UNIVERSITY OF CALIFORNIA

Santa Barbara

Receptor recognition and inhibitory mechanisms of contact dependent growth inhibition systems

A thesis submitted in partial satisfaction of the

requirements for the degree Master of Science in

Biochemistry and Molecular Biology

by

Ian Hoyt Matthews

Committee in charge:

Professor Christopher S. Hayes, Chair

Professor David A. Low

Professor Frederick Dahlquist

June 2022

The thesis of Ian Hoyt Matthews is approved.

_____
Frederick Dahlquist

_____
David Low

_____
Christopher Hayes, Committee Chair

June 2022

Receptor recognition and inhibitory mechanisms of contact-dependent growth inhibition systems

ACKNOWLEDGEMENTS

I will forever be thankful for my time in the Hayes Lab as both an undergraduate and a graduate student. Working in this setting has fundamentally changed me as a both a student and a person and has demonstrated to me what it means to be a good scientist. I am grateful to every person whom I interacted with in the lab – the unwavering support that I received kept me motivated to come in each day. None of this would have been possible without Nicole Chan's leadership throughout my time in the lab as an undergraduate, which provided me with the foundations I needed to begin my own projects. To Dr. Fernando Garza-Sánchez, I will forever cherish our late-night conversations and your willingness to help at any time, by any means possible, without question. To Michael Costello, thank you for challenging me to always learn more and for reminding me to have fun.

I am thankful to Dr. Christopher Hayes, who challenged me to push myself as a scientist and showed me what it means to master a craft. His advising and contagious excitement towards discovery made my difficulties in the lab surmountable. Finally, I am especially grateful to Dinh Quan Nhan for his patient teaching, moral support, and friendship.

ABSTRACT

Receptor recognition and inhibitory mechanisms of contact dependent growth inhibition systems

By

Ian Hoyt Matthews

Bacteria occupy nearly every environmental niche on Earth, including extremities of salinity, temperature, pressure, and pH[1]. In each of these settings, they share space and resources with other organisms and form a variety of symbiotic relationships[2]. In some cases, bacteria have evolved to deliver toxic effectors into the environment[3], or directly into nearby organisms[4,5] to provide themselves with a growth advantage over their neighbors. A number of secretion systems have been identified which allow bacteria to translocate effectors across their membranes, as well as the membranes of targeted organisms[6]. In Gram-negative bacteria, contact-dependent Type Vb secretion systems (T5SS) recognize specific surface epitopes on neighboring bacteria and deliver toxic proteins into their cytosol[7–9]. Sibling cells are protected from intoxication by expression of an immunity protein which binds and inactivates cognate toxic effectors[10,11]. This process, termed contact-dependent growth inhibition (CDI) is associated with kin recognition[8,12], genetic stability[13], biofilm formation[14,15] and pathogenesis[16]. The secretory pathway of CDI systems across the membranes of toxin-producing cells appears highly conserved[17]. However, the mechanisms underlying target cell

recognition, traversal across target cell membranes, as well as the processes by which toxins exhibit their toxicity, are highly variable and in some cases not well understood[8,11,18,19]. In chapter 1, I review the arsenal of systems used by Gram-negative bacteria to translocate proteins across their membranes, with special focus on Type Vb CDI systems. In chapter 2, I identify novel inner membrane proteins co-opted by the cytoplasm-entry domains of CDI systems. Additionally, I find that some unique entry domains the recognize same inner membrane proteins, suggesting differences in recognized epitopes. In chapters 3 and 4, I investigate potential growth inhibition mechanisms of two protein effectors found in CDI systems from *Enterobacter cloacae*. First, I cover an effector domain from *E. cloacae* S611 with homology to SAM-binding domains and propose that it could act as a toxic methyltransferase. Then, I investigate an effector domain from *E. cloacae* UCI49 with predicted homology to glutaminases and cysteine proteases, where I identify potential protein targets via mass spectrometry. Finally, in chapter 5 I discuss potential future directions in the field of CDI.

TABLE OF CONTENTS

I. Introduction

Abstract

A plethora of secretion systems in Gram negative bacteria power and/or facilitate the export of a variety of molecules destined for the environment or for the cytosol of other cells. Pathways such as the general secretory pathway are highly traveled routes for most proteins destined beyond the cytosol of the producing cell. On the other hand, many systems have evolved to specifically recognize and secrete a handful of effectors. In some cases, they rely on the Sec system for transport of substrates into the periplasm, and in other cases they span multiple membranes. Here, I briefly cover the the general secretory pathway and Type I-VI secretions systems, with special focus on Type V systems and specifically on Type Vb contact dependent growth inhibition (CDI) systems.

The General Secretory Pathway

Most gene products in Gram negative bacteria bound for destinations beyond the cytoplasm encode a hydrophobic amino-terminal signal peptide that enables co-translational or post-translational secretion into the periplasm. During post-translational secretion, the nascent signal peptide retards initial folding and allows binding by promiscuous chaperones including SecB[20]. SecB then associates with the ATPase SecA at the inner membrane and hands off the protein for interaction with SecYEG[21,22]. The SecYEG complex forms a helical pore in the inner membrane capable of expanding its lumen[23,24], as well as opening laterally toward the inner membrane[23,25]. Cycles of ATP hydrolysis by SecYEG-bound SecA pump coordinated substrates through the lumen of SecYEG while the signal peptide remains associated with the lipid bilayer proximal to the lateral gate[24–26]. A second associated complex,

SecDFYajC, binds the substrate in the periplasm and further powers translocation via conformational changes driven by the proton motif force (PMF)[27]. When translocation nears completion, the signal peptide can be proteolytically removed by a membrane associated signal peptidase[24]. While post-translational secretion is typically reserved for proteins destined beyond the cytosolic membrane, a co-translational pathway delivers inner membrane proteins[28]. In this process, the signal peptide interacts with a recognition protein, SRP, and the complex associates with the SecYEG complex[24]. Energy from translational elongation provides a power source for translocation across the opened lateral gate of the pore [28], assisted by the inner membrane protein YidC[29]. Combined, pathways using the Sec system are responsible for the export of the majority of the bacterial secretome[23,24,30].

Type I-IV and Type VI Secretion Systems

Type I secretion systems (T1SS) present a simple model for translocation across Gram-negative membranes. A continuous transport pathway is formed across both host membranes consisting of an ABC transporter in the inner membrane, TolC or a TolC-like porin that bridges the outer membrane and periplasm, and a membrane fusion protein in the inner membrane that mediates interactions between the two[31,32]. Assembly of these components is induced by interaction of the ABC transporter with a secretion signal at the extreme C-terminus of the cargo that then leads to active transport of the cargo into the periplasmic channel and subsequent facilitated diffusion into the extracellular environment[32,33]. In contrast, Type 2 secretion systems (T2SS) are formed from the assembly of multi-protein subcomplexes in the inner membrane, periplasm, and outer membrane, transporting folded periplasmic proteins across the outer membrane[34]. Following Sec or Tat-mediated secretion into the periplasm,

effectors likely associate with the periplasmic lumen of the outer membrane pore complex[35,36]. Recognition of a secretion signal on the effector then induces activity of a cytoplasmic ATPase, which drives polymerization of inner membrane-associated pseudopili[37]. As the pseudopili extend through the periplasmic space and the outer membrane porin, they drive opening of an extracellular gate and push the effector outside of the cell[38].

Type 3 secretion systems (T3SS) are made up of a similarly complex macromolecular assembly, spanning both bacterial membranes[39–41]. This assembly, termed the needle complex, is made up of assembled monomers which extend the apparatus beyond the LPS to enable contact with a host cell. Interestingly, this machine is closely related to the flagellar structure and shares similar export pathways to that of flagellar subunits[40]. Contact with a host cell triggers secretion and assembly of a pore complex in the targeted cell's membrane, allowing the delivery of unfolded toxic effectors[42]. In *Salmonella typhimurium*, T3SS has also been found to be necessary for invasion of eukaryotic host cells and formation of *Salmonella*-containing vacuoles[43]. Type 4 secretion systems (T4SS) can similarly target eukaryotic cells for delivery of effectors, but also perform interbacterial conjugation[44,45]. These systems form 12-protein complexes spanning both membranes, while a hollow pilus assembled from pilin monomers extends from the cell[46]. Recognition interactions between T4SS and host cells in some cases mediate adhesion to targeted cells and delivery of toxic effectors, although the mechanisms surrounding receptor binding and membrane translocation are not well understood[47,48].

Type VI Secretion Systems (T6SS) are reminiscent of the contractile tail structures of bacteriophages[49]. T6SS complexes span both membranes and form massive, rod-like tubular structure composed of Hcp monomers, while at the tip of the rod lies a trimeric VgrG cap and

PAAR domain-containing protein[50,51]. Some toxic effectors are loaded into the "cargo bay" of the Hcp tube, while specialized effectors encode fusions to PAAR domains, placing them at the tip of the contractile sheath[52]. During secretion, the system undergoes a forceful contraction, anchored by the baseplate, which penetrates the T6SS-producing cell's outer membrane, as well as those of any adjacent cells within its trajectory[51]. Given the lack of specificity in firing, these systems are upregulated by quorum sensing, limiting expression to scenarios in which other cells are likely to be nearby[52]. T6SS are responsible for anti-eukaryotic activities[53] as well as interbacterial competition[54], capable of releasing an arsenal of diverse toxic effectors with each contraction.

Type Va Vc, Vd, and Ve Secretion Systems

Type V secretion systems can further be classified into five distinct subtypes, denoted Type Va through Ve. Universal among subtypes is the presence of a translocator, which forms a beta-barrel in the outer membrane, and a passenger, which is exported through the translocator. Passengers tend to remain tethered to the translocator on the cell surface, forming semi-rigid extensions through various structural motifs[4,55]. Type V proteins are first targeted to the periplasm through Sec-dependent secretion via a cleavable signal sequence. Once in the periplasm, the translocator is assembled into the membrane by the Bam complex[4]. However, the system lacks an apparent external energy source to power passenger translocation across the outer membrane[4,56]. The energy powering passenger export is thought to come from co-translocational folding, as the passenger remains in a less stable, partially unfolded conformation in the periplasm mediated by chaperones[4,57–59].

In Type Va systems, termed "classic autotransporters," the translocator and passenger are domains of the same protein. Membrane insertion of the C-terminal translocation domain leads to export of the N-terminal passenger to the cell surface, where a fused cargo may be presented[56,57,60]. Passenger domains usually form beta helices, which stack as long beta sheets extending away from the membrane[55,61]. Enzymatic cargoes, such as IgA protease from *Nisseria meningitidis,* undergo autoproteolysis for liberation into the extracellular environment[62]. Other cargoes, like the adhesins presented by pertactin from *Bordetella pertussis*, remain associated with the cell surface[61].

The genetic arrangements of Type Vc systems bear similarity to that of classic autotransporters, but instead form trimers on the cell surface[4]. The C-terminal translocation domain of each monomer forms a third of the outer membrane beta-barrel, while the oligomerized passenger domains form a coiled coil structure[55,63]. Cargoes at the tip of the filament tend to function as adhesins, as is the case for the characterized collagen-binding autotransporter YadA from *Yersinia enterocolitica*[64]. The exact mechanism underlying passenger translocation through the trimeric beta-barrel is poorly understood, although co-secretory folding is likely involved[57].

Type Vd systems have only recently been characterized, appearing similar to classic autotransporters but containing an additional polypeptide translocation associated (POTRA) domain linking the passenger and translocator[56,57]. POTRA domains are common among porins that export protein substrates, including the Type Vb systems, the Bam complex, and porins in mitochondria and chloroplasts[65–67]. The first and best characterized protein of this system, PlpD from *Pseudomonas aeruginosa*, is cleaved from the cell surface after export and exhibits lipase activity[68]. The authors who identified this system postulate that the POTRA

domain could be important in recruiting a processing factor or enhancing export of the passenger domain.

Type Ve systems are termed "inverse autotransporters" due to the relocation of the translocation domain to the N-terminus rather than the C-terminus. The passengers also utilize structural motifs distinct from other autotransporters, such as immunoglobulin-like repeats[55–57]. A notable example is intimin, an adhesin produced by diarrheagenic *Escherichia coli* that binds to a bacteria-produced transmembrane receptor inserted into the host membrane via a type III secretion system[69]. Similar to Type Vc, the majority of the identified Ve autotransporters remain associated with the cell surface and function in adhesion[70].

Type Vb Secretion Systems and Contact Dependent Inhibition

In contrast to single protein autotransporters, type Vb systems divide the translocator and passenger between two proteins. They are thus termed "two partner secretion" (TPS) systems, where TpsB forms the translocator in the outer membrane and TpsA forms the passenger. In *E. coli* and other enterobacteria, TPS systems have been identified to be involved in contact-dependent growth inhibition (CDI)[10]. Cells carrying CDI systems (CDI^+ cells) are termed "inhibitors," while CDI^- cells may be referred to as "targets". During CDI, CdiB (TpsB) exports and presents CdiA (TpsA) on the inhibitor cell surface, where upon recognition of a specific receptor on an adjacent bacterial cell, a toxic payload is delivered across both target cell membranes into the cytoplasm.

The translocator, CdiB, belongs to the Omp85 family of outer membrane porins which are found across eukaryotes[66], didermic bacteria, and their relatives, including mitochondria and chloroplasts[67]. The C-terminal region of CdiB and related TpsB proteins form membrane-

associated beta-barrels comprised of 16 beta strands, with eccentric lumens containing diameters around 30 Å[71]. Meanwhile, the N-terminus forms a helical plug as well as two periplasmic POTRA repeat domains[65]. POTRA domains have been demonstrated to mediate substrate specificity, as exchanging the POTRA domains between different TpsBs allows recognition of different TpsA passengers[72]. The extreme N-terminal helix (H1) allows an additional form of regulation by occluding the beta-barrel lumen in the absence of CdiA secretion. In FhaC, a CdiB homolog from *Bordetella pertussis*, spin labeling measurements between the distal tip of H1 and extracellular or periplasmic residues indicate a conformational change that slides the helix into the periplasm during secretion of FHA (TpsA)[73]. Additionally, in a crystal structure of FhaC lacking substrate, the extracellular loop 6 (L6) extends into the lumen of the beta-barrel, forming a "lid-lock" structure[74,75]. L6 contains a conserved motif necessary for secretion[74,76] and protease site insertions indicate that it becomes extracellularly available in the presence of FHA[77]. This suggests a similar regulatory role to that of H1, although while displacement of H1 is transient during secretion[73,75], L6 may form stable interactions with neighboring extracellular loops or with FHA. Given the high degree of structural similarity between FhaC and *E. coli* CdiB, these findings likely bear functional significance to the mechanisms underlying CdiA translocation.

CdiA is a large multidomain protein, varying in mass between species from 180 to 630 kDa[7]. Its extreme N-terminus bears a signal sequence for targeting to the periplasm via the Sec pathway, after which the peptide is proteolytically removed. The mature N-terminus harbors the two-partner secretion (TPS) domain, which interacts with the periplasmic POTRA domains of CdiB. TPS domains form a conserved three face beta-helical backbone characteristic of filamentous hemagglutinin (FHA) in *B. pertussis*[78]. Excursions from this backbone are more

variable and are thought to mediate substrate specificity through a transient beta-augmentation mechanism conserved between various POTRA-extended peptide interactions[79,80]. Thus, a given TPS domain will only interact with its cognate POTRA domain to trigger secretion. This domain is followed by the FHA-1 domain, given its name due to its repetitive beta-helical motifs with high homology to *B. pertussis* FHA. The size of this domain varies across CDI proteins, ranging from around 500 residues to nearly 4000[17]. In FHA, the beta-helices stack upon those in the TPS domain, forming a rigid filament that extends from the cell surface after translocation through FhaC[78].

Downstream of the FHA-1 domain resides the receptor binding domain (RBD). The RBD has been demonstrated to bind epitopes on the outer membrane of closely related species and plays a critical role in the specificity of target cell recognition[8]. The RBD region is highly variable between different *cdiA* genes, and in *E. coli* four distinct classes are recognized by sequence identity. Classes 1-3 bind the outer membrane porins BamA[14], heterotrimeric OmpC-OmpF[12], and tsx[8] respectively, while class 4 RBDs target a core phosphorylated heptose in LPS[81]. The extracellular components targeted by receptor binding domains are highly variable, and thus RBDs tend to recognize the corresponding receptors of only closely related species[8]. Downstream of the RBD is an extended tyrosine-proline rich region, termed the YP domain, which is necessary for cell surface presentation and therefore likely forms contacts with the inhibitor cell surface or with CdiB[17]. This domain links directly to the FHA-2 domain, which bears resemblance to FHA-1, although structural modeling indicates that it contains many beta-strand excursions of varying length which change the number of residues between the beta-helical, FHA-like repeats. FHA-2 has been shown to associate with the surface of the target cell and is thought to form a pore for translocation of the rest of the C-terminus of CdiA into

the target cell periplasm[17]. Downstream of FHA-2 is a region termed the "pre-toxin" (PT) domain due to its proximity to the extreme C-terminal toxin[17]. This domain ends in a conserved "VENN" motif (or "ELYN" in *Burkholderia* species[7]) that has been identified as a cleavage site that liberates the C-terminus of CdiA into the target cell periplasm. Processing immediately C-terminal to the final asparagine residue has been shown to be crucial for proper delivery of toxin to the target cytosol. The PT domain has been postulated to be important in this cleavage process, perhaps carrying autoproteolytic acvitity[9,17].

While majority of CdiA is highly conserved between species, considerable variability exists in the previously covered RBD, as well as the post-VENN C-terminus of CdiA (CdiA-CT). This region may contain one or two domains, with the extreme C-terminal domain possessing toxic activity and the N-terminal "entry" domain mediating translocation across the inner membrane. Entry domains have previously been characterized through mutagenesis of target bacteria and selection for CDI-resistant mutants. Many factors identified by these screens are inner membrane proteins which confer resistance to toxicity through native delivery pathways, but not through internal toxin expression[18]. For example, CdiA-CT^{EC3006} from *E. coli* isolate EC3006 requires the glucose-specific phosphotransferase system PtsG for inhibition of target cells during co-culture, but cells expressing cytoplasmic CdiA-CT^{EC3006} exhibit toxicity in a PtsG-independent manner. Additionally, when this entry domain is swapped with distinct CdiA-CTs, those fusions are endowed with PtsG-dependent delivery[18]. Interactions between entry domains and inner membrane proteins have been shown to mediate translocation through a mechanism that, although unknown, does not rely on the hijacked protein's native import functions and is dependent on the PMF[82]. One potential exception to this observation may exist for entry domains targeting the Sec machinery, such as those found

in CdiA-CT_{o10}^{EC869} and CdiA-$CT^{GN05224\ 83}$. The introduction of a bulky side chain into the lumen of SecY confers partial resistance to their CdiA-CT activities, and full resistance is observed when coupled with disruptions of SecY associated proteins PpiD or YgfM. The necessity of an available lumen may indicate that these CdiA-CTs travel backwards through the export machinery and may later insert into the membrane as a step in translocation of the toxin domain. Despite the potential exception of these entry domains, current findings suggest a universal translocation mechanism across the inner membrane, despite the expansive heterogeneity of entry domains.

While the toxin activities of CdiA-CTs are largely uncharacterized[7], the majority of characterized toxins harbor various nuclease activities. The first characterized toxin from *E. coli* isolate EC93 appears to form pores in the inner membrane that dissipate the proton motive force and cause reversible changes in cell morphology[84]. Better characterized toxin domains include CdiA-$CT^{Dd3937-2}$ from *Dickeya dadantii* 3937 CDI module 2, which nonspecifically degrades DNA in the targeted cell[11]. Other toxin domains target RNA instead, such as CdiA-CT^{ECL} from *Enterobacter cloacae* which cleaves 16S rRNA[85] and CdiA-$CT^{STECO31}$ from *E. coli* STEC_O31 which cleaves $tRNA^{Glu}$ at a specific site near the anticodon[19]. Some toxins require specific co-factors in the cell for function, such as CdiA-CT^{EC869} which requires EF-Tu to cleave targeted tRNAs[86] and CdiA-$CT^{UPEC536}$ which requires the biosynthetic enzyme CysK to perform a similar tRNase function[87]. In the latter case, binding to CysK stabilizes the toxin's fold by anchoring its C-terminus and forming an interaction interface that increases thermostability[88]. Low thermostability may be a trend among CdiA-CTs, which must remain unfolded in the inhibitor periplasm and subsequently cross 3 membranes to reach the target cell's cytosol.

In addition to the two proteins encoded by Type Vb secretion systems, many CDI systems encode an additional gene downstream of *cdiA* which functions as an antitoxin to a cognate CdiA-CT[10,11]. This gene, termed *cdiI*, prevents genetically similar cells from inhibiting one another by providing specific immunity against the toxin deployed by CdiA. For example, cells expressing $CdiI^{UPEC535}$ are protected from inhibition when co-cultured with cells expressing $CdiA^{UPEC536}$ but exhibit growth inhibition when co-cultured with cells expressing $CdiA^{EC93}$ [11]. When a chimera is generated containing a fusion of CdiA-$CT^{UPEC536}$ to $CdiA^{EC93}$, cells expressing $CdiI^{UPEC536}$ are protected. Crystal structures of CdiI-CdiA-CT complexes illustrate a specific binding interaction between the two cognate proteins, where the bound CdiA-CT is rendered inactive either by occlusion of its catalytic site[89] or through an allosteric mechanism[90]. Thus, CdiA-CT-CdiI interactions bear resemblance to classic toxin-antitoxin (TA) systems like colicins and plasmid TA modules, but are delivered via a completely heterologous, contact-dependent mechanism.

Mechanism of CDI Delivery

The secretion, surface presentation, and delivery of CdiA occurs in a highly controlled manner through a series of stable intermediates. First, CdiB is targeted to the target cell outer membrane via signal peptide-mediated export through the Sec machinery into the periplasm and assembly into the outer membrane aided by the Bam complex. Then, CdiA follows a similar Sec-mediated pathway to the periplasm, where it may begin interactions with CdiB. Chaperones in both the cytosol and periplasm prevent full folding of CdiA until the protein is presented on the surface of the cell[58]. Following signal peptide removal, the TPS domain at the mature N-terminus recognizes the POTRA domains of CdiB, which initiates secretion of the

extended polypeptide through the lumen of the porin[80]. Co-secretional folding powers assembly of stacking beta-helices of the FHA-1 domain, which accounts for the majority of the N-terminal half of the protein. CdiA is too large to occupy the CdiB lumen in a folded state[74], so this folded region may interact with the barrel's extracellular loops or may form some other interaction for tethering to the outer membrane.

Past models of CDI describe the delivery mechanism as a "toxin on a stick", whereby the entire protein is immediately secreted, folded and presented on the surface, with CdiA-CT forming the most distal tip of the filament[91]. Presumably, the RBD in the middle of the folded filament then contacts a target cell and the toxin is deposited in the target periplasm via an unknown mechanism. However, recent work by Ruhe *et al.,* 2018[17] has shed light on the cell surface presentation of CdiA and part of its delivery into target cells. They show that initially, the FHA-1 domain forms an extended rigid filament ending at the receptor binding domain. Thus, the RBD is presented at the far end of the filament while the C-terminal region of the RBD as well as the YP domain form an extended polypeptide chain that crosses the outer membrane back into the periplasm. The domains C-terminal to the YP region, including FHA-2, the pre-toxin domain, the cytoplasmic entry domain, and the effector domain remain sequestered in the periplasm in an unfolded state. This partially secreted hairpin-like structure is held stably on the cell surface until the RBD encounters its cognate receptor on a neighboring cell. Folding of the RBD in the presence of the receptor triggers export and subsequent folding of the C-terminal half of CdiA. Based on the predicted structural model, the FHA-2 domain is thought to fold into beta helices that stack on top of the FHA-1 and RBD beta helices and extend toward the target cell membrane. Beta-strand spacers between these FHA-2 repeat sequences may form a pore capable of translocating the rest of the C-terminus of CdiA into the

target cell periplasm. Thus, the energy of folding could power transport across the target cell outer membrane, explaining why no energy source has been attributed to this step in CDI, unlike colicins which use the Tol and Ton systems to power their entry[92].

Delivery of the pre-toxin domain and CdiA-CT into the target cell periplasm could trigger autoproteolytic cleavage at the VENN sequence, liberating CdiA-CT from the rest of the polypeptide. The cytoplasm entry domain of the free CdiA-CT may then recognize periplasmic epitopes of its cognate inner membrane receptor and mediate inner membrane translocation through an unknown, PMF-dependent manner. Once inside the cell, the highly variable effector domain exhibits toxic activity by interfering with core cellular processes to inhibit growth. Cells carrying cognate immunity proteins would avoid effector-mediated growth inhibition by binding and inactivating CdiA-CT.

Conclusion of Introduction

While the Sec pathway performs general cellular functions, Type I-VI secretion systems offer highly specialized pathways out of the cell and sometimes into targeted eukaryotic or bacterial cells. In the case of T2SS and T5SS, the general secretory pathway is necessary to deliver the desired effectors into the periplasm for interaction with the secretory apparatus. In contrast, T1SS, T3SS, T4SS, and T6SS span both membranes, transporting effectors from the cytosol to their destined locations either in the extracellular milieu or the inside of another cell. At a glance, CDI seems to be one of the simplest pathways, requiring only two proteins, CdiA and CdiB for specific translocation across up to three membranes to reach the target cell cytosol. However, the large, multidomain CdiA performs complex functions and undergoes multiple structural rearrangements during delivery. Some steps in this

dynamic pathway have recently become better understood, including the static presentation of CdiA on the cell surface and the export of the full protein after receptor binding[8,17]. Other steps, such as presumed liberation of CdiA-CT by the pre-toxin domain and translocation across the target cell inner membrane, are poorly understood. Additionally, the characterized activities of CDI effector domains currently remain limited to nucleases[19,85,93,94] and pore formers[14,84], despite evidence that much greater diversity exists[95]. It is my hope that the work performed here sheds light on the diversity and mechanisms underlying the cytoplasm entry domains and effector domains of various CdiA-CTs.

II. Identification of Inner Membrane Proteins Involved in CDI

Abstract

Contact dependent growth inhibition (CDI) systems are made up of two partners, CdiA and CdiB, which coordinate to deliver a toxic effector from the periplasm of a producing "inhibitor" cell to the cytoplasm of a receiving "target" cell[7]. One critical step in CDI delivery involves liberation of the C-terminus of CdiA from the rest of the large protein, releasing a two-domain protein, termed CdiA-CT, into the target cell periplasm[17,95]. Free CdiA-CT must then traverse the target cell inner membrane to access the cytosol and perform its toxic activity. The mediator of the translocation step has been localized to the N-terminal "cytoplasm-entry" domain of CdiA-CT, while toxic functions are attributed to the C-terminal effector domain[18,96]. Additionally, it has been found that cytoplasm-entry domains require specific proteins in the target cell inner membrane in order to perform translocation via an unknown mechanism[18]. These domains exhibit high polymorphism, and unique inner membrane proteins have been identified to be required to translocation via various domains. Here, I use transposon mutagenesis to identify permissive factors involved in resistance to specific CdiA-CTs and demonstrate that these factors are likely required for translocation across the cytoplasmic membrane. While some of the identified factors are novel, including AroP, AmpG, MtlA, and YajC, others are previously identified, including GltJK and FtsH. In the latter two cases, dissimilarities between genetically distinct cytoplasm entry domains which target the same proteins are postulated to recognize distinct epitopes on the periplasmic surface.

Introduction

Targeting of CDI systems to neighboring cells requires the recognition of multiple specific epitopes. The first target-recognition event involves a binding event between the receptor binding domain and an extracellularly available motif on the target cell surface[8]. Four classes of RBDs have been identified in *E. coli* which bind to distinct epitopes on either outer membrane porins[8,12,14] or components of LPS[81]. After RBD-mediated deployment of FHA-2 and translocation of the C-terimnus of CdiA across the target cell outer membrane, a second receptor recognition event occurs. Here, the cytoplasm entry domain of proteolytically-liberated CdiA-CT recognizes periplasmic epitopes of inner membrane proteins[18,82]. Many recognized inner membrane proteins have been identified for various CDI systems, including MetI, PtsG, FtsH, YciB, RbsC, GltJK, SecY, and AcrB[14,18,83]. While some of these proteins use ATP or the transfer of high energy phosphates to power the import of their native substrates, others have no known import function. For example, AcrB forms part of the AcrAB-TolC multidrug efflux pump, which uses the proton motive force to export molecules from the cytoplasm[97]. Interestingly, the involvement of AcrB in the import of CdiA-CT^{EC93} appears to be independent of its native function, as cells containing mutations in TolC or AcrA are still sensitive to CDI[14]. This may indicate that in CDI, inner membrane proteins function primarily as specific receptors that localize the CdiA-CT to the inner membrane, where a general translocation mechanism takes place for entry into the cytosol.

CDI systems in enterobacteria are thought to encode at least 29 distinct families of cytoplasm entry domains, determined by primary sequence identity (unpublished data). Currently, only a third of those families have been linked to a specific inner membrane protein or IM protein complex[14,18,83] (unpublished data). Identification of factors linked to

uncharacterized entry domains could yield insight into the range of targets for receptor recognition and the mechanism underlying the final translocation step in CDI. Here, I identify AmpG, MtlA, YajC, and AroP as novel inner membrane proteins presumably involved in translocating CdiA-CTs across the cytoplasmic membrane. Additionally, I find that two previously recognized CDI-associated inner membrane proteins, FtsH and GltJK, are associated with novel cytoplasm entry domains, suggesting that these entry domains may recognize unique epitopes on the associated inner membrane proteins.

Mariner Transposon Mutagenesis and Selection for CDI-Resistant Mutants

CDI-associated factors have previously been identified via mutagenesis of CDI-susceptible bacteria and selection for CDI-resistant mutants[8,12,14,18,86]. Randomized mutagenesis of *E. coli* cells is commonly performed using a variety of mutagenic agents including chemical mutagens, UV light, and transposable elements. While the former two approaches generate single nucleotide changes that lack easy traceability, transposable elements generate large insertions and can be engineered to carry resistance markers as well as other components necessary for identifying their location in the genome[98]. Regardless of the mutagenic approach, enrichment of CDI-resistant mutants from pools of mutagenized cells takes advantage of the fact that CDI-sensitive cells often experience a drastic decrease in viability during co-culture with CDI^+ inhibitor cells. Meanwhile, CDI-resistant cells continue to grow normally. Over multiple rounds of exposure to CDI^+ cells, resistant mutants will vastly outnumber sensitive mutants, allowing the simple isolation of an isogenic resistant colony, followed by recovery of an inserted genetic marker or whole-genome sequencing.

To generate mutagenized target cells for selection, independent pools of MG1655 Δ*wzb* *E. coli* were mated with a donor strain carrying a mobilizable pSC189 plasmid. Target cells lacking the colonic acid biosynthetic *wzb* gene were chosen as mutations upregulating biosynthesis and formation of capsule have been shown to block CDI, leading to accumulation of undesirable resistant mutants[14]. Inhibitor cells were generated for co-culture selections carrying chimeric fusions of various CdiA-CTs to $CdiA^{EC93}$ from *E. coli* isolate EC93, lacking $CdiA\text{-}CT^{EC93}$. These chimeras allow for targeted selection for factors associated specifically with the CdiA-CT, as the receptor binding domain of $CdiA^{EC93}$ recognizes the essential outer membrane protein BamA, which is unlikely to accumulate viable transposon insertions[14]. Potential genes linked to CDI resistance should thus be limited to factors associated with the specific fused CdiA-CT.

Candidate CdiA-CTs for selection were chosen by the identity of their cytoplasm entry domains, which appear distinct by primary sequence from those previously identified. Three of the selected CdiA-CTs bear characterized toxin domains, including $CdiA\text{-}CT^{EC16}$ from *Erwinia chrysanthemi* EC16 which cleaves 16S rRNA[85], $CdiA\text{-}CT^{Dd3937}$ from *Dickeya dadantii* which degrades DNA[11], and $CdiA\text{-}CT^{DBS100}$ from *Citrobacter rodentium* DBS100 which acts as a cysteine protease (unpublished data). The other selected CdiA-CTs include $CdiA\text{-}CT^{WPP163}$ from *Pectobacterium parmentieri* WPP163, $CdiA\text{-}CT^{S611}$ from *Enterobacter cloacae* S611, and $CdiA\text{-}CT^{UCI49}$ from *E. cloacae* UCI49. Enrichment of *mariner* transposon-mutagenized pools against each chimeric inhibitor yielded resistant mutants after 2 to 4 rounds of co-culture, from which single colonies were isolated and tested for resistance. To confirm that the CDI-resistant phenotype of individual colonies was caused by *mariner* transposon insertion, the transposon-associated kanamycin marker was transduced using P1 phage into

CDI-sensitive non-mutagenized MG1655 Δ*wzb E. coli*. Surprisingly, multiple enriched pools across the tested chimeras exhibited CDI-resistant phenotypes which were not linked to a transposon marker.

CdiA-CT from EC16 Recognizes Known CDI-Associated Factor GltJK

Enrichment of three independent transposon-mutagenized pools for mutants resistant to CdiA-CT^{EC16} yielded two linked mutants harboring insertions in either *gltJ* or *gltK* (Figure 1A-C). GltJ and GltK are inner membrane proteins that complex with the ATP-binding protein GltL and periplasmic binding protein GltI to form an ABC transporter for import of L-glutamate and L-aspartate[99]. All four proteins are encoded within the same operon, with *gltJ* and *gltK* most downstream. To ensure that identified insertions do not simply induce polar effects on the *gltIJKL* operon, in frame insertions in each gene were tested in co-culture with chimeric *cdiA*^{EC93}-*CT*^{EC16} (termed CDI^{EC16}) inhibitors. Loss of either *gltJ* or *gltK* was sufficient to confer CDI^{EC16} resistance and complementation of the respective genes on a plasmid restored wild-type levels of inhibition (Figure 1C). Additionally, Δ*gltI* and Δ*gltL* cells were sensitive to CDI^{EC16}, confirming that only the membrane-associated proteins are required for delivery.

Interestingly, these proteins have previously been reported as CDI-associated receptors for cytoplasm entry domains from *Photorhabdus luminescens* TTO1[18] and *Burkholderia multivorans* CGD2M[96]. It was found that importer activity is not necessary for uptake of *P. luminescens* CdiA-CT, as Δ*gltL* cells retain CDI-sensitivity. This is also the case for CdiA-CT^{EC16}. Alignment of the CdiA-CTs reveals little significant homology between any of their N-terminal cytoplasm entry domains aside from two highly conserved Cys residues which are

predicted to form separate disulfides with less conserved cysteines (Figure 1D). In the case of *B. multivorans* CGD2M, it was reported that this entry domain does not recognize *E. coli* GltJK (although it does recognize *E. coli* GltJ in complex with *B. multivorans* GltK, perhaps indicating that GtlK residues form the majority of the epitope while GltJ is important for proper presentation of GltK)[96]. However, in the case of CdiA-CT^{TTO1}, screens identifying association of GltJK with were performed in *E. coli*. Lack of sequence homology between TTO1 and EC16 may suggest either that these sequences form similar structures with the similar activities, or that they may recognize distinct epitopes of the GltJK complex. Comparison of structural models of the two entry domains generated by AlphaFold2[100,101] show that both have high alpha-helical content, a property consistent among CDI entry domains (Figure 1E). Although two disulfide-linked helices are conserved, most of the domains are structurally dissimilar, supporting the possibility that each entry domain recognizes a distinct region of the GltJK surface.

AroP, AmpG, MtlA, and YajC are Novel CDI-Associated Inner Membrane Proteins

Enrichment of transposon pools and selection of these pools against *cdiA^{EC93}* fusions with *cdiA-CT*s from Dd3937, WPP163, S611, and C. rod yielded insertions in *aroP, ampG, mtlA, and yajC*, respectively (Figures 2A&B, 3A&B, 4A&B, 5A&B). In each case, in frame insertions generated by the Keio collection[102] into each of the respective genes led to CDI-resistance, and complementation with the corresponding plasmid-borne gene rescued CDI-sensitivity (Figure 3C, 4C, 5C).

AroP is an inner membrane permease that imports the aromatic amino acids Phe, Tyr, and Trp using the PMF[103,104]. It is encoded as a single gene and is not predicted to complex

with other inner membrane proteins that could potentially share a CdiA-CT^{Dd3937} interaction surface. Topology models propose 12 transmembrane helices, as well as only 2 minimal periplasmic excursions determined by fusions with alkaline phosphatase[105]. The periplasmic loops of inner membrane proteins have previously been proposed to form the recognition epitopes for CDI entry domains[18], and the minimal available interaction surfaces in the periplasm of AroP may make it an attractive model to study the mechanism of CDI translocation. Interestingly, transposon-linked mutants in *aroP* are not fully resistant to growth inhibition by CDI^{Dd3937}, with inhibitors retaining a ~10-fold growth advantage after 3 hours of co-culture (Figure 2A, bottom panel). This could suggest an alternative, suboptimal entry pathway for CdiA-CT^{Dd3937} across the cytoplasm involving a separate inner membrane protein. Alternatively, AroP could be recognized in complex with another periplasmic epitope, where loss of AroP makes interactions with the entry domain suboptimal and thus reduces inhibition. This protein is unlikely to be a co-factor for DNase activity of the effector domain, as *in vitro* reactions demonstrate high processivity against plasmid DNA[11], presumably in the absence of AroP.

AmpG is an inner membrane permease that facilitates the import of cell wall degradation products using the proton motive force[106]. It works alongside the cytosolic amidase AmpD to induce expression of beta-lactamase, AmpC, and plays a role in cell wall recycling in Gram-negative bacteria[107]. AmpG has no known inner membrane partners, making it likely that it is the only inner membrane protein with recognition epitopes for CdiA-CT^{WPP163}. Topology mapping of AmpG via generation of fusion proteins indicates an even more minimal periplasmic landscape than is present in AroP[108], suggesting that very little context is required for recognition by the WPP163 entry domain. To confirm that AmpG is necessary for passage

across the cytoplasmic membrane rather than functioning as a co-factor for toxic activity, the *cdiA-CT*^{WPP163}*-cdiI*^{WPP163} complex was internally expressed in cells under an arabinose inducible promoter. To eliminate the immunity protein and allow growth inhibition, a modified SsrA tag was fused to C-terminus of CdiI^{WPP163} for ClpXP-mediated degradation[109]. Induction of this construct with arabinose showed no difference in growth inhibition between wild-type and Δ*ampG* cells (Figure 3D), indicating that the inner membrane protein is not required for the activity of endogenously expressed CdiA-CT. Therefore, AmpG is likely co-opted by the cytoplasm entry domain of CdiA-CT^{WPP163} for traversal of the cytoplasmic membrane.

In contrast to the two previous inner membrane proteins, topology maps of the CdiA-CT^{S611}-associated MtlA demonstrate more significant periplasmic loops for interaction with the entry domain[110]. MtlA is a phosphotransferase system (PTS) powered by phosphoenolpyruvate which imports and phosphorylates D-mannitol[111]. As opposed to many PTS proteins, MtlA is a fusion of the IIA, IIB, and IIC components, covalently linking the membrane transporter to the phosphotransfer machinery[112]. Although CDI cytoplasm entry domains have been reported to function independently of associated import functions[18], it's possible that the CdiA-CT^{S611} entry domain interacts with the periplasmic loops of MtlA in a similar manner to its substrate to mediate recognition. To confirm that the inner membrane protein is not involved in its uncharacterized mechanism of inhibition, an internal expression constructs was generated similar to that of CdiA-CT^{WPP163}. This construct showed no difference in inhibition between wild-type and Δ*mtlA* cells, indicating that endogenously expressed CdiA-CT^{S611} bypasses the requirement for MtlA.

Compared to inhibition levels of the other CdiA-CT fusions explored in this section, CdiA-CT^{S611} exhibited at least 10-fold less inhibition during co-culture with susceptible target cells. It was therefore hypothesized that low expression of MtlA in co-culture conditions could be responsible for lower inhibition levels when compared to fusions targeting constitutively expressed inner membrane proteins. Transcriptional de-repression of *mtlA* in the presence D-mannitol, which binds the repressor MtlR, has been found to increase expression 20-fold[113]. However, co-culture inhibition of CDI-sensitive cells was not significantly different in the presence of D-mannitol (Figure 4D). This may indicate that even low levels of inner membrane proteins are sufficient to translocate overexpressed CdiA-CTs into the cytoplasm, suggesting that translocation across the cytoplasmic membrane is not a rate-limiting step of CDI.

Enrichment of transposon mutants against CdiA-CT^{DBS100} from *C. rodentium* DBS100 resulted in three sequenced insertions in a protein of unknown function, YajC. CDI^{DBS100}-resistant cells were also resistant to delivery of another CdiA-CT from *Yersinia kristensenii* ATCC 33638, which bears highly similar entry domain and a distinct effector domain[94], confirming that the requirement for YajC is directly related to the cytoplasm entry domain. The inner membrane protein is encoded in the *yajC-secDF* operon and has been reported to form part of the general secretory pathway SecYEG-SecDF-YajC-YidC holo-translocon[114]. Thus, it's possible that other components of the holotranslocon may contribute to the periplasmic binding epitope of CdiA-CT^{DBS100}. Transposon insertions into these other genes are not expected to be viable as they are all essential, potentially explaining why only *yajC* insertions were recovered. It's also possible that transposon insertion into *yajC* could exhibit a polar effect on *secDF* downstream in the operon. However, complementation of the transduced mutants with plasmid-borne *yajC* was sufficient to restore CDI^{DBS100} sensitivity. Additionally,

in-frame Keio insertions exhibited a similar CDI-resistant phenotype that could be restored by complementation with *yajC* (Figure 5C). Therefore, it is clear that YajC is necessary for recognition and unlikely that SecD or SecF contribute to the binding epitope of CdiA-CT^{DBS100}, as polar effects generated by *mariner* transposons require only YajC provided in *trans* to restore sensitivity (Figure 5D). However, contacts between YajC and the SecYEG complex have been postulated, suggesting that these proteins may contribute to a binding epitope. This is furthered by the size of YajC, which contains only one transmembrane helix and a significant periplasmic region. Most of this periplasmic region is potentially buried during assembly with the rest of the holo-translocon, resulting in a mixture of periplasmic regions from YajC and the surrounding proteins. Selection of UV mutants against CdiA-CT^{DBS100} and sequencing of *yajC* from resistant mutants yielded multiple strains with nonsense mutations in the locus which conferred resistance, as well as a single point mutation, V72G. This mutation was confirmed to be responsible for CDI-resistance, as complementation with plasmid-borne *yajC* fully restored CDI sensitivity (Figure 5D). Based upon a crystal structure of YajC in complex with AcrB[115] and AlphaFold2-predicted monomer structure, V72 resides in the hydrophobic core of the periplasmic domain. It's unlikely that this mutation would prevent expression or presentation of YajC on the cytoplasmic membrane, but disruption of hydrophobic packing could drastically change the fold of this domain, rendering it unrecognizable by CdiA-CT^{DBS100}. While this may not reveal an obvious point of contact between the two domains, it does confirm that the periplasmic region of the inner membrane protein is specifically recognized during CDI delivery.

CdiA-CT from *E. cloacae* UCI49 Recognizes FtsH

Enrichment of transposon mutagenized target cells against CdiA-CT^{UCI49} yielded no significant resistance after three rounds of selection (Figure 6A). This is expected to be the case if all associated factors are essential and do not tolerate transposon insertions. A position-specific iterative BLAST of the cytoplasmic entry domain revealed distant homology to a previously characterized entry domain from CdiA^{ECL}, which is known to target FtsH for translocation[18]. Alignment of CdiA-CT^{UCI49} with CdiA-CT^{ECL} as well as FtsH-targeting CdiA-CT^{EC536} reveals little homology at the level of primary sequence (Figure 6B). However, co-culture of chimeric CdiA-CT^{UCI49} with target cells lacking FtsH demonstrates a clear dependence upon the inner membrane (Figure 6C). The CDI-resistant phenotype can be reversed by complementation with plasmid-borne *ftsH,* confirming its involvement with this CDI system. In addition to the lack of similarity in primary sequence, comparison of the entry domains AlphaFold2 model of CdiA-CT^{UCI49} and a crystal structure of CdiA-CT^{EC536} [88] shows little structural similarity. This could indicate that this novel entry domain recognizes distinct periplasmic epitopes from the previously identified FtsH-targeting domains.

Discussion

Transposon mutagenesis has continually proved to be an effective strategy for the identification of permissive factors involved in CDI[15,18]. Here, pools of transposon-mutagenized *E. coli* were selected for resistance to various *cdiA-CT*s fused to the previously characterized *cdiA^{EC93}* scaffold[10,14]. Novel CDI-associated inner membrane proteins including AroP, Mtla, AmpG, and YajC highlight the diversity of proteins co-opted by the cytoplasm entry domains of various CdiA-CTs. The functional dissimilarity between the identified

proteins reinforces evidence that translocation across the cytoplasm of target cells is not related to import functions of involved inner membrane protein[18]. Instead, these proteins likely act as periplasmic receptors, triggering a PMF-dependent delivery mechanism facilitated by the cytoplasm entry domain of CdiA-CT[82]. It's possible that this mechanism could involve direct interactions of the entry domain with the lipid bilayer, as a family of these domains has been identified to form molten-globule-like structures[116].

In addition to the novel inner membrane proteins identified here, some CdiA-CTs were identified to be associated with previously identified factors including GltJK and FtsH[18,96]. Given the lack of primary sequence and predicted structural homology between the entry domains characterized here and those characterized previously, it's possible that each entry domain recognizes distinct epitopes on the cell surface of the respective inner membrane protein. Further study of interactions with GltJK could yield new insights into the mechanism of entry or contact points between the entry domain and periplasmic epitopes. In a similar manner to the methodology described previously[96], pieces of GltJK from *E. coli* could be grafted onto unrecognizable GltJK from *B. multiovorans*. It's possible that regions determined to be necessary for translocation of *P. luminescens* TTO1 and *E. chrysanthemi* EC16 would be different, confirming the recognition of distinct epitopes. Identification of important single residues could also be easily done with UV mutagenesis now that the associated inner membrane protein has been identified. Perhaps single point mutations causing resistance to only one entry domain and not the other could be used to map distinct recognition epitopes.

Although many CDI-associated inner membrane proteins have been identified here, many recognized *cdiA-CTs* harbor genetically distinct entry domains from those previously identified[18,116] (unpublished data). To reveal the true diversity of periplasmic epitopes targeted

by CdiA-CTs, further mutagenesis should be performed. These screens are also able to identify other CDI-associated factors, such as extracellular recognition epitopes or co-factors required for toxicity[8,12,81,88]. A systematic search for more of these factors has the potential to provide important insights into the cellular processes co-opted for import of toxic effectors, as well as the mechanisms of import and toxicity.

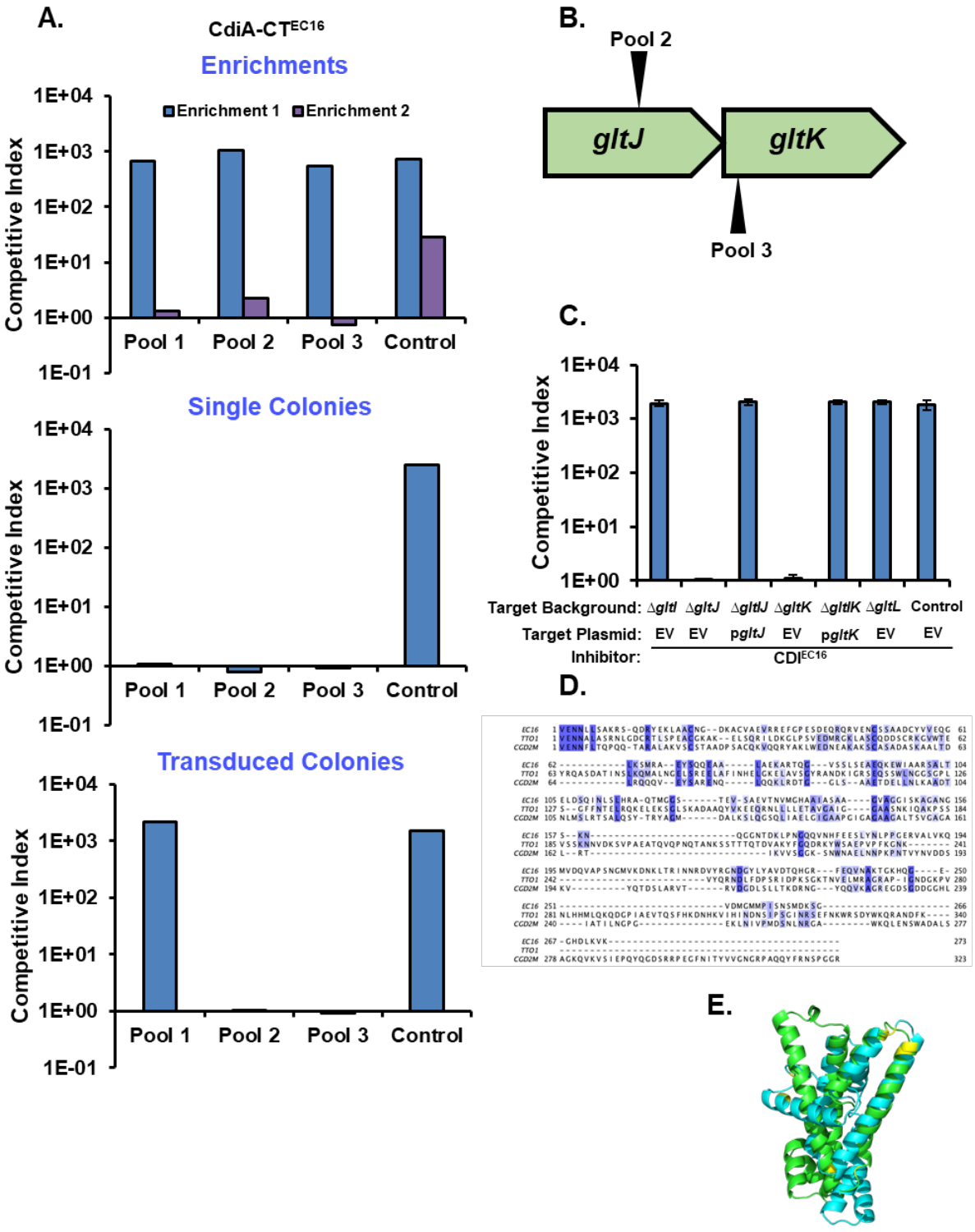
A.
CdiA-CT^EC16
Enrichments
Enrichment 1
Enrichment 2
Competitive Index
1E+04
1E+03
1E+02
1E+01
1E+00
1E-01
Pool 1
Pool 2
Pool 3
Control
Single Colonies
Transduced Colonies
B.
Pool 2
gltJ
gltK
Pool 3
C.
Target Background: ΔgltI ΔgltJ ΔgltJ ΔgltK ΔgltK ΔgltL Control
Target Plasmid: EV EV pgltJ EV pgltK EV EV
Inhibitor: CDI^EC16
D.
E.

Figure 1. Selection for CdiA-CT^{EC16}-Resistant Mutants Reveals a Requirement for GltJK

A. Selection of transposon mutagenized CDI-sensitive CH7367 pools against CdiA-CT^{EC16}. Single colonies from resistant pools were competed (middle graph) to confirm their resistance. CH7367 cells transduced with transposon-associated kanamycin resistance markers from respective CDI^{R} single colonies were competed (bottom graph). In each case CH7286 cells were used as a CDI-sensitive control.

B. Location and orientation of transposon insertions in *gltJK* for resistant, transduced colonies. Upper and lower markers denote insertions in the "forward" and "reverse" orientations of the ORF respectively.

C. Competitive indices of CDI^{EC16} chimeric inhibitors co-cultured for 3 hours with indicated target cells.

D. Multiple sequence alignment of CdiA-CTs from *E. chrysanthemi* EC16, *P. luminescens* TTO1, and *B. multivorans* CGD2M, beginning at the conserved VENN motif.

E. Structural alignment of AlphaFold2 models of CdiA-CT entry domains from *E. chrysanthemi* EC16 (green) and *P. luminescens* TTO1 (blue).

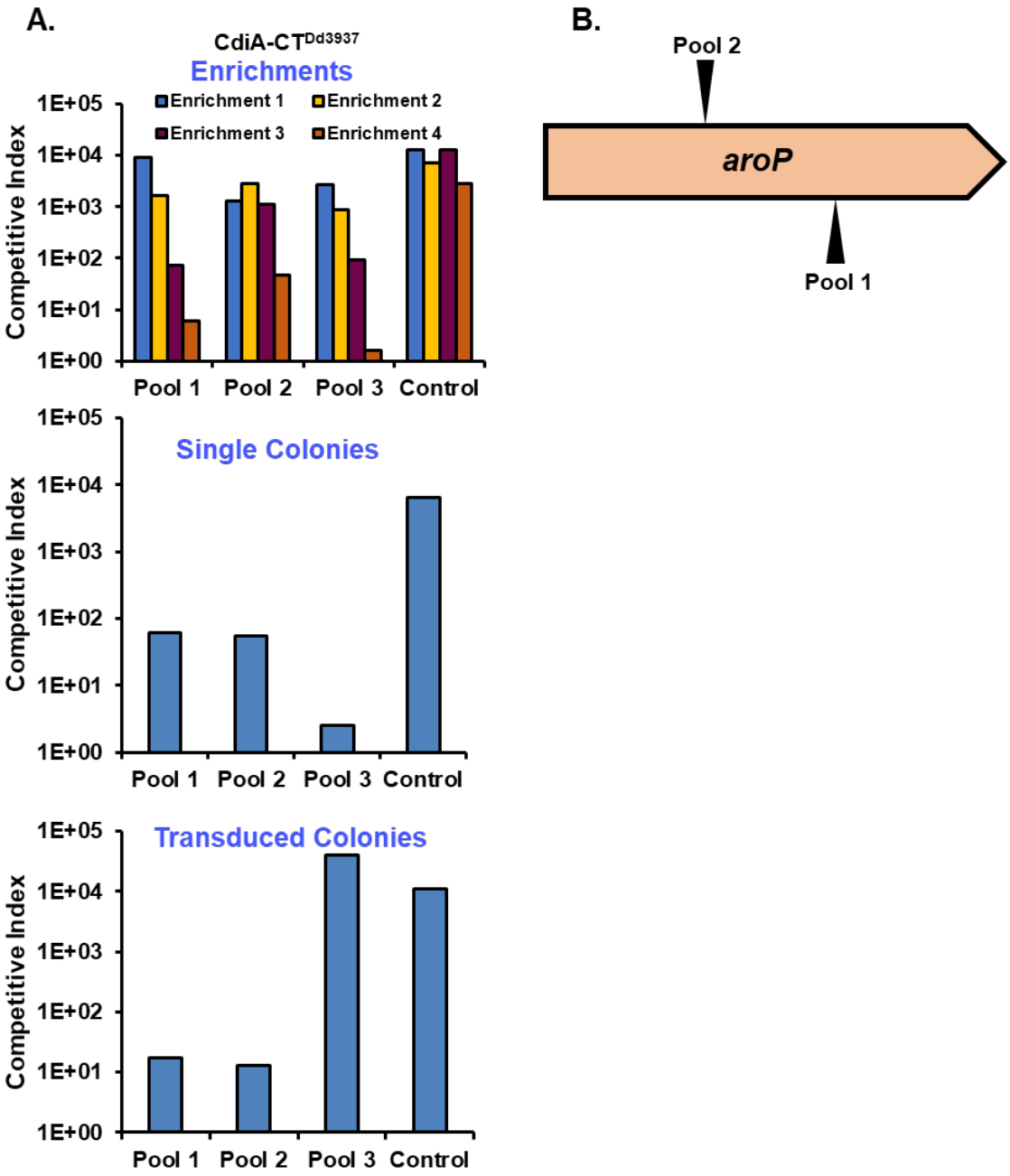

Figure 2. Selection for CdiA-CT^{Dd3937}-Resistant Mutants Suggests Involvement of AroP.

A. Selection of transposon mutagenized CDI-sensitive CH7367 pools against CdiA-CT^{Dd3937}. Single colonies from resistant pools were competed (middle graph) to confirm their resistance. CH7367 cells transduced with transposon-associated kanamycin resistance markers from respective CDI^{R} single colonies were competed (bottom graph). In each case CH7286 cells were used as a CDI-sensitive control.

B. Location and orientation of transposon insertions in *aroP* for resistant, transduced colonies. Upper and lower markers denote insertions in the "forward" and "reverse" orientations of the ORF respectively.

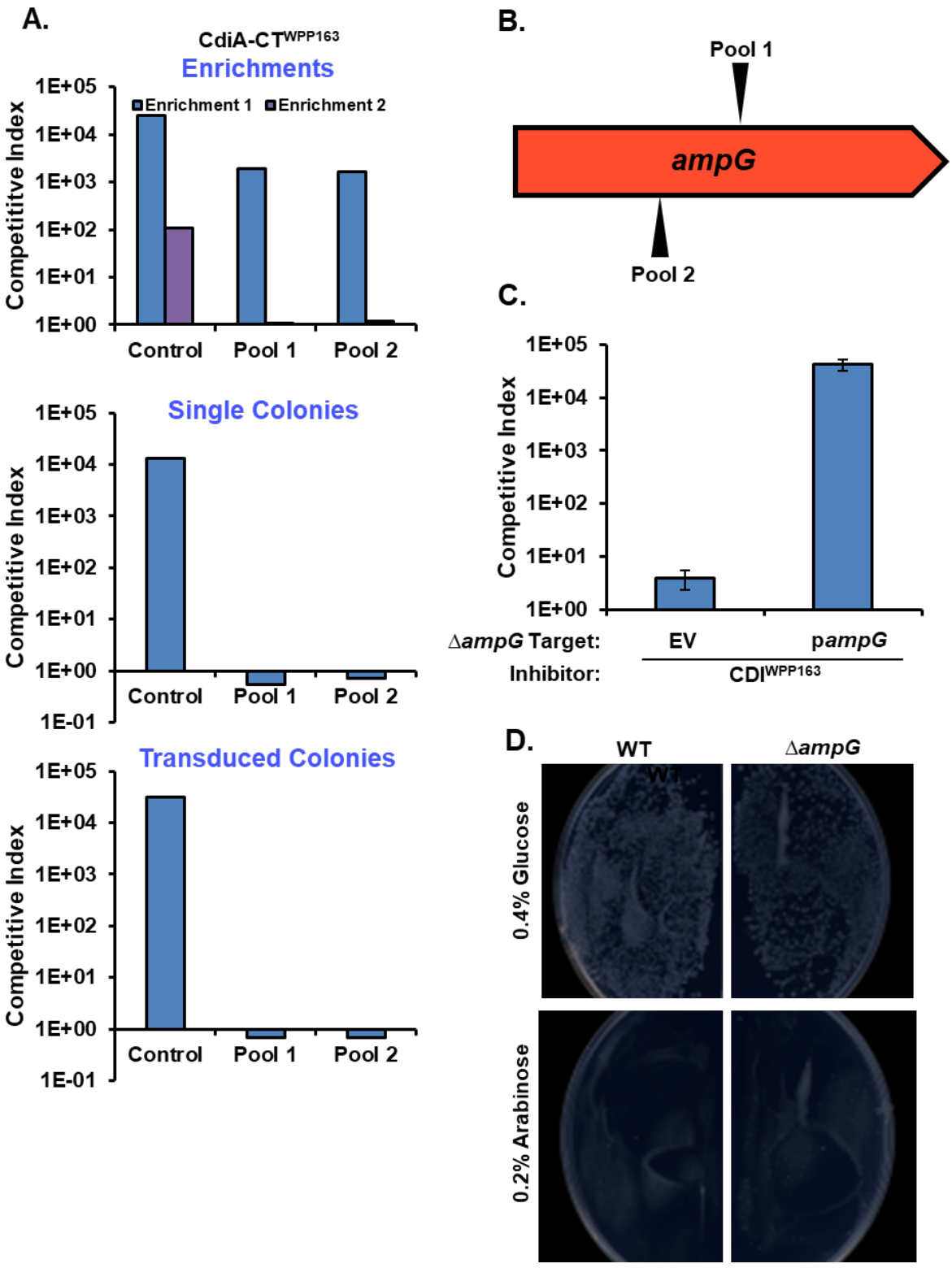
A.
CdiA-CT^WPP163
Enrichments
Enrichment 1
Enrichment 2
Competitive Index
1E+05
1E+04
1E+03
1E+02
1E+01
1E+00
Control
Pool 1
Pool 2
Single Colonies
1E-01
Transduced Colonies
B.
Pool 1
ampG
Pool 2
C.
ΔampG Target:
EV
pampG
Inhibitor:
CDI^WPP163
D.
WT
ΔampG
0.4% Glucose
0.2% Arabinose

Figure 3. Selection for CdiA-CT^{WPP163}-Resistant Mutants Reveals a Requirement for AmpG.

A. Selection of transposon mutagenized CDI-sensitive CH7367 pools against CdiA-CT^{WPP163}. Single colonies from resistant pools were competed (middle graph) to confirm their resistance. CH7367 cells transduced with transposon-associated kanamycin resistance markers from respective CDI^{R} single colonies were competed (bottom graph). In each case CH7286 cells were used as a CDI-sensitive control.

B. Location and orientation of transposon insertions in *ampG* for resistant, transduced colonies. Upper and lower markers denote insertions in the "forward" and "reverse" orientations of the ORF respectively.

C. Competitive indices of CDI^{WPP163} chimeric inhibitors co-cultured for 3 hours with indicated target cells.

D. Transformation of a *cdiA-CT^{WPP163}-cdiI^{WPP163}-DAS* construct into wild-type CH7286 cells (WT) or Δ*ampG* cells, followed by plating of transformants on LB-agar containing 20μg/mL tetracycline and either 0.4% glucose or 0.2% arabinose.

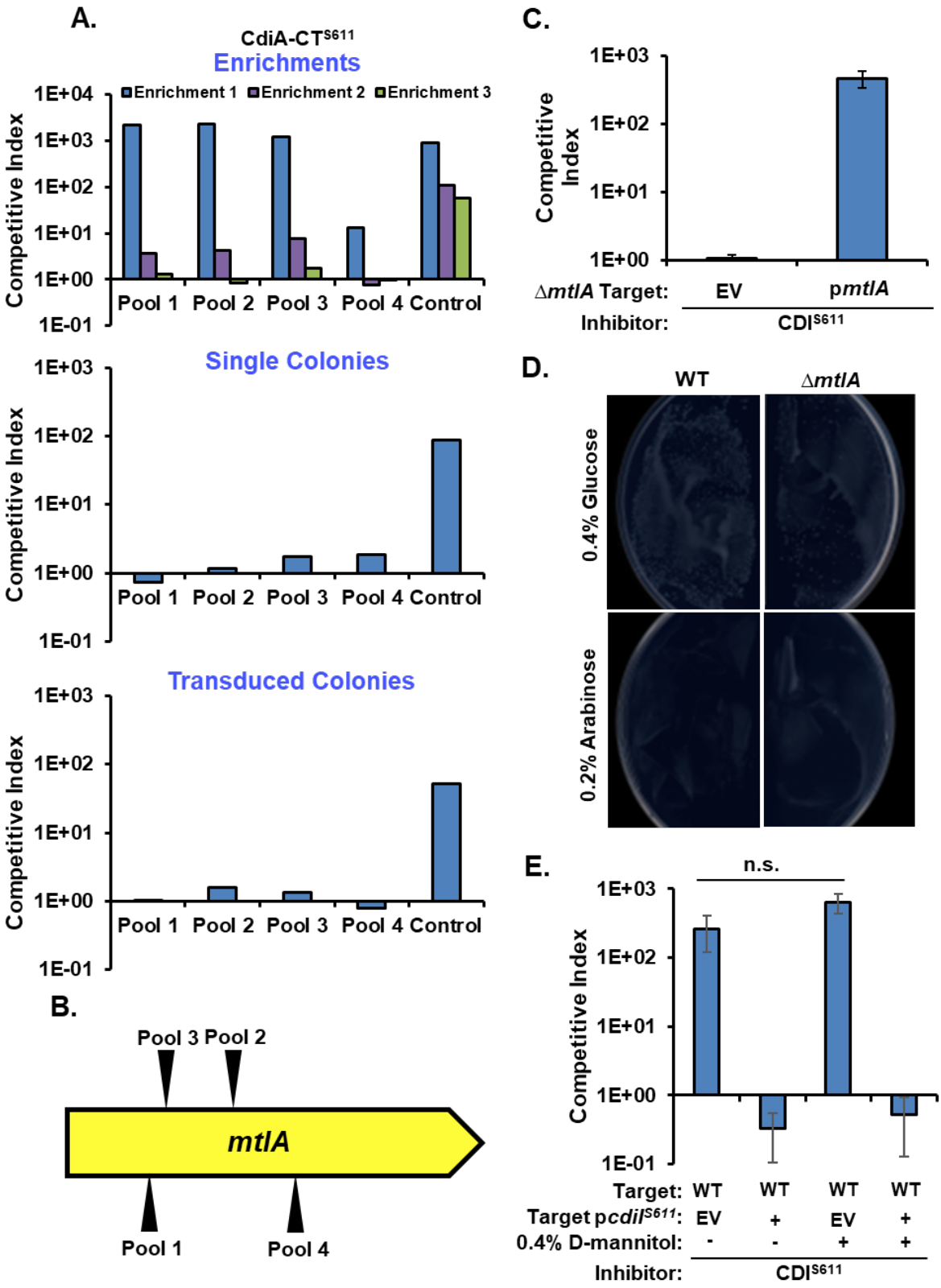
A.
CdiA-CT^{S611}
Enrichments
Enrichment 1
Enrichment 2
Enrichment 3
Competitive Index
1E+04
1E+03
1E+02
1E+01
1E+00
1E-01
Pool 1
Pool 2
Pool 3
Pool 4
Control
Single Colonies
Transduced Colonies
B.
Pool 3
Pool 2
mtlA
Pool 1
Pool 4
C.
ΔmtlA Target:
EV
pmtlA
Inhibitor:
CDI^{S611}
D.
WT
ΔmtlA
0.4% Glucose
0.2% Arabinose
E.
n.s.
Target:
Target pcdiI^{S611}:
0.4% D-mannitol:
Inhibitor:
CDI^{S611}

Figure 4. Selection for CdiA-CT^{S611}-Resistant Mutants Reveals a Requirement for MtlA.

A. Selection of transposon mutagenized CDI-sensitive CH7367 pools against CdiA-CT^{S611}. Single colonies from resistant pools were competed (middle graph) to confirm their resistance. CH7367 cells transduced with transposon-associated kanamycin resistance markers from respective CDI^{R} single colonies were competed (bottom graph). In each case CH7286 cells were used as a CDI-sensitive control.

B. Location and orientation of transposon insertions in *mtlA* for resistant, transduced colonies. Upper and lower markers denote insertions in the "forward" and "reverse" orientations of the ORF respectively.

C. Competitive indices of CDI^{S611} chimeric inhibitors co-cultured for 3 hours with indicated target cells.

D. Transformation of a *cdiA-CT^{S611}-cdiI^{S611}-DAS* construct into wild-type CH7286 cells (WT) or Δ*mtlA* cells, followed by plating of transformants on LB-agar containing 20μg/mL tetracycline and either 0.4% glucose or 0.2% arabinose.

E. Competitive indices of CDI^{S611} chimeric inhibitors co-cultured for 3 hours with indicated target cells in either the presence or absence of 0.4% D-mannitol. Targets bore plasmids either as empty vector controls (EV) or with the cognate *cdiI^{S611}* immunity gene.

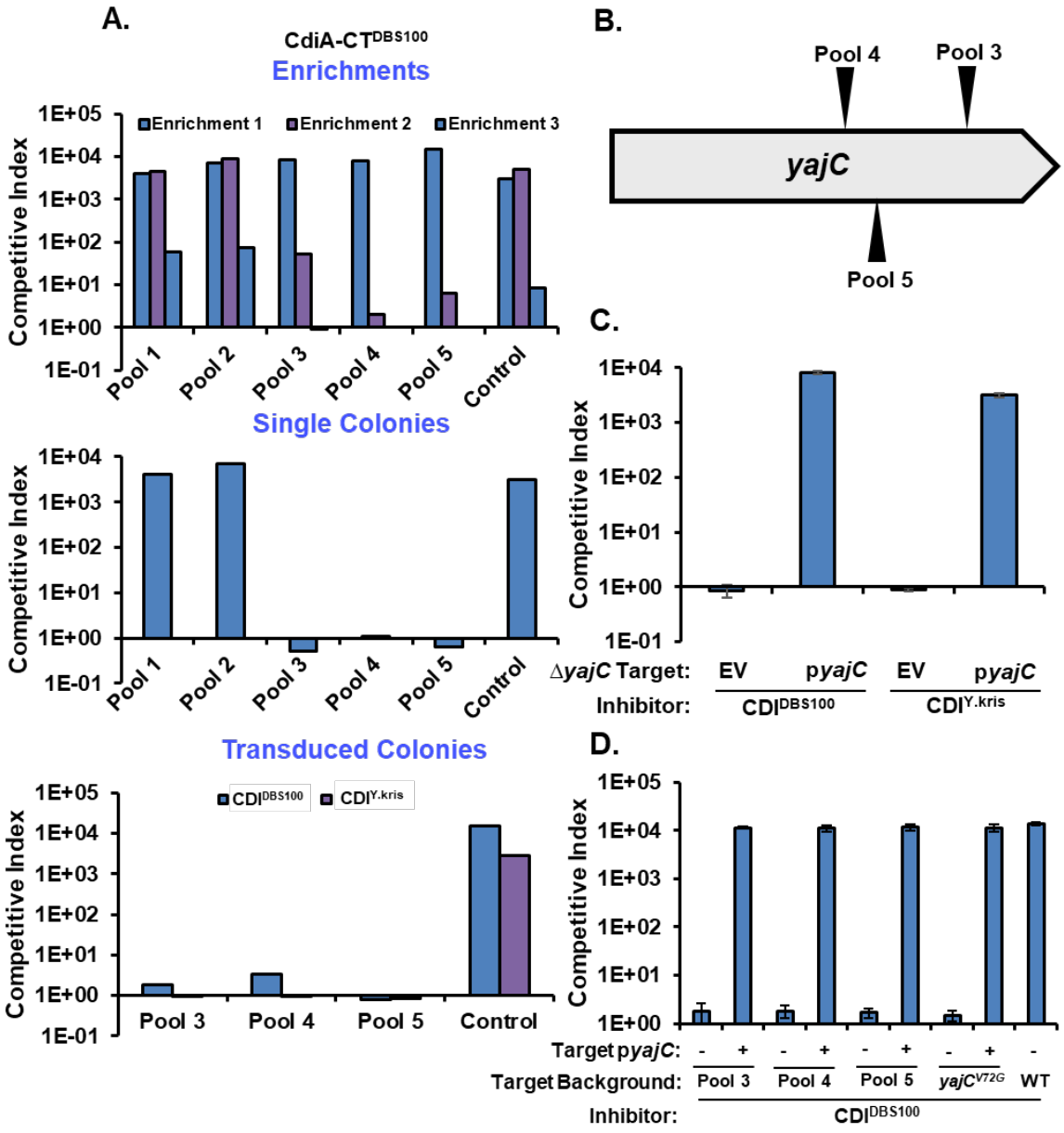

Figure 5. Selection for CdiA-CT^{DBS100}-Resistant Mutants Reveals Involvement of YajC.

A. Selection of transposon mutagenized CDI-sensitive CH7367 pools against CdiA-CT^{DBS100}. Single colonies from resistant pools were competed (middle graph) to confirm their resistance. CH7367 cells transduced with transposon-associated kanamycin resistance markers from respective CDI^{R} single colonies were competed against either CDI^{DBS100} or CDI$^{Y.kris}$ chimeric inhibitors (bottom graph). In each case CH7286 cells were used as a CDI-sensitive control for both inhibitors.

B. Location and orientation of transposon insertions in *yajC* for resistant, transduced colonies. Upper and lower markers denote insertions in the "forward" and "reverse" orientations of the ORF respectively.

C-D. Competitive indices of CDI^{DBS100} chimeric inhibitors co-cultured for 3 hours with indicated target cells. In Figure 5D, the "Pools" refer to isogenic linked transposon mutants from the bottom panel of Figure 5A.

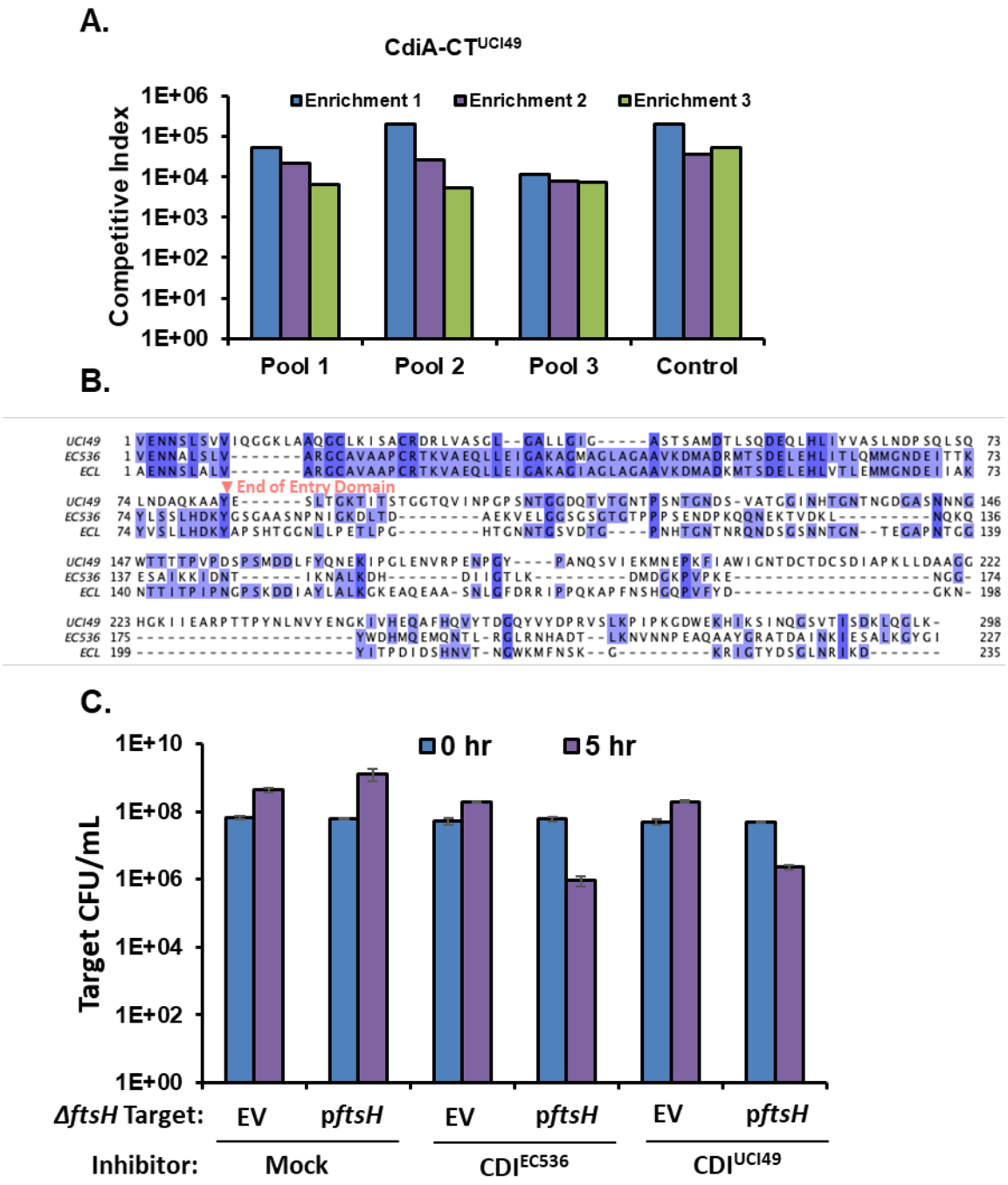

Figure 6. CDI^{UCI49} Requires FtsH for Delivery into Target Cells.

A. Three rounds of enrichment of transposon mutagenized CDI-sensitive CH7367 pools against CdiA-CT^{UCI49}. CH7286 cells were used as a CDI-sensitive control.

B. Multiple sequence alignment of CdiA-CTs from *E. cloacae* UCI49, *E. coli* EC536, and *E. cloacae* ATCC 13047

C. Target CFU/mL of mock and chimeric CDI^{UCI49} and CDI^{EC536} inhibitors co-cultured for 5 hours with indicated target cells.

Materials and Methods

Table 1. Bacterial Strains

Strains	Genotype	Source
X90	F′ *lacIq lac′ pro′/ara Δ(lac-pro) nal1 argE(Am) rif*^{R} *thi-1.*	-
MC4100	*F- [araD139]B/r Δ(argF-lac)169* &lambda- e14- flhD5301 Δ(fruK-yeiR)725 (fruA25)‡ relA1 rpsL150(strR) rbsR22 Δ(fimB-fimE)632(::IS1) deoC1* Rif^{R}	18
CH120010	MC4100 *ΔgltL::kan* Rif^{R} Kan^{R}	18
CH12007	MC4100 *ΔgltI::kan* Rif^{R} Kan^{R}	18
CH12008	MC4100 *ΔgltJ::kan* Rif^{R} Kan^{R}	18
CH12009	MC4100 *ΔgltK::kan* Rif^{R} Kan^{R}	18
CH2552	EPI100 *pir+* Tp^{R}	18
MFDpir	MG1655 *RP4-2-Tc::[ΔMu1::aac(3)IV-ΔaphA-Δnic35-ΔMu2::zeo] ΔdapA::(erm-pir) ΔrecA* Apr^{R} Zeo^{R} Erm^{R}	167
MG1655	K-12 *F– λ– ilvG– rfb-50 rph-1*	-
CH43	MG1655Δ*ftsH* Δ*lpxC::kan* Kan^{R}	168
CH7157	X90 *DclpX DclpA::kan* Kan^{R}	169
CH3778	MG1655 *Δwzb ΔarfB bamA(Δ2014-2043)*	This Study
CH7367	MG1655 *Δwzb*	17
CH7286	MG1655 *Δwzb::kan* Kan^{R}	17
CH8420	MG1655 *Δwzb ΔampG::kan* Kan^{R}	This Study
CH8508	MG1655 *Δwzb ΔyajC::kan* Kan^{R}	This Study
CH8827	MG1655 *Δwzb ΔmtlA::kan* Kan^{R}	This Study

Abbreviations: AmpR , ampicillin-resistant; CmR , chloramphenicol-resistant; KanR , kanamycin-resistance; RifR , rifampicin-resistant; TetR , tetracycline-resistant; TpR , trimethoprim-resistant

Table 2. Plasmids

Plasmid	Description	Source
pCH12025	pTrc99aKX::*gltJ*, IPTG-inducible expression of *gltJ,* Amp^R	18
pCH12132	pTrc99aKX::*gltK,* IPTG-inducible expression of *gltK,* Amp^R	18
pCH13171	Constitutive expression of chimeric $cdiA^{EC93}$-CT^{EC536} and $cdiI^{EC536}$, Cm^R	18
pCH14361	Constitutive expression of chimeric $cdiA^{EC93}$-$CT^{Y.kris}$ and $cdiI^{Y.kris}$, Cm^R	94
pCH2005	Constitutive expression of chimeric $cdiA^{EC93}$-CT^{UCI49} and $cdiI^{UCI49}$, Amp^R	This Study
pCH2006	Constitutive expression of chimeric $cdiA^{EC93}$-CT^{WPP163} and $cdiI^{WPP163}$, Amp^R	This Study
pTrc99a	IPTG-Inducible Expression Plasmid, Amp^R	GE Healthcare
pCH475	pTrc99a::*ftsH,* IPTG-inducible expression of *ftsH,* Amp^R	18
pSC189Δ	Mobilizable plasmid with R6Kγ replication origin. Carries the *mariner* transposon containing kanamycin-resistance cassette, Amp^R Kan^R	171
pCH450	pACYC184 Derivative with *E. coli araBAD* promoter, Tet^R	82
pCH8422	pCH450::*cdiA-CT-cdiI-DAS* (*P. parmienteri* WPP163_0433), Arabinose Inducible Degradation Construct, Tet^R	This Study
pCH8510	pTrc99a::*yajC*, IPTG-inducible expression of *yajC,* Amp^R	This Study
pCH8539	Constitutive expression of chimeric $cdiA^{EC93}$-CT^{S611} and $cdiI^{S611}$, Amp^R	This Study
pCH8826	Constitutive expression of chimeric $cdiA^{EC93}$-CT^{DBS100} and $cdiI^{DBS100}$, Amp^R	This Study
pCH8828	pCH405Δ::*mtlA*, constitutive expression of *mtlA*, Tet^R	This Study
pCH8849	pCH450::*cdiA-CT-cdiI-DAS* (*E. cloacae* S611), Arabinose Inducible Degradation Construct, Tet^R	This Study
pCH8865	Constitutive expression of chimeric $cdiA^{EC93}$-CT^{EC16} and $cdiI^{EC16}$, Amp^R	This Study
pCH8867	Constitutive expression of chimeric $cdiA^{EC93}$-CT^{Dd3937} and $cdiI^{Dd3937}$, Cm^R	This Study
CH8846	pTrc99a::*yajC* (V72G), IPTG-inducible expression of *yajC* (V72G), Amp^R	This Study

Abbreviations: AmpR , ampicillin-resistant; CmR , chloramphenicol-resistant; KanR , kanamycin-resistance; RifR , rifampicin-resistant; TetR , tetracycline-resistant; TpR , trimethoprim-resistant

Table 3. Oligonucleotides

Oligo Number	Name	Sequence	Description	Source
CH5838	UCI49-cdiI-Xho-rev	5'- TTT CTC GAG TTA TGC ATC ATA TCC AGC ATT TTT G -3'	Reverse primer for cloning UCI49 CdiA-CT into the CdiA(EC93) inhibitor chimera	This Study
CH5782	mtlA-Xho-rev	5'- TTT CTC GAG TTA CTT ACG ACC TGC CAG C -3'	reverse primer to amplify MG1655 mtlA for cloning into pCH400-series plasmids	This Study
CH5781	mtlA-Eco-for	5'- TTT GAA TTC ATG TCA TCC GAT ATT AAG ATC AAA GTG -3'	forward primer to amplify MG1655 mtlA for cloning into pCH400-series plasmids	This Study
CH5759	S611-cdiI-Spe-rev	5'- TTT ACT AGT TTC TTT TGC ATT ATA AGG CTT AAT TGC -3'	Reverse primer for generation of the CdiA-CT-CdiI-DAS S611 construct with pCH450	This Study
CH5758	S611-CT-Nco-for	5'- TTT CCA TGG GTT ATT TAT ATG CAG ATG AAG ATA AAG CG -3'	Forward primer for cloning S611 CdiA-CT into the CdiA(EC93) inhibitor chimera and generation of the CdiA-CT-CdiI-DAS S611 construct with pCH450	This Study
CH5709	ampG-Xho-rev	5'- TTT CTC GAG TTA CGT CAG ATG CGT TTT TCG -3'	reverse primer to amplify MG1655 ampG for cloning into pCH400-series plasmids	This Study
CH5708	ampG-EcoR1-for	5'- TTT GAA TTC ATG TCC AGT CAA TAT TTA CG -3'	forward primer to amplify MG1655 ampG for cloning into pCH400-series plasmids	This Study
CH5707	S611-cdiI-Xho-rev	5'- TTT CTC GAG TTA TTC TTT TGC ATT ATA AGG CTT AAT TGC -3'	Reverse primer for cloning S611 CdiA-CT into the CdiA(EC93) inhibitor chimera	This Study
CH5687	WPP163-cdiI-Spe-rev	5'- TTT ACT AGT TCC TTT ATT GAT ATA AAT AGC ATC GC -3'	reverse primer to amplify cdiI of WPP163_0433 for DAS construct and purification	This Study
CH5686	WPP163-CT-Nco-for	5'- TTT CCA TGG TGG AGA ATA ACT ATC TGT CCA G - 3'	forward primer to amplify cdiA-CT of WPP163_0433 for DAS construct and purification	This Study
CH4738	UCI49-cdiI-Spe-rev	5'- TTT ACT AGT TGC ATC ATA TCC AGC ATT T -3'	Reverse primer for generation of the CdiA-CT-CdiI-DAS UCI49 construct with pCH450	This Study
CH4734	MGH20/UCI49C-Kpn/Nco-for	5'- TTT GGT ACC ATG GTT GAG AAT AAC TCG CTG AG -3'	Forward primer for cloning S611 UCI49-CT into the CdiA(EC93) inhibitor chimera and generation of the CdiA-CT-CdiI-DAS UCI49 construct with pCH450	This Study
CH2260	mariner-rev-seq	5' - CAA GCT TGT CAT CGT CAT CC - 3'	reverse sequencign oligo for rescue cloned plasmids	18
CH2255	mariner-for-1	5' - GAG CGG GAC TCT GGG GTA CG - 3'	forward sequencing oligo for rescue cloned plasmids	This Study

Generation of Mariner-Transposon Pools:

Overnight cultures of transposon donors (CH5951) and recipients (CH7367) were diluted into fresh cultures and grown at 37°C in shaking LB broth until OD_{600} of 0.6. Donors

were grown in the presence of 600 μM DAP. Donors and targets were mixed at a 2:1 ratio and 75 μL of this mixture was spotted onto an LB-agar plate. Each independent transposon-mutagenized pool comes from an independent mixture and plate spot. Spotted mixtures were incubated 37˚C for 4 hours, then transferred to 500 μL M9. Resuspended cell mixtures were diluted 10 fold and 100 fold, and each dilution (including the undiluted mixture) was spread on separate LB-agar plates containing 50 μg/mL kanamycin. The next day, cells from each dilution in a given pool were resuspended in M9 stocked in 50% glycerol to form the transposon-mutagenized pools for future selections.

Enrichment of Mariner-Transposon Pools:

Overnight cultures of transposon mutagenized pools were grown in 50 μg/mL kanamycin, along with the respective inhibitor (grown in 150 μg/mL ampicillin). Overnight cultures were diluted to OD_{600} = 0.1 and grown for 1.5 hours. The optical density of each fresh culture was then measured and target cells and inhibitors were mixed by resuspending each to OD_{600} = 0.1 in 10 mL of LB. Co-cultures were incubated in baffled 125 mL flasks at 37˚C for 3 hours with shaking. Prior to incubation, a time = 0 point was taken by diluting cells 10-fold into M9, followed by further 10-fold serial dilution for spot plating. Aliquots were again taken after 3 hours and serial diluted, followed by spotting 10 μL of dilution on LB-agar containing either kanamycin (50 μg/mL) or ampicillin (150 μg/mL) to measure target and inhibitor CFU/mL. Finally, 100 μL of the 10^{-1}, 10^{-2}, and 10^{-3} dilutions were spread on LB-agar with 50 μg/mL kanamycin and incubated overnight at 37˚C. The next day, spread plates were harvested with M9 and used to inoculate fresh cultures at an OD_{600} = 0.1 for further selections. Once pools were judged to likely be resistant to the given inhibitor, determined by CFU/mL counts,

single colonies were selected from pools and co-cultured with the corresponding inhibitors in the same manner as above. Single colony strains demonstrating resistance (a competitive index close to 1) were then selected for transduction of the transposon-associated kanamycin marker into a non-mutagenized *E. coli* K-12 background.

P1 Phage Transduction of Transposon Markers and Confirmation of Transposon-Linkage:

CDI-resistant isogenic isolates (donors), along with a CDI-sensitive MG1655 Δ*wzb* recipient strain (CH7367), were grown in overnight cultures along with the corresponding antibiotics. Overnight cultures of donor strains were diluted 1:100 into LB media containing 0.2% D-Glucose and 5 mM $CaCl_2$. Fresh cultures were grown until slightly turbid, followed by addition of chloroform-extracted P1 phage at 1:25 dilution. Cultures were monitored until visibly cleared and lysates were prepared by extraction of cleared culture with chloroform at a 1:5 ratio. Overnight recipient cultures resuspended in LB containing 100 mM $MgSO_4$ and 5 mM $CaCl_2$ were mixed at a 1:1 v/v ratio with prepared lysate at either no dilution or 10X dilution. Controls were generated containing either recipient cells and LB at a 1:1 ratio, or P1 phage and LB at a 1:1 ratio. Mixtures were incubated without shaking at 37°C for 30 minutes, followed by addition of an equal volume of 1M Na-Citrate and 5 volumes of LB, then allowed to recover with shaking at 37°C for 2 hours. Recovered cells were then pelleted and resuspended in a small volume of LB, then spread on LB-agar plates supplemented with kanamycin (50 μg/mL). The next day, single colonies were streaked onto fresh LB-agar-kanamycin plates and incubated overnight. Single colonies from these plates were competed against the respective inhibitors in the manner described in the section above to confirm

linkage of the transposon-associated kanamycin marker to CDI-resistance. Strains exhibiting resistance at this stage were selected for rescue cloning of the transposon marker.

Rescue cloning:

Transduced colonies shown to be CDI-resistant in competition co-culture with the selected inhibitor were selected for recovery of the genomic transposon marker. First, genomic DNA (gDNA) was purified from overnight cultures by phenol/chloroform extraction and ethanol precipitation. Then, 1 µg of gDNA was digested in 30 µL reaction containing 1 µL EcoRI restriction enzyme and 3 µL 10X NEB Cutsmart. Digests were incubated at 37˚C for 6 hours, followed by heat inactivation at 75˚ for 5 minutes. Reactions were cooled slowly and ATP was added to a final concentration of 1.5 mM, followed by addition of 2 µL of purified T4 ligase. Ligations were incubated at 16˚C overnight. The next day, 10 µL of ligation mixture was transformed into TSS-competent CH2552 cells with heat shock at 42˚C and recovery in LB at 37˚C for 3 hours. Cells were then pelleted, resuspended in a small volume of LB, and spread on LB-agar plates supplemented with 50 µg/mL of kanamycin. Colonies selected the next day from this plate were grown in LB-kanamycin, followed by harvesting of plasmids. An aliquot of plasmid was checked for presence of an EcoR1 site by digest with the enzyme followed by gel electrophoresis. Viable plasmids were then sent for sequencing, using primers binding to conserved sequences on either end of the transposon.

Competition Co-Cultures

Overnight cultures of targets were grown in 50 µg/mL kanamycin and inhibitors were grown in either grown in 150 µg/mL ampicillin (for pET-derivative inhibitors) or 60 µg/mL

chloramphenicol (for pDAL879-derivate inhibitors). Overnight cultures were diluted to OD_{600} = 0.1 in fresh LB without antibiotics and grown with shaking for 1.5 hours at 37˚C. The optical density of each fresh culture was then measured using a spectrophotometer and target cells and inhibitors were mixed by resuspending each to OD_{600} = 0.1 in 10 mL of LB. Co-cultures were incubated in baffled 125 mL flasks at 37˚C for 3 hours (unless otherwise stated) with shaking. Prior to incubation, a time = 0 point was taken by diluting cells 10-fold into M9, followed by further 10-fold serial dilution for spot plating. Aliquots were again taken at the final time point and serial diluted, followed by spotting 10 µL of dilution on LB-agar containing either kanamycin (50 µg/mL) or ampicillin (150 µg/mL) to measure target and inhibitor CFU/mL. Competitive indices were calculated as the ratio of inhibitors:target CFU/mL at the final time point divided by the ratio of inhibitors:target CFU/mL at the initial time point.

For the competitions performed in figure 6C, all incubation was performed at 30˚C rather than 37˚C to allow growth of cells lacking *ftsH*.

Multiple Sequence Alignments

Sequences selected for multiple sequence alignment were submitted together to Uniport Align, followed by formatting and coloring with Jalview[117].

Structural Alignment of Entry Domains

A structural alignment was generated for the entry domains of *E. chrysanthemi* EC16 and *P. luminescencs* TTO1. First, the respective CdiA-CT protein sequences were submitted separately to the AlphaFold2 server. Then, the resultant .pdb files were imported into PyMol and aligned relative to the disulfide bridge shown in yellow.

Internal Expression of Selected cdiA-CTs

Expression of *cdiA-CT*^{S611} and *cdiA-CT*^{WPP163} was performed by first generating a construct consisting of the respective cognate *cdiA-CT-cdiI* pair in a pCH450-DAS backbone plasmid (Tet^{R}). This plasmid introduces a pBAD arabinose inducible promoter, and an ssrA(DAS) tag at the 3' end of the immunity gene. Translation of this sequence generates a suboptimal degradation tag at the C-terminus of CdiI. These constructs, stored in CH8849 and CH8422 respectively, were transformed into either wild-type CH7286 cells or cells with the corresponding inner membrane protein knockout. After ice-cold incubation of cells and plasmid and heat shock at 42˚C, cells were recovered in LB and 0.8% glucose for 1 hour at 37˚C. After recovery, cells were pelleted, resuspended in a small volume of LB, then plated on LB-agar plates supplemented with 20 μg/mL tetracycline and either 0.4% glucose or 0.2% arabinose. Plates were incubated overnight at 37˚C, and the following day were imaged.

III. Characterization of a CDI Effector with Homology to Methyltransferases

Abstract

Contact dependent growth inhibition (CDI), is a phenomenon in which bacteria deploy type V secretion systems (T5SS) to inhibit the growth of neighboring bacteria[10]. CDI is carried out by two proteins CdiA, which forms a filament capable of binding to target cell receptors and delivering a toxic payload into their cytoplasm, and CdiB, which transports CdiA across the outer membrane of the CDI-producing cell[63]. While some toxic effectors delivered via this machinery have been characterized[19,93,94], the majority of effectors identified in nature remain mysterious. Structural predictions of a CDI effector from *Enterobacter cloacae* S611 indicate homology to *S*-adenosylmethionine (SAM)-binding domains and suggest that the effector could act as a SAMase. Here, a potential SAMase phenotype of intoxication with CDI^{S611} is investigated, revealing that the effector is unlikely to degrade SAM and instead may function as a SAM-dependent methyltransferase.

Introduction

Of the CDI effectors currently characterized, the vast majority target nucleic acids as DNases[11], tRNases[19,118], rRNases[93] or general RNases[94]. However, toxic effectors employed by other anti-bacterial secretion systems highlight the variety of mechanisms by which growth inhibition can occur. Type VI effectors have been identified which target membranes, peptidoglycan, cell division, essential proteins, and small molecules to compete with adjacent cells[119]. Gram-negative bacteriocins such as colicin M and pesticin also interfere with the formation and structural integrity of peptidoglycan[120]. Given that many CDI effectors are

currently uncharacterized, it seems likely that they could exhibit similar, if not broader, diversity. *In silico* structural modeling and crystallography of uncharacterized domains can often offer unique insights into protein functions via comparison to databases of known protein structures. In the previous chapter, I identified MtlA as an inner membrane protein co-opted by the cytoplasm entry domain of CdiA-CT from *Enterobacter cloacae* S611 (see Chapter 2 Figure 4). In this chapter, I investigate the effector domain of this CdiA-CT, which is predicted to have structural homology to S-adenosyl methionine binding domains.

Structural Modeling Predicts a SAM-Binding Rossman Fold

Recent advances in structural modeling of proteins, notably AlphaFold2[100,101], has yielded new insights into the potential functions of previously uncharacterized CdiA-CTs. Structural prediction of CdiA-CT^{S611} and subsequent interrogation of the PDB database reveals strong homology to class 1 methyltransferases, specifically to their *S*-adenosylmethionine (SAM) binding domains (Table 1, Figure 1A). In most methyltransferases, including the top matches to CdiA-CT^{S611}, these domains are used to coordinate SAM while an adjacent domain binds the substrate of methyltransfer. Transfer of the active methyl group is achieved simply by bringing the substrate in its proximity, after which the highly reactive group exchanges bonds to neutralize the sulfur cation[121]. The predicted SAM-binding fold strongly resembles a Rossman fold, found across proteins that coordinate nucleotide derivatives[122,123]. Additionally, CdiA-CT^{S611} and relatives contain a conserved XGXG motif common among SAM-binding domains[124] (Figure 1B). This motif follows an N-terminal beta-sheet in the structure, forming a beta-turn that cradles SAM in the binding pocket[123].

Despite homology to SAM-binding domains, CdiA-CT^{S611} notably lacks an obvious substrate binding domain, as CdiA-CTs typically contain only a cytoplasm entry domain and effector domain. This could indicate that CdiA-CT^{S611} does not participate in methyltransfer, but instead degrades SAM to starve the cells of the essential cofactor. This is analogous to a recently discovered Type 6 effector, Tse6, which contains an NAD^+ binding domain but lacks a substrate binding domain for expected ADP-ribosylation reactions[125]. Tse6 has been found to instead degrade NAD^+ and $NADP^+$ to inhibit the growth of targeted cells[125,126]. Similarly, phage enzymes have been identified which function as SAM lyases and hydrolases to block restriction modification systems during infection[127,128]. Other SAM-processing enzymes have been identified including a variety of SAM-halogenases, although they perform normal cell functions rather than contributing to toxicity[129]. One issue with toxic mechanisms targeting the degradation of SAM is that the co-factor and its natural degradation products are constantly cycled and synthesized in the cell under native conditions[130]. As a result, targeted cells could potentially counteract the depletion of SAM by upregulating biosynthesis to restore growth. If CdiA-CT^{S611} acts a SAMase, perhaps this could explain the relatively low inhibition levels of the *cdiA*^{EC93}*-cdiA-CT*^{S611} fusion construct explored in the previous chapter.

Investigation of CdiA-CT^{S611} SAMase Activity

It has previously been reported that expression of T3 SAM hydrolase in *E. coli* causes inhibition of growth and slight cell elongation[131]. This is likely directly related to depletion of the SAM pool, as temperature sensitive mutations in SAM synthetase (MetK) cause the formation of filamentous cells at nonpermissive temperatures[132]. To explore gross morphological changes associated with CDI^{S611}, inhibitor and target cells expressing

fluorescent markers were co-cultured (Figure 1C). When mixed with mock CDI$^-$ inhibitor cells, both targets and inhibitors exhibit similar sizes as well as uniform fluorescence by DAPI staining. When mixed with inhibitor cells expressing CDI^{S611}, target cells become slightly elongated relative to the inhibitors, with some filaments forming. Many target cells also stain more brightly with DAPI, indicating increased cell permeability which could be associated with loss of cell viability. This phenotype was further explored via internal expression of a construct containing *cdiA-CT^{S611}-cdiI^{S611}* under an arabinose-inducible promoter, with a modified SsrA degradation tag encoded at the C-terminus of *cdiI*[109]. This construct was either suppressed in cells by addition of D-glucose or induced with L-arabinose for expression of CdiA-CT^{S611} and ClpXP-mediated degradation of the cognate immunity protein. Cells expressing CdiA-CT^{S611} exhibited significant inhibition of growth compared to those undergoing catabolite repression (Figure 1D). At 2 hours post-induction, the morphology of cells expressing the effector was slightly elongated, with some filaments forming.

While the elongation phenotype may align with observed morphology changes caused by SAM-depletion, this phenotype is associated with a broad range of cellular defects including the activities of disparate CDI effectors[11,18]. To more closely examine an effect on SAM levels *in vivo*, plasmid DNA from cells internally expressing CdiA-CT^{S611} was harvested and assessed for endogenous methylation. Under normal conditions, K-12 *E. coli* strains express Dam methylase, which methylates both adenine nucleotides in the double stranded 5'-GATC-3' motif[133]. If CdiA-CT^{S611} degrades SAM, newly synthesized DNA may lack Dam methylation. This has been observed during internal expression of phage-encoded SAM hydrolases. The methylation status of Dam sites can be probed using restriction endonucleases which also recognize this site. Endonuclease MboI cleaves the unmethylated GATC motif[134],

while DpnI cleaves the doubly methylated motif[135]. Plasmid pBluescript harvested from cells lacking Dam methylase was found to be susceptible to digest by MboI but protected from DpnI digestion (Figure 2A). 2 hours after arabinose induction of *cdiA-CT*^{S611} in cells expressing Dam methylase, harvested pBluescript was susceptible to DpnI but not MboI digestion, indicating unperturbed activity of Dam *in vivo*.

The ability of methyltransferases to protect DNA from digestion in the presence of CdiA-CT^{S611} was additionally probed *in vitro* using a restriction protection assay. SAM incubated with purified CdiA-CT^{S611} was added to a solution containing linearized pBluescript and BamHI methyltransferase (M.BamHI). The methylation status of the single BamHI cut site in pBluescript was then probed by digestion with BamHI endonuclease, which recognizes fully unmethylated GGATCC sites[136]. DNA methylation by M.BamHI in the absence of CdiA-CT^{S611} pretreatment showed only partial protection from digestion (Figure 2B). Interestingly, pretreatment of SAM with CdiA-CT^{S611} resulted in slightly less digestion rather than more, providing no evidence of significantly depleted SAM. An alternative approach to monitor a direct enzymatic interaction between CdiA-CT^{S611} and SAM used HPLC to resolve the nucleotide derivative from potential degradation products after co-incubation. This method takes advantage of the absorbance of the adenine group of SAM, which absorbs maximally at 260 nm. Common SAM byproducts that share the nucleobase and thus absorb at this wavelength include *S*-adenosyl-L-homocysteine (SAH) and 5'-methyl-thioadenosine (MTA). Isocratic elution of SAM and SAH in 1-heptanesulfonate buffer generated distinct peaks (Figure 2C). When SAM was incubated with purified CdiA-CT^{S611}, no change in elution time was observed. Additionally, the height of the peak corresponding to SAM remained relatively

invariant, indicating that no unobservable products were formed either. In combination, these *in vitro* and *in vivo* findings suggest that CdiA-CT^{S611} does not degrade SAM.

CdiA-CT^{S611} May Act as a Methyltransferase

Despite the lack of evidence of SAMase activity, the strong predicted homology of CdiA-CT^{S611} to SAM-binding domains indicates that some SAM-dependent activity may underly toxicity. The most likely remaining mechanisms would involve the methyltransfer. Common targets for this actiivty include DNA, RNA, proteins, and small molecules. Of these, small molecule and tRNA methyltransferases are the predominant matches to CdiA-CT^{S611} by structural homology (Table 1). Reassessment of the AlphaFold2 model based on these criteria identified a basic groove which intersects the predicted SAM binding site (Figure 3A). This groove could be used to bind nucleic acids, and its dimensions of around ~11 Å could accommodate single stranded RNA. As an initial probe, RNA was extracted from cells internally expressing *cdiA-CT^{S611}* under inducing or suppressing conditions (Figure 3B). No drastic change in total RNA is observed during induction of the effector, although there may be some change in abundance of 23S rRNA.

Discussion

The data provided here strongly suggest that *S*-adenosylmethionine is not a direct target of CdiA-CT^{S611}. It's possible that at physiological levels of effector delivery, degradation of SAM is not a viable mechanism for growth inhibition, as has been observed across the phage SAMases[137–140]. These enzymes, which are the best characterized SAMases, only decrease growth rates of host cells when overexpressed[140]. Additionally, the growth inhibitory

phenotype associated with overexpression of these proteins could simply come from the detraction of transcriptional and translational machinery from necessary host processes, rather than by a mechanism related to the enzyme and SAM levels themselves. In fact, expression of phage SAMases has been used to rescue Δ*ilvA* leucine auxotrophs by derepression of the *met* operon[139]. In combination with these observations, the experiments performed here monitoring plasmid DNA methylation patterns *in vitro* and *in vivo* fail to establish a connection between effector toxicity and SAM levels. This has raised the possibility that CdiA-CT^{S611} instead acts as a methyltransferase. Analysis of the predicted structure of the effector domain indicates that it could interact with single stranded nucleic acids. This effector could, for example, methylate specific conserved residues in rRNA or tRNA to block vital functions like aminoacylation. This type of toxicity has not previously been described, and if present would demonstrate a particularly remarkable mechanism for the perturbation of cellular function.

Many important experiments stand out which follow up on the data presented here. Primarily, it is critical to demonstrate a binding interaction between SAM and CdiA-CT^{S611}. While structural predictions appear to have high confidence in the homology of the effector domain, there is yet to be experimental evidence of an interaction. One approach to identify interactions between the protein and its potential substrate could use radiolabeled SAM or SAH, as has been described previously[141,142]. Alternatively, NMR could detect shifts in resonance in the presence of SAM or SAH, indicating binding interactions. With experimental evidence of binding, an interaction of CdiA-CT^{S611} with nucleic acids appears have the most potential for success. Incubation of purified CdiA-CT^{S611} with RNA followed by co-purification could identify bound RNAs, although determing the identity of the bound RNA

may be challenging. These discoveries could uncover a completely novel mechanism of toxicity among antibacterial effectors.

Rank	PDB ID	Z-score	rmsd	Description
1	6kji	11.3	3.0	Fungal Polyketide C-Methyltransferase
2	3kkz	11.3	3.1	Uncharacterized Protein QLES9 from *Bacteroides fragilis*
3	6uak	11.0	2.5	Peptide C-terminal Methyltransferase
4	2glu	11.0	2.8	YcgJ protein from *Bacillus subtilis*
5	5ufm	10.8	2.4	1,6-Didesmethyltoxoflavin N-Methyltransferase from *Burkholderia thailandensis*
6	3sm3	10.8	2.8	Q8PUK2_METMA Methyltransferase from *Methanosarcina mazei*
7	7nzi	10.8	2.6	TrmB M7G46 tRNA Methyltransferase from *Bacillus subtilis*
8	3e05	10.5	2.6	Precorrin-6y C5,15-Methyltransferase
9	7dmb	10.4	2.7	Polyketide Methyltransferase
10	2o57	10.4	3.0	Sarcosine Dimethylglycine Methyltransferase

Table 1. Predicted Structural Homologs of CdiA-CT^{S611}.
The AlphaFold2 model of the effector domain from CdiA-CT^{S611} was submitted to the Dali server for comparison to other structures in the PDB. The top 10 matches in the corresponding PDB-90 are shown above.

A.

B.

"XGXG" Motif

```
ECL_S611                1 PNTIYNQQLAKEAEKAGFLSAP-QACGTLNIGAGNRPISGAYNISSPDYPMANGVHAGDANDLSQIASGSQSKIVIENPYGF  81
Pantoea_agglomerans     1 PNSIYNQQLVKDAEKSGYYSSP-TQCGILNIGAGNKPIEGAYNISHPDYPKSAGVYSGDANNLSNVATGSQKTIIMENPYGF  81
Cronobacter_malonaticus 1 ----------------FYDKP-QECGILNIGAGNRPIEGAYNISHPDYPKGPGVYAGDANDLSNTATGSQTKIIMENPYGF  64
Snodgrassella_alvi      1 ----YATKIKEIAKGNKYLSKP-QQCGTLNIGAGNKPIEGAYNISHPDHPMANGVHAGDANKLSNIATGSQNKIIMENPYKY  77
Frischella_perrara      1 ----------------YLSEP-EQCGTLNIGAGLNPIEGAYNISHPDYPMAPGVHVGDAYDLSNIATRSQNKIIMDNPFGY  64
Gilliamella_apicola     1 --------------KKRYLKSA-EQDGTLVIGAGLNPIEGAYNISHPAHPMAPGVFAGDAHNLSNIATGSQKTIIMDNPYGY  67
Moraxella_catarrhalis   1 ----------------YLSKP-VYKGTLNIGAGLKPIPNAYNISHPNYPMAPNVYAGNADNLAGINSQSQSLIIMQNPYGF  64
Acetonema_longum        1 ----------------YLKEPATQNGTLNIGAGSRPTDGAYNIDI--DPKVSGVNSGNMTNFSKIKTGSQSKIIIDNPYDY  63
Pseudomonas_kribbensis  1 ----------------YLDKPANTDGSLNIGAGSNPIEGYYNIDI--DPKTPGVHAGNATDLSGIKSGSQSHINMDNPYGF  63

ECL_S611               82 QPFNSEVLRVLADDGAIIVKGTWD------NKNISKIEKVAERNGFFIVEKNII-DNDGYKQSDG-SPIAKDKLREYTFKRK 155
Pantoea_agglomerans    82 KPFNDEILRVLDKNGTMVVTGTWN------NKALKNIEKVAESKGFILIEKNVK-SSKGFLQSDG-NPINNPTVTEYQFRRK 155
Cronobacter_malonaticus 65 EPFNDEVVRVLDQNGTIIVKGTWN------NPKIKSIEKKAKKYGFTLTEKNVI-PSTGFSQTDG-KPIANDTVTEYIFKK- 137
Snodgrassella_alvi     78 DPLNSEILRVLSSNGTITIKGSLS------NGTLKNLEKRASDKGLVLVNKTKV-PNTGYTQTNG-KPIGSSELIQYTFKKK 151
Frischella_perrara     65 DPLNDEVLRVLNDGGTIIIRGVDGKI----NKYLKKLEAKAETAGLTLENKQRI-LSKGYLHTDGTTPIKSEFIDEYEFKRK 141
Gilliamella_apicola    68 APLNDEVLRVLKKDGTIIIRGSEN------NKHLRKIEEIAKLKDLQLISKQKV-LSAGYKQTSG-APIQGKEIDEFIFKKQ 141
Moraxella_catarrhalis  65 NPLNPEIIRVLHPNGKIVITASLNTKGQINNKFANQAIKEAESKGFKV-SKKPV-QNNGFNQSDG-NPIKSESFIEITITKK 143
Acetonema_longum       64 DPLNPEVLRVLSQDGEIVLTGSRS-----NI-EKNQWLKNLDEKGLTIKERSEVLNDGSYKTTDG-QPIKSKKLDRYVIVKK 138
Pseudomonas_kribbensis 64 DPLNPEILRVLSENGQITITGSAY-----ANKYIKKSLKRIEELGLKIVSQTKV-DPKGFKTIEG-EQIGSKSLDRFIIER- 137
```

C.

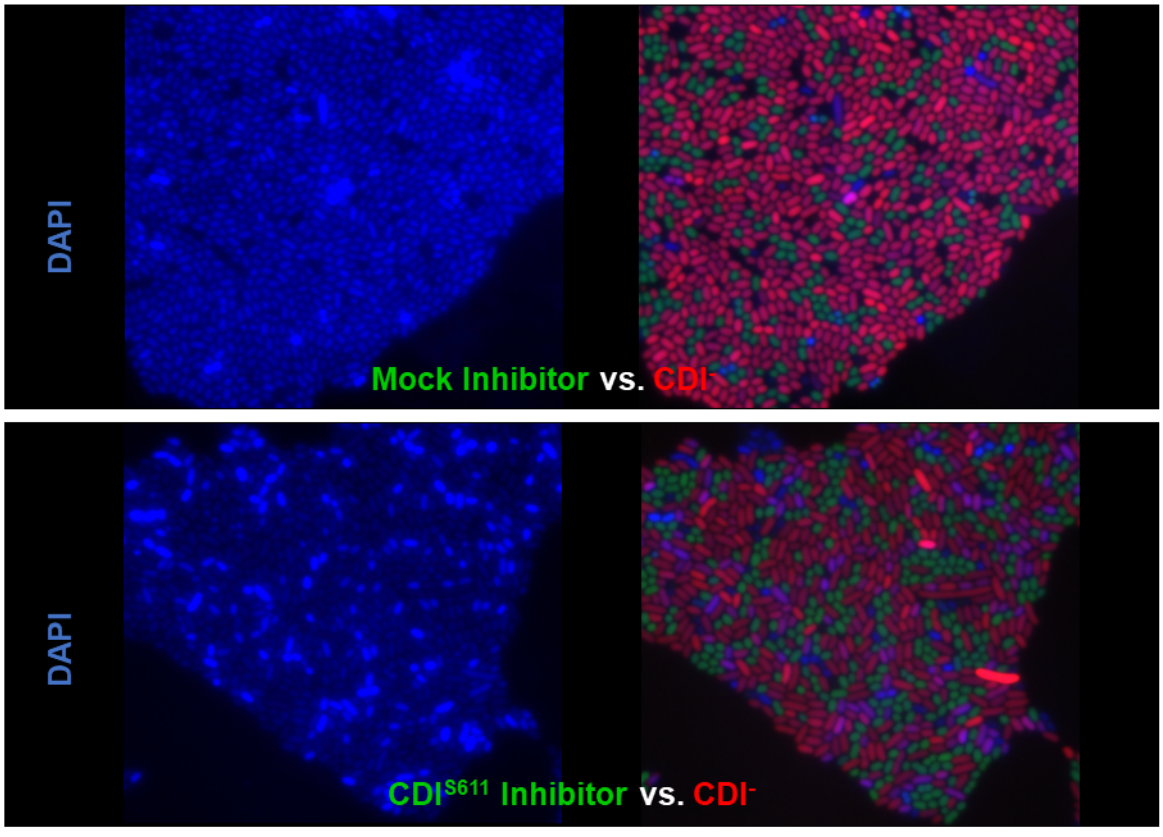

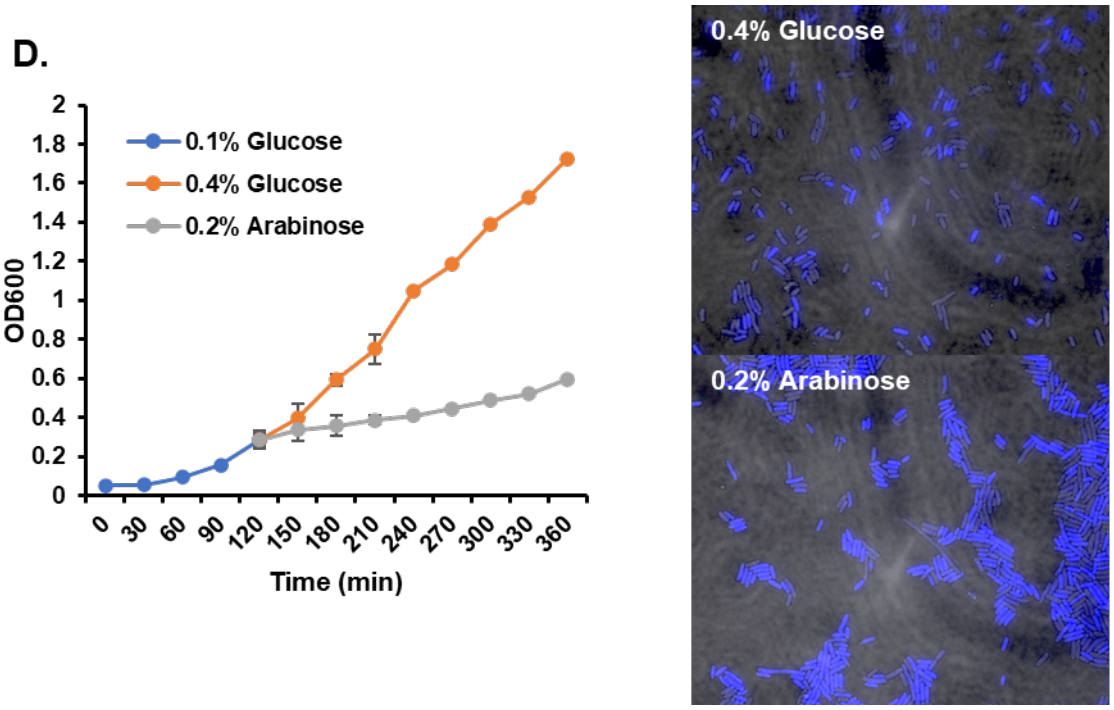

Figure 1. CdiA-CT^{S611} Bears Homology to SAM-Binding Domains and Causes Moderate Elongation of Targeted Cells.

A. AlphaFold2 model of the effector domain of CdiA-CT^{S611} with *S*-adenosylhomocysteine (SAH) placed into the proposed binding pocket. The protein is colored from the N-terminus (blue) to the C-terminus (red)

B. Multiple sequence alignment of the effector domain of CdiA-CT^{S611} with various related CdiA effector domains from indicated species.

C. Fluorescent microscopy of mKate-expressing target cells co-cultured GFP-expressing mock inhibitors (top panel) or CDI^{S611} inhibitors (bottom panel). Images were taken after 5 hours of co-culture, spotting on 1% agarose and DAPI staining.

D. (Left) Growth curve of internal expression of *cdiA-CT^{S611}* in X90 *E. coli* cells, with expression either induced using 0.2% arabinose or suppressed using 0.4% glucose after OD_{600} = 0.25. (Right) After 2 hours post-induction, samples were taken for fluorescence microscopy and prepared used the same method as Figure 1C.

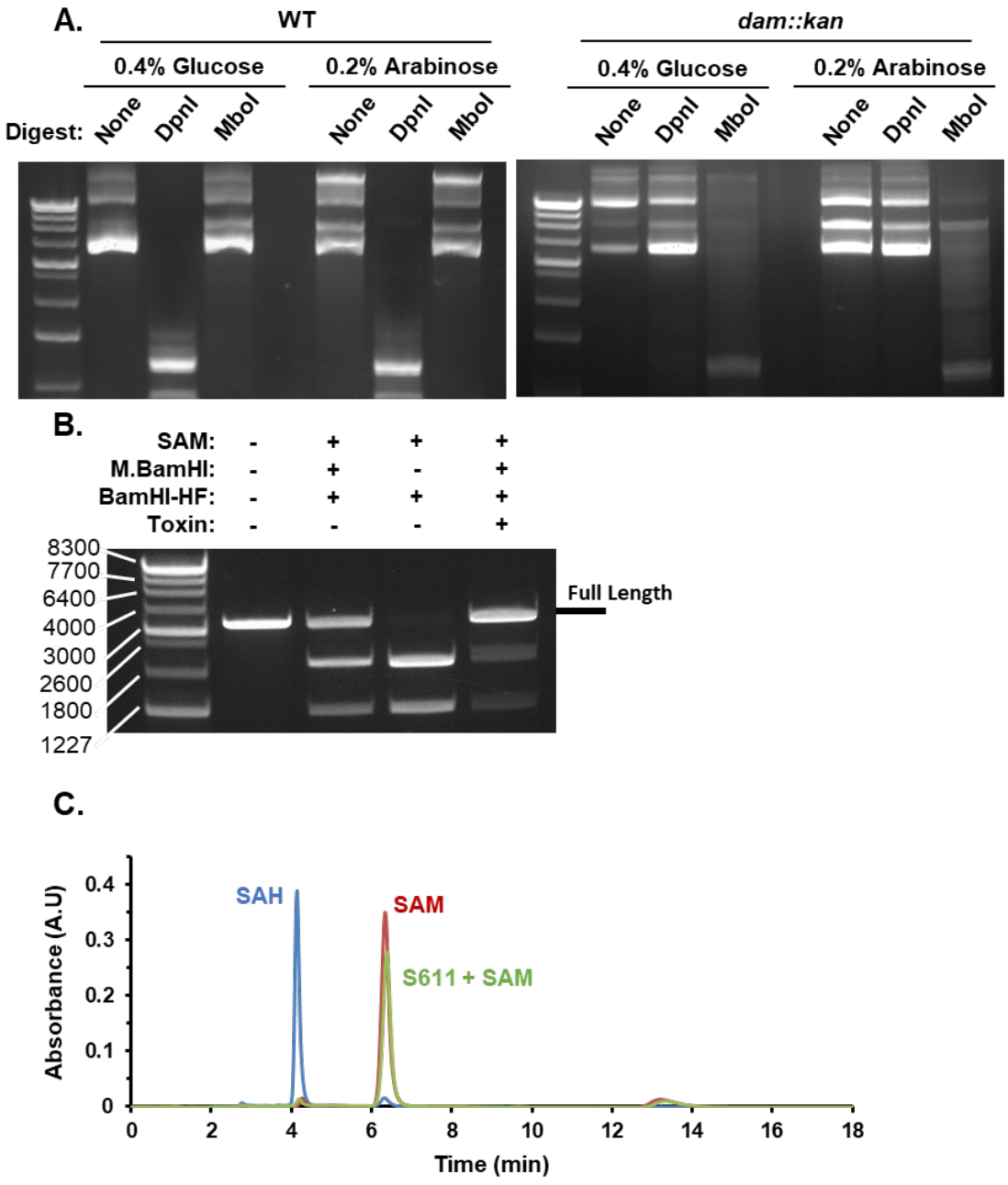
A.
WT
dam::kan
0.4% Glucose
0.2% Arabinose
0.4% Glucose
0.2% Arabinose
Digest:
None
DpnI
MboI
None
DpnI
MboI
None
DpnI
MboI
None
DpnI
MboI
B.
SAM:
M.BamHI:
BamHI-HF:
Toxin:
8300
7700
6400
4000
3000
2600
1800
1227
Full Length
C.
SAH
SAM
S611 + SAM
Absorbance (A.U)
0.4
0.3
0.2
0.1
0
0
2
4
6
8
10
12
14
16
18
Time (min)

Figure 2. CdiA-CT^{S611} Does Not Bear Noticeable SAMase Activity *in vivo* or *in vitro*.
A. Internal expression of *cdiA-CT^{S611}* in wild-type MG1655 CH7286 (WT) cells or MG1655 Δ*dam::kan* cells. After reaching an OD_{600} around 0.25, the effector was induced or suppressed using 0.2% arabinose or 0.4% glucose, respectively. 2 hours post-induction, plasmid DNA was purified from cultures and digested with the indicated enzymes, followed by electrophoresis on a 1% agarose-TAE gel stained with ethidium bromide.
B. Restriction protection assay with ScaI-linearized pBluescript DNA and the indicated reaction components. Briefly, SAM and CdiA-CT^{S611} were incubated prior to addition of substrate DNA and BamHI-methyltransferase (M.BamHI). After 1 hour of incubation with methyltransferase, plasmid DNA was digested with BamHI and electrophoresed on a 1% agarose-TAE gel stained with ethidium bromide.
C. HPLC of 500 pmol of SAM (red) or SAH (blue) standards eluted isocratically on a C18 column. In SAM + S611 (green), 500 pmol of SAM was incubated with 2 μM purified CdiA-CT^{S611} for 1 hour in reaction buffer prior to loading.

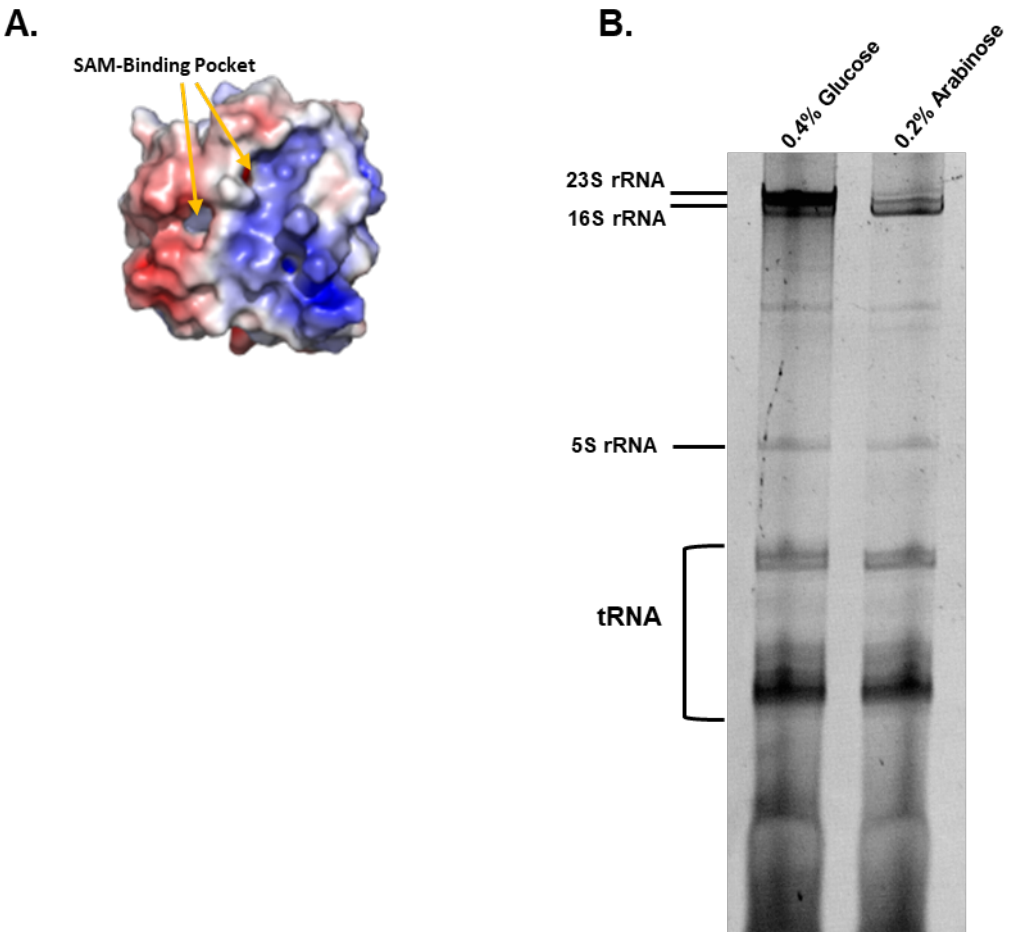

Figure 3. CdiA-CT^{S611} May Interact with RNA
A. Space filling AlphaFold2 model of CdiA-CT^{S611} with the proposed SAM-binding pocked indicated. Red regions indicate negative charges and blue regions indicate positive charges, with gradation by charge density.
B. Urea-PAGE of purified RNA samples taken from cells internally expressing *cdiA-CT^{S611}* 2-hours post induction (Figure 1C).

Materials and Methods

Table 2. Bacterial Strains

Strain	Genotype	Source
MC4100	F- *[araD139]B/r Δ(argF-lac)169* &lambda- e14- flhD5301 Δ(fruK-yeiR)725 (fruA25)‡ relA1 rpsL150(strR) rbsR22 Δ(fimB-fimE)632(::IS1) deoC1* Rif^R	-
CH2445	MC4100 *galK::sYFP2opt-cat* Rif^R Kan^R	Sanna Koskiniemi
CH2016	X90 *(DE3) Δrna ΔslyD::kan* Rif^R Kan^R	170
CH7157	X90 *ΔclpX ΔclpA::kan* Kan^R	169
CH3778	MG1655 *Δwzb ΔarfB bamA(Δ2014-2043)*	This Study
X90	F′ *lacIq lac′ pro′/ara Δ(lac-pro) nal1 argE(Am) rif*^{R} *thi-1.*	-
CH2567	MC4100 *mKate2::cat* Cm^R	This Study
CH10546	MG1655 *Δdam::kan* Kan^R	This Study

Abbreviations: AmpR , ampicillin-resistant; CmR , chloramphenicol-resistant; KanR , kanamycin-resistance; RifR , rifampicin-resistant; TetR , tetracycline-resistant; TpR , trimethoprim-resistant

Table 3. Plasmids

Plasmid	Genotype	Source
pCH8536	pMCSG63::*H6-TEV-cdiA-CT-cdiI (ECL S611)*, IPTG inducible expression with T7 promoter for purification, Amp^R	This Study
pCH1286	Constitutive expression of chimeric $cdiA^{EC93}$-CT^{S611} and $cdiI^{S611}$, Amp^R	This study
pCH8849	pCH450::*cdiA-CT-cdiI-DAS (E. cloacae* S611*),* Arabinose Inducible Degradation Construct, Tet^R	This study

Abbreviations: AmpR , ampicillin-resistant; CmR , chloramphenicol-resistant; KanR , kanamycin-resistance; RifR , rifampicin-resistant; TetR , tetracycline-resistant; TpR , trimethoprim-resistant

Table 4. Oligonucleotides

Oligo Number	Name	Sequence	Description	Source
CH5759	S611-cdiI-Spe-rev	5'- TTT ACT AGT TTC TTT TGC ATT ATA AGG CTT AAT TGC -3'	Reverse primer for generation of the CdiA-CT-CdiI-DAS S611 construct with pCH450	This Study
CH5758	S611-CT-Nco-for	5'- TTT CCA TGG GTT ATT TAT ATG CAG ATG AAG ATA AAG CG -3'	Forward primer for cloning S611 CdiA-CT into the CdiA(EC93) inhibitor chimera and generation of the CdiA-CT-CdiI-DAS S611 construct with pCH450	This Study
CH5707	S611-cdiI-Xho-rev	5'- TTT CTC GAG TTA TTC TTT TGC ATT ATA AGG CTT AAT TGC -3'	Reverse primer for cloning S611 CdiA-CT into the CdiA(EC93) inhibitor chimera and for into an N-terminal H6 purification construct pMCSG63	This Study
CH5706	S611-CT-Kpn-for	5'- TTT GGT ACC GAG AAC CTG TAC TTC CAA TAT TTA TAT GCA GAT GAA GAT AAA GCG -3'	forward primer to amplify E. cloacae S611 cdiA-CT and cdiI for N-terminal his6 purification in pMCSG63	This Study
CH5637	pCH405D-seq-for	5'-CGG CAC CTC GCT AAC GGA TTC ACC-3'	Forward sequencing primer for pCH405delta, upstream of the EcoR1 site	This Study

Prediction of Structural Homology

Submission of the CdiA-CT^{S611} protein sequence to AlphaFold2 yielded a predicted .pdb file, which was then submitted to the EMBL Dali Protein Structure Comparison Server (http://ekhidna2.biocenter.helsinki.fi/dali/) . The top 10 matches of this search from the PDB-90 output were selected for inclusion.

AlphaFold2 Modeling of the CdiA-CT^{S611} Effector Domain

The generated AlphaFold2 model for CdiA-CT^{S611} was imported into PyMol for further modeling. To overlay SAH into the proposed active pocket of the domain, the structure of the top match from the Dali PDB-90, Fungal Polyketide C-Methyltransferase (PDB ID 6kji), was imported into the same PyMol session file. Alignment of the two using the PyMol in-built function placed SAH from the 6kji crystal structure into the CdiA-CT^{S611} proposed binding

pocket. SAH was then extracted form the 6kji structure, leaving the CdiA-CT^{S611}-SAH modeled complex.

Multiple Sequence Alignments

Sequences selected for multiple sequence alignment were submitted together to Uniport Align, followed by formatting and coloring with Jalview. Sequences included in the alignment in Figure 1B were chosen by BlastP of the effector domain of CdiA-CT^{S611} (bounds of the domain were determined from the AlphaFold2 model).

Fluorescence Microscopy

Cells taken from either co-culture or monocultures were spotted on 1% agarose pads, prepared as previously described[143]. 2-3 µL of cells were spotted on a ~1 cm^2 pad and left to dry at room temperature. 1 drop of 4′,6-diamidino-2-phenylindole (DAPI) was added and a microscope slide was placed over the samples. Images were collected on an Echo Revolve fluorescent microscope and adjusted using ImageJ. In competition co-cultures destined for fluorescence microscopy, CH8906 and CH7092 inhibitors were competed against CH2567 targets.

Competition Co-Cultures

Overnight cultures of targets were grown in 50 µg/mL kanamycin and inhibitors were grown in either grown in 150 µg/mL ampicillin (for pET-derivative inhibitors) or 60 µg/mL chloramphenicol (for pDAL879-derivate inhibitors). Overnight cultures were diluted to OD_{600} = 0.1 in fresh LB without antibiotics and grown with shaking for 1.5 hours at 37˚C. The optical

density of each fresh culture was then measured using a spectrophotometer and target cells and inhibitors were mixed by resuspending each to OD_{600} = 0.1 in 10 mL of LB. Co-cultures were incubated in baffled 125 mL flasks at 37˚C for 3 hours (unless otherwise stated) with shaking. Prior to incubation, a time = 0 point was taken by diluting cells 10-fold into M9, followed by further 10-fold serial dilution for spot plating. Aliquots were again taken at the final time point and serial diluted, followed by spotting 10 µL of dilution on LB-agar containing either kanamycin (50 µg/mL) or ampicillin (150 µg/mL) to measure target and inhibitor CFU/mL. Competitive indices were calculated as the ratio of inhibitors:target CFU/mL at the final time point divided by the ratio of inhibitors:target CFU/mL at the initial time point.

Internal Expression and Growth Curves of cdiA-CT^{S611}

Expression of *cdiA-CT^{S611}* and was performed by first generating a construct consisting of the respective cognate *cdiA-CT^{S611}-cdiI^{S611}* pair in a pCH450-DAS backbone plasmid (Tet^{R}). This plasmid introduces a pBAD arabinose inducible promoter, and an ssrA(DAS) tag at the 3' end of the immunity gene. Translation of this sequence generates a suboptimal degradation tag at the C-terminus of CdiI. This construct, stored in CH8849 was transformed into wild type CH7286 cells or CH10546 Δ*dam::kan* cells. After ice-cold incubation of cells and plasmid and heat shock at 42˚C, cells were recovered in LB and 0.8% glucose for 1 hour at 37˚C. After recovery, cells were pelleted, resuspended in a small volume of LB, then plated on LB-agar plates supplemented with 20 µg/mL tetracycline and either 0.4% glucose or 0.2% arabinose. Plates were incubated overnight at 37˚C.

The next day, transformants plated on 0.4% glucose were harvested with a sterile swab and used to inoculate 60 mL of LB containing 15 µg/mL tetracycline to an optical density at

600 nm around ~0.05. The OD_{600} of the culture was measured every 30 minutes with a spectrophotometer while shaking at 37˚C. Once reaching an OD_{600} near 0.25 (or after 2 hours), cultures were split into two 20 mL fractions and were supplemented with either 0.2% arabinose (for induction) or 0.4% glucose (for suppression). OD_{600} was continually monitored over the course of 4-5 hours post-induction. For microscopy of cells during internal expression, samples were taken at 2 hours post-induction. For analysis of plasmid methylation, 5 mL of cells were harvested at 2 hours post-induction for plasmid purification.

Assessment of In Vivo Levels of Plasmid Methylation

At 2-hours post induction or suppression of internal expression (described above) plasmid DNA was harvested from cells. 1-2 µg of purified plasmids were incubated in 20 µL reaction buffer with 2 µL of 10X CutSmart and either no restriction enzyme or 1 µL of DpnI or MboI. After incubation at 37˚C for 1 hour, DNA was loaded on a 1% agarose-TAE gel, run at 100 V for 30 minutes, then stained with ethidium bromide and imaged.

Protein Purification

An expression vector of *cdiA-CT*^{S611} was generated by cloning the *cdiA-CT-cdiI* immunity pair into *pMCSG63*, containing a N-terminal polyhistidine tag fusion under a T7 promoter. This plasmid was transformed into CH2016, an expression strain of X90 carrying the DE3 lysogen with T7 polymerase and knockouts of *rna* and *slyD*. An overnight culture of this strain (CH8536) was grown in LB + 150 µg/mL ampicillin and used to inoculate 200 mL LB supplemented with 150 µg/mL ampicillin at OD_{600} = 0.1. After the optical density reached ~0.6, expression of CdiA-CT was induced by addition of 1.5 mM isopropyl ß-D-1-

thiogalactopyranoside (IPTG). After 2 hours of induction, cells were harvested by centrifugation at 6,000 rpm for 10 minutes and resuspended in 10 mL 6M Guanidine HCl + 30 mM Imidazole. After a freeze-thaw cycle at -80˚C and centrifugation at 10,000 rpm for 10 minutes, clarified lysates were added to 60 µL Ni-NTA and incubated at 4˚C for 1 hour with rotating. Bound Ni-NTA protein-complexes were then collected by centrifugation and removal of supernatant, followed by two 10 mL washes in 6M Guanidine HCl + 30 mM Imidazole. After two washes, the Ni-NTA was added to an elution column and washed with urea lysis buffer (ULB) supplemented with 30 mM Imidazole. Finally, proteins were eluted in successive 200 µL volumes of (ULB) containing 250 mM Imidazole. Elutions were assayed with Bradford reagent and combined for dialysis against 1L 20 mM Tris-HCl pH 7.5, 150 mM NaCl, and 10 mM B-mercaptoethanol (BME) overnight. Dialyzed protein was quantified by measurement of A_{280} and purity was confirmed via SDS-PAGE and staining with Coomassie before performing experiments.

Plasmid Protection Assay

S-adenosylmethionine and BamHI methyltransferase (M.BamHI) were acquired from NEB. First, 500 pmol SAM was incubated with 2 µM purified CdiA-CT^{S611} in 10 µL reaction buffer containing 1 µL 10X CutSmart. This mixture was incubated at 37˚C for 1 hour. Control samples lacking either of these components were instead incubated at 37˚C for 1 hour in reaction buffer. After incubation, 500 ng of ScaI-linearized pBluescript was added to the reaction, along with 2 units of M.BamHI, and the reaction volume was brought up to 20 µL with water and 1 µL CutSmart buffer. This reaction mixture was incubated at 37˚C for 1 hour, followed by heat inactivation at 75˚C for 5 minutes and purification of plasmid DNA. 35 µL

of purified plasmid DNA was then supplemented with 4 µL of CutSmart and 1 µL of BamHI restriction endonuclease and incubated at 37˚C for 1 hour. After digestion, 6X NEB DNA loading dye was added, and the mixture was loaded onto a 1% agarose-TAE gel. The gel was run at 100V for 30 minutes, followed by staining with ethidium bromide and imaging.

HPLC

HPLC as performed on a Waters Breeze HPLC Machine, using a reverse phase C18 column. A buffer was prepared containing 10 mM 1-heptanesulfonic acid, 40 mM K_2HPO_4 and 20% methanol, adjusted to pH 4 with H_3PO_4. SAM and SAH were acquired from NEB, and standards were run on HPLC by injection of 500 pmol of metabolite diluted into 100 µL of buffer. The small molecules were eluted isocratically with the described buffer and absorbance was measured at 257 nm. In the case of SAM+CdiA-CT^{S611}, 500 pmol of SAM was incubated at 37˚C with 2 µM purified CdiA-CT^{S611} for 1 hour prior to injection.

RNA Extraction

Cell samples were taken 2 hours post-induction of internally expressed *cdiA-CT^{S611}*, described above. First, the OD_{600} of internal expression cultures was measured, and the volume of cells removed was calculated by $2/OD_{600}$. Samples were immediately mixed with ice-cold methanol and pelleted at 10,000 rpm for 10 minutes. Pellets were briefly dried and placed on ice, followed by lysis with ThermoFisher TRIzol reagent, followed by purification with chloroform extraction. Purified RNA was ethanol precipitated and washed in ethanol prior to dissolution in 10 mM sodium acetate + 1 mM EDTA. RNA then underwent a freeze-thaw cycle at -80˚C and was quantified with a nanodrop. 10 µg of purified RNA was loaded in a pre-

warmed Urea-PAGE gel and run at 300V for 15 minutes, followed by staining with ethidium bromide and imaging.

IV. Characterization of a CDI Effector with Homology to Glutaminases

Abstract

Contact dependent growth inhibition (CDI) is a phenomenon in which a Type V Secretion System (T5SS) delivers toxic effector cargoes into neighboring cells to gain a growth advantage[10,91]. Currently, toxic cargoes have been characterized which exhibit nuclease and pore forming activity, although the full genetic diversity CDI effectors has been only minimally explored.[19,84,93] Here, I investigate a CDI effector from *Enterobacter cloacae* UCI49 predicted to have homology to protein glutaminases and cysteine proteases and find that it uses a Cys-Asp-His catalytic triad to perform its activity. Additionally, I search for the identity of the effector's substrate by affinity purification and find that unique bands co-purify with the inactive effector domain. Western blotting and mass spectrometry reveal two essential proteins, protein release factor 2 (RF2) and the riboflavin biosynthetic enzyme (RibD), that specifically co-purify, although their involvement in toxicity remains unknown.

Introduction

While in the previous chapter I explored the potential inhibitory mechanisms of a CDI effector from *Enterobacter cloacae* bearing homology to SAM-binding methyltransferases, in this chapter I explore another uncharacterized CdiA-CT from *E. cloacae* UCI49. Work in Chapter 2 demonstrated that the cytoplasm entry domain of CdiA-CT^{UCI49} requires FtsH for translocation into the cell (see Chapter 2 Figure 6). Structural prediction of the extreme C-terminal effector domain by AlphaFold2[100,101] predicts significant homology to bacterial and human protein glutaminases, specifically to their processive domains (Table 1). These enzymes catalyze a deamidation reaction that turns glutamine into glutamate, releasing ammonia[144].

While similar in structure to transglutaminase enzymes, they do not perform transpeptidation[145]. During normal cellular function, glutaminases are important for glutamine metabolism[146], protein stability via the N-degron pathway[147], and post-translational modification[148]. CdiA-CT^{UCI49} was also predicted to have homology to cysteine proteases, including SseI from *Salmonella enterica* and *Pasteurella multocida* toxin (PMT). It was therefore hypothesized that CdiA-CT^{UCI49} could exhibit glutaminase or protease activity towards essential proteins found in the *E. coli* cytosol to mediate growth inhibition.

CdiA-CT^{UCI49} Contains a Conserved Cys-Asp-His Active Site

While glutaminases and proteases perform different functions, they share a highly conserved Cys-Asp-His active site, where the nucleophilic cysteine performs catalysis[149]. Analysis of the predicted structural model of CdiA-CT^{UCI49} confirmed the presence of this catalytic triad within the effector domain between residues Cys205-His248-Asp259 (Figure 1A). Additionally, a second cysteine, Cys202 was located nearby the presumed active site nucleophile. This is a common occurrence in enzymes bearing this catalytic triad, as the activity of the nucleophilic cysteine may be regulated by pH via formation of a disulfide in oxidizing conditions[149]. In CDI, this could function to inactivate the effector domain during secretion arrest in the reducing environment of the inhibitor periplasm[150] and maintain inactivity after delivery, prior to inner membrane translocation. After entry into the oxidizing cytoplasm, the disulfide may then be broken to liberate the nucleophilic cysteine and enable activity.

To confirm that Cys205 is necessary for growth inhibition, a construct containing *cdiA-CT^{UCI49}-cdiI^{UCI49}-DAS* encoding the C205A mutation was internally expressed in cells under

an arabinose-inducible promoter. Cells expressing wild-type *cdiA-CT*^{UCI49} exhibited slow growth even during suppression of the effector with glucose, while induction with arabinose completely blocked the growth of cells over 2 hours (Figure 1B). However, cells expressing the C205A mutation with or without induction experienced similar, robust growth rates, which were higher than both conditions bearing wild-type *cdiA-CT*^{UCI49}. This demonstrates the necessity of Cys205 for effector activity and reinforces the prediction that it participates in a conserved Cys-Asp-His catalytic triad. As a search for clues regarding the targeted proteins whose disturbance could lead to gross cell defects, cells expressing wild-type *cdiA-CT*^{UCI49} at 2 hours post-induction were observed under the microscope (Figure 1C). Although no obvious morphological defects were present, this knowledge could prove useful when narrowing down candidate protein targets.

Co-Purification of Potential CdiA-CT^{UCI49}-Related Protein Factors

Given that the C205A mutation renders CdiA-CT^{UCI49} inactive, it was hypothesized that the mutant protein would bind stably to its substrate. A polyhistidine tag was appended to the N-terminus of the inactive effector domain for expression and non-denaturing purification with Ni-NTA resin. When compared to the native purification of a similarly prepared cysteine protease effector from *C. rodentium* DBS100 (Unpublished data), two unique co-purifying bands appear near 40 kDa and 60 kDa (Figure 2A). These bands could be co-purified reproducibly and appeared despite high salt and imidazole stringency during washes. To probe for potential binding between the CdiA-CT$^{UCI49\ C205A}$ bait and the co-purified proteins, a denaturing wash with 6 M Guanidine-HCl was performed prior to elution from the resin (Figure 2B). Notably, the band near 40 kDa could be completely eluted via denaturation. This

could occur if the co-purifying protein is bound by folded CdiA-CT$^{UCI49\ C205A}$ and released upon denaturation of the interaction interface. Alternatively, it's possible that this protein does not interact with CdiA-CT^{UCI49} and instead binds to Ni-NTA in its folded state, where denaturation reduces its affinity for the resin. Tentatively, this co-purifying protein was named UIP40 (UCI49-Interacting Protein at 40 kDa).

Investigation of Interactions Between CdiA-CT^{UCI49} and Protein Release Factors

Interrogation of the proteome of *E. coli* revealed only a handful of essential cytosolic proteins with 6 kDa of the estimated size. Notable among this list are the protein release factors RF1 and RF2, as they contain a highly conserved GGQ motif residing in an easily accessible loop region[151]. In this motif, the backbone of the glutamine residue performs hydrolysis of tRNA-bound polypeptides during translation termination and ribosome rescue[152]. Glutaminase activity could inactivate class 1 release factors, resulting in ribosome stalling and growth inhibition. To determine whether release factors co-purify with inactive CdiA-CT^{UCI49}, constructs containing either full length CdiA-CT or only the toxin domain, with or without cognate immunity, were purified in non-denaturing conditions in a background expressing FLAG-tagged RF2 (Figure 3A). This purification background lacks knockouts of *rna* and *slyD*, which have intrinsic Ni-NTA affinity and are commonly co-purified with this method[153]. Western blotting against FLAG-tagged RF2 revealed its elution alongside full length CdiA-CT^{UCI49} constructs with or without immunity, but not with the effector domain alone. Additional blotting against RF1 indicate show that it does not co-purify. Interestingly, although RF2 cannot be UIP40 based on its lack of elution with the effector domain construct used previously, it's possible that it could interact with the full-length protein in an immunity

independent manner. Immunity independent interactions with CdiA-CTs have previously been reported as co-factors necessary for proper folding and toxic activity[88,118,125].

While blotting indicated that class 1 release factors are not substrates, a ribosome-stalling phenotype was still investigated. To do this, CDI^{UCI49}-susceptible cells were either treated with streptomycin to induce stalling[154] or incubated with inhibitor cells. These target cells harbor a modified *ssrA* allele, *ssrA(DD)*, which encodes a non-degradable ssrA tag that is appended to polypeptides during ribosome rescue[155]. Additionally, target cells carry a reporter construct encoding mutant *rbsK*, where rare arginine codons near the 3' end of the open reading frame have been repaired to codons corresponding to more common arginine tRNAs for higher fidelity translation. This modified sequence undergoes negligible ssrA-tagging during normal conditions, allowing for direct monitoring of induced ribosome stalling by accumulation of RbsK-SsrA(DD)[156]. Total protein staining by Coomassie R-250 and western blot against SsrA(DD) shows an accumulation of tagged proteins during treatment with streptomycin (Figure 3B). Co-culture with a mock inhibitor similarly shows accumulation of tagged proteins, but co-culture with inhibitors expressing the previously described $CdiA^{EC93}$-CT^{UCI49} (CDI^{UCI49}) chimera shows no increase in tagging. Loss of target cell viability during both streptomycin treatment and co-culture with CDI^{UCI49} inhibitors confirmed that target cells were successfully intoxicated (Figure 3C). These data may indicate that CdiA-CT^{UCI49} does not directly interfere with translation, instead stopping some other essential cellular process which leads to a decrease in translation initiation and therefore less ssrA tagging. As a final measure for activity, target cells carrying a FLAG tag on *prfB* (RF2) were co-cultured with CDI^{UCI49} inhibitors and lysates were subjected to western blot (Figure 3D-E). Consistent migration of RF2-FLAG across all time points confirms no cysteine protease

activity directed towards the release factor. Although potential glutaminase activity could not be monitored by migration via SDS-PAGE, the experiments performed previously here indicate that toxic activity towards RF2 is unlikely.

Mass Spectrometry of CdiA-CT$^{UCI49\ C205A}$ Native Purification Reveals Potential Interactors

To precisely determine the identity of the protein bands that previously co-purified with CdiA-CT$^{UCI49\ C205A}$ (Figure 2A-B), an elution was subjected to trypsinization and LC-MS. Analysis of the co-purified proteins with a percent coverage above 65% revealed a handful of proteins known to be essential, as well as a few expected contaminants (Table 2). For example, human keratin was quickly excluded. Additionally, *E. coli* proteins which are known to bind Ni-NTA, including Fur, Crp, and GlmS, appeared with high coverage and are less likely to be candidate targets[153]. The protein with highest coverage identified as essential to cell growth is RibD, a two-domain reductase and deaminase involved in riboflavin biosynthesis[157]. At a mass of ~40.3 kDa, this protein is a promising candidate for UIP40. Other proteins identified with high coverage within ~6 kDa of 40 kDa include AdhP, HisB, GutQ, XerD, GldA, AstC, and KdsD, all of which are nonessential and therefore unlikely to be targets of toxin activity. Additionally, many of these proteins have intrinsic Zn^{2+}-binding activity or histidine-rich sequences, making it likely that they bound directly to the Ni-NTA rather than to CdiA-CT$^{UCI49\ C205A}$ during purification.

If RibD is targeted by the effector domain of CdiA-CT^{UCI49}, a defect in riboflavin biosynthesis would be expected to lead to cell inhibition. *E. coli* and many Gram-negative bacteria rely on biosynthetic enzymes to generate riboflavin for a variety of cellular processes

and are unable to import the nutrient from the extracellular environment[157]. However, some bacteria, including Gram-negative bacteria such as *Agrobacterium tumefaciens* and Gram-positive bacteria such as *Bacillus subtilis* encode membrane transporters for riboflavin and analogs[158,159]. To test whether decreased intracellular riboflavin levels in target cells leads causes growth inhibition, co-culture media was supplemented with high concentrations of riboflavin. Although *E. coli* are unable to actively import the nutrient, high concentrations (>1 mM) are thought to diffuse into cells by mass action and this has been found to be sufficient to rescue riboflavin auxotrophs[160]. However, co-culture of wild-type CDI-susceptible cells with cells expressing chimeric CDI^{UCI49} in the presence of 1.5 mM riboflavin led to no noticeable rescue of growth inhibition (Figure 4). As an alternative approach, the riboflavin ABC transporter *ribU* from *B. subtilis* 168 was expressed in *E. coli* target cells during co-culture. This similarly provided no rescue of growth inhibition. To more closely investigate a disruption of RibD, it was hypothesized that overexpression of the protein could rescue growth inhibition. However, this similarly had no effect on co-culture inhibition. While not necessarily conclusive, these findings suggest that RibD is not a target of CdiA-CT^{UCI49} activity and could instead be a cytosolic cofactor.

Discussion

Despite experimental attempts to uncover the toxic activity of CdiA-CT^{UCI49}, its targets and specific effect on cells remains largely mysterious. It is clear that the effector contains a Cys-Asp-His triad, conserved among glutaminases and cysteine proteases, making it likely that it exhibits one of these activities. Attempts to co-purify associated proteins were inconclusive as two candidates, protein release factor 2 (RF2) and the dual-functional riboflavin biosynthetic

enzyme, RibD, appear unrelated to activity of the toxin. However, their appearance in purifications of the inactive mutant, verified by western blotting or mass spectrometry, could indicate a role in toxicity. Perhaps one of these proteins act as a co-factor, providing thermodynamic stability to the effector domain in a similar manner to previously identified co-factors for CDI effectors[88,118]. RF2 is an enticing candidate co-factor, given its abundance in cells and high conservation among bacterial species[161]. To confirm any interactions indicative of a co-factor, demonstration of *in vitro* binding interactions between the protein and CdiA-CT^{UCI49} is necessary.

To further investigate potential targets of the CdiA-CT, mass spectrometry of co-purified samples could still pose a viable route. Perhaps comparison of nondenaturing purifications of inactive CdiA-CT with or without cognate CdiI could narrow the list of candidates. Additionally, specific confirmation of activity of the effector domain would prove useful. In some cases, glutaminases have been reported to undergo self-deamidation[162]. Evidence of this process in CdiA-CT^{UCI49} would confirm glutaminase activity. An alternative and promising route to characterization of this effector domain could use BioID processes to identify interacting proteins[163]. For example, CdiA-CT could be fused to a peroxidase like APEX2, which in the presence of biotin-phenol and hydrogen peroxide generates biotin-phenoxy radicals that react rapidly with nearby proteins and can be selectively purified[164]. This is likely a promising approach to the characterization of many diverse and mysterious CDI effectors, especially those suspected to interact with proteins.

Rank	PDB ID	Z-score	rmsd	Description
1	4w79	7.3	3.0	Human N-terminal Glutamine Amidohydrolase
2	2zk9	7.3	3.3	Protein Glutaminase from *Chryseobacterium proteolyticum*
3	3c9q	6.9	2.8	Human C8orf32
4	6kgj	6.7	2.9	Human Glutamine Hydrolase
5	2ksv	6.5	3.2	Protein glutaminase from *Chryseobacterium proteolyticum*
6	4g2b	6.3	2.9	Virulence Factor SseI from *Salmonella enterica*
7	2ebh	6.2	3.5	Thiol Protease from *Pasteurella multocida* Toxin
8	1evu	4.6	3.2	Human Factor XIII Transglutaminase
9	4fgp	4.6	2.6	Periplasmic Protease from *Legionella pneumophila*
10	5lq7	4.5	3.3	Cysteine Protease from *Salmonella enterica*

Table 1. Predicted Structural Homologs of CdiA-CT^{UCI49}.
The AlphaFold2 model of the effector domain from CdiA-CT^{UCI49} was submitted to the Dali server for comparison to other structures in the PDB. The top 10 matches in the corresponding PDB-90 are shown above.

Protein ID	Gene	Length	Mass (kDa)	Percent Coverage	Protein Description	Essential
P0A9A9	fur	148	16.7	100	Ferric uptake regulation protein	No
P0AA43	rsuA	231	25.8	97.8	Ribosomal small subunit pseudouridine synthase A	No
P25539	ribD	367	40.3	87.5	Riboflavin biosynthesis protein RibD	Yes
P0ACJ8	crp	210	23.6	84.8	cAMP-activated global transcriptional regulator CRP	No
P21599	pykA	480	51.3	84.4	Pyruvate kinase II	No
P0A8E1	ycfP	180	17.8	83.9	UPF0227 protein YcfP	No
P0AF63	nsrR	141	15.6	83.7	HTH-type transcriptional repressor NsrR	No
P39451	adhP	336	35.3	81	Alcohol dehydrogenase, propanol-preferring	No
P64588	yqjI	207	23.4	80.7	Transcriptional regulator YqjI	No
P17169	glmS	609	66.8	80.5	Glutamine--fructose-6-phosphate aminotransferase	Yes
P0A6T5	folE	222	24.8	79.7	GTP cyclohydrolase 1	Yes
None	UCI49	165	18.5	78.8	Bait	No
P06987	hisB	355	40.2	78	Histidine biosynthesis bifunctional protein HisB	No
P17115	gutQ	321	34	76	Arabinose 5-phosphate isomerase GutQ	No
P60906	hisS	424	47	75.9	Histidine--tRNA ligase	Yes
P0ACR4	yeiE	293	32.7	75.8	HTH-type transcriptional regulator YeiE	No
P0A9R7	ftsE	222	24.4	75.2	Cell division ATP-binding protein FtsE	Yes
P0A7J0	ribB	217	23.3	74.2	3,4-dihydroxy-2-butanone 4-phosphate synthase	Yes
P0A8P8	xerD	298	34.2	73.2	Tyrosine recombinase XerD	No
P0A9S5	gldA	367	38.7	71.7	Glycerol dehydrogenase	No
P35527	KRT9	623	62	70.8	Keratin, type I cytoskeletal 9	No
P77581	astC	406	43.6	70.4	Succinylornithine transaminase	No
P45395	kdsD	328	35.2	70.1	Arabinose 5-phosphate isomerase KdsD	No
P13645	KRT10	584	58.8	69.7	Keratin, type I cytoskeletal 10	No
P0AGI8	trkA	458	50.3	69.7	Trk system potassium uptake protein TrkA	No
P0AED9	dcm	472	53.4	69.5	DNA-cytosine methyltransferase	No
P0C8J6	gatY	284	30.8	69.4	D-tagatose-1,6-bisphosphate aldolase subunit GatY	No
P0ADZ4	rpsO	89	10.3	68.5	30S ribosomal protein S15	No
P13035	glpD	501	56.7	67.7	Aerobic glycerol-3-phosphate dehydrogenase	No
P0A6Z6	nikR	133	15	67.7	Nickel-responsive regulator	No
P32664	nudC	257	29.6	67.3	NAD-capped RNA hydrolase NudC	No
P27306	sthA	466	51.5	66.7	Soluble pyridine nucleotide transhydrogenase	No
P04264	KRT1	644	66	66.1	Keratin, type II cytoskeletal 1	No
P31658	hchA	283	31.1	65.4	Protein/nucleic acid deglycase 1	No
P0A9N4	pflA	246	28.2	65	Pyruvate formate-lyase 1-activating enzyme	No

Table 2. Mass Spectrometry of CdiA-CT$^{UCI49\ C205A}$ Co-Purification.
All hits determined by mass spectrometry with a percent coverage above 65 are shown, including the protein identifier, gene name for *E. coli* K-12, corresponding protein length and mass from the Uniprot database (ID UP000271721) . Each gene was determined to be essential by query of the Shigen Profling of *E. coli* database for strain MG1655. The CdiA-CT$^{UCI49\ C205A}$ bait protein is highlighted in red, and contaminants from human keratins are highlighted in yellow.

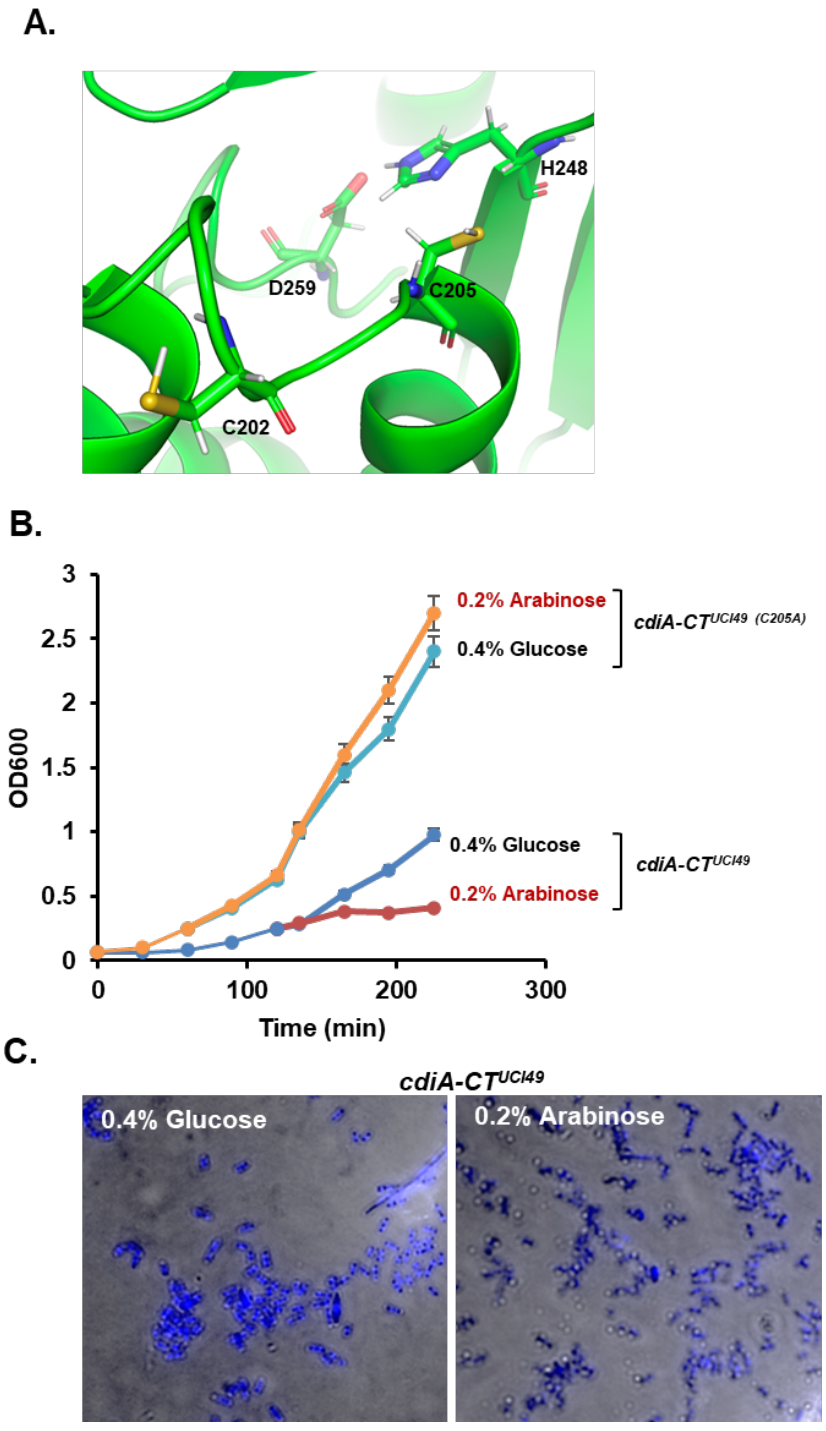

Figure 1. CdiA-CT^{UCI49} Bears a Cys-Asp-His Catalytic Triad Necessary for Growth Inhibition.

A. Carton of the Cys-Asp-His active site in the AlphaFold2 model of the effector domain of CdiA-CT^{UCI49}.

B. Growth curve of internal expression of either *cdiA-CT*^{UCI49} or *cdiA-CT*$^{UCI49\ C205A}$ in X90 *E. coli* cells, with expression either induced using 0.2% arabinose or suppressed using 0.4% glucose after OD_{600} = 0.25.

C. After 2 hours post-induction of *cdiA-CT*^{UCI49} from Figure 1B, samples were taken for fluorescence microscopy by spotting on a 1% agarose pad and staining with DAPI.

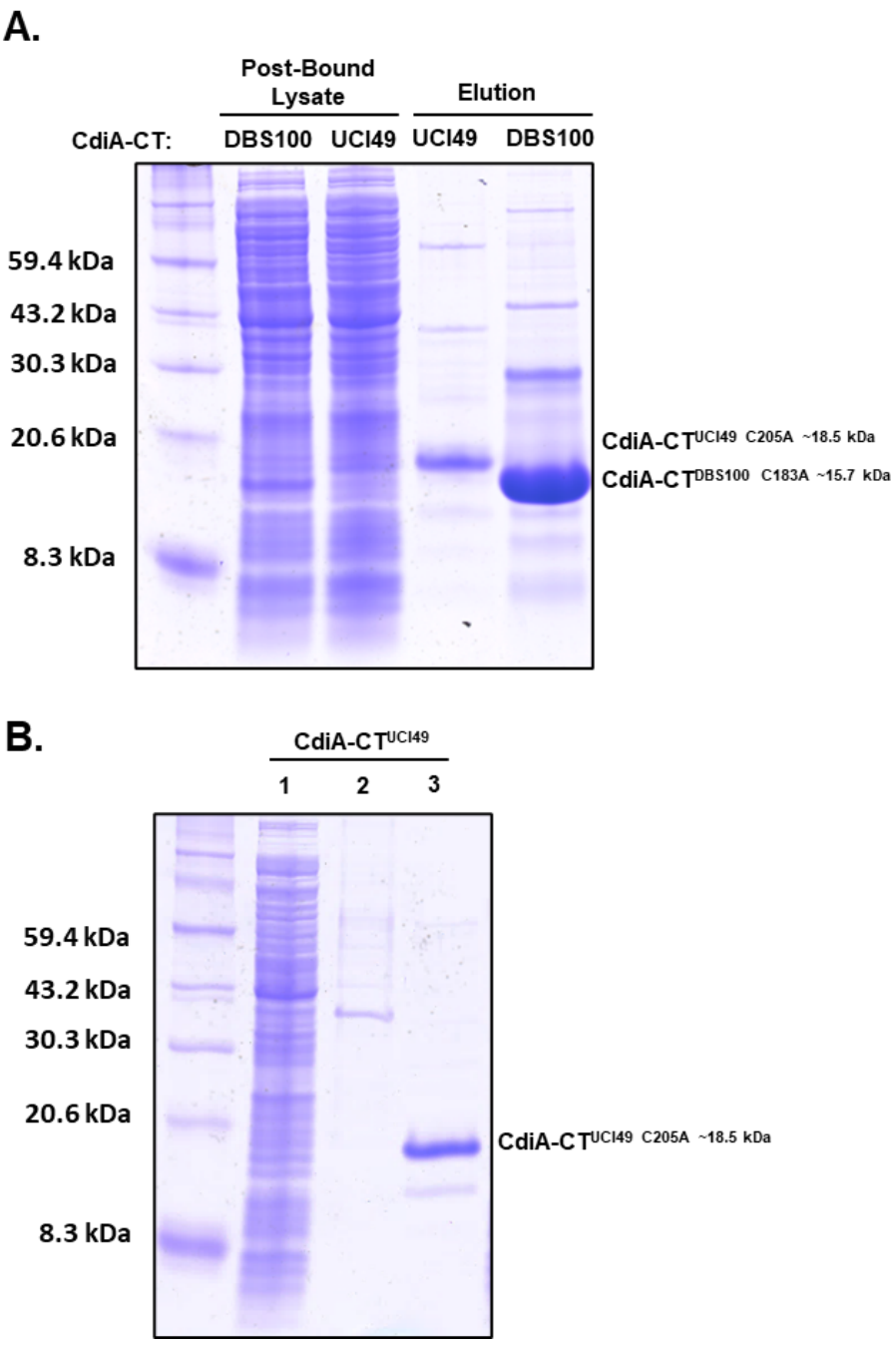

Figure 2. Native Purification of CdiA-CT$^{UCI49\ C205A}$ Reveals Unique Co-Purifying Bands.

A. Native Ni-NTA affinity purificiation of polyhistidine-tagged CdiA-CT$^{UCI49\ C205A}$ and CdiA-CT$^{DBS100\ C183A}$. Each construct includes only the effector domains (lacking the N-terminal entry domain). Lysates were sampled after binding to NiNTA.

B. Native Ni-NTA affinity purification of polyhistidine-tagged CdiA-CT$^{UCI49\ C205A}$. A sample of clarified cell lysate was taken after Ni-NTA binding (1). Following washes of Ni-bound proteins with non-denaturing buffer, a single denaturing wash in 6M Guanidine H-Cl. was performed (2). This elution was followed by washes in non-denaturing buffer and native elution in 300 mM Imidazole (3).

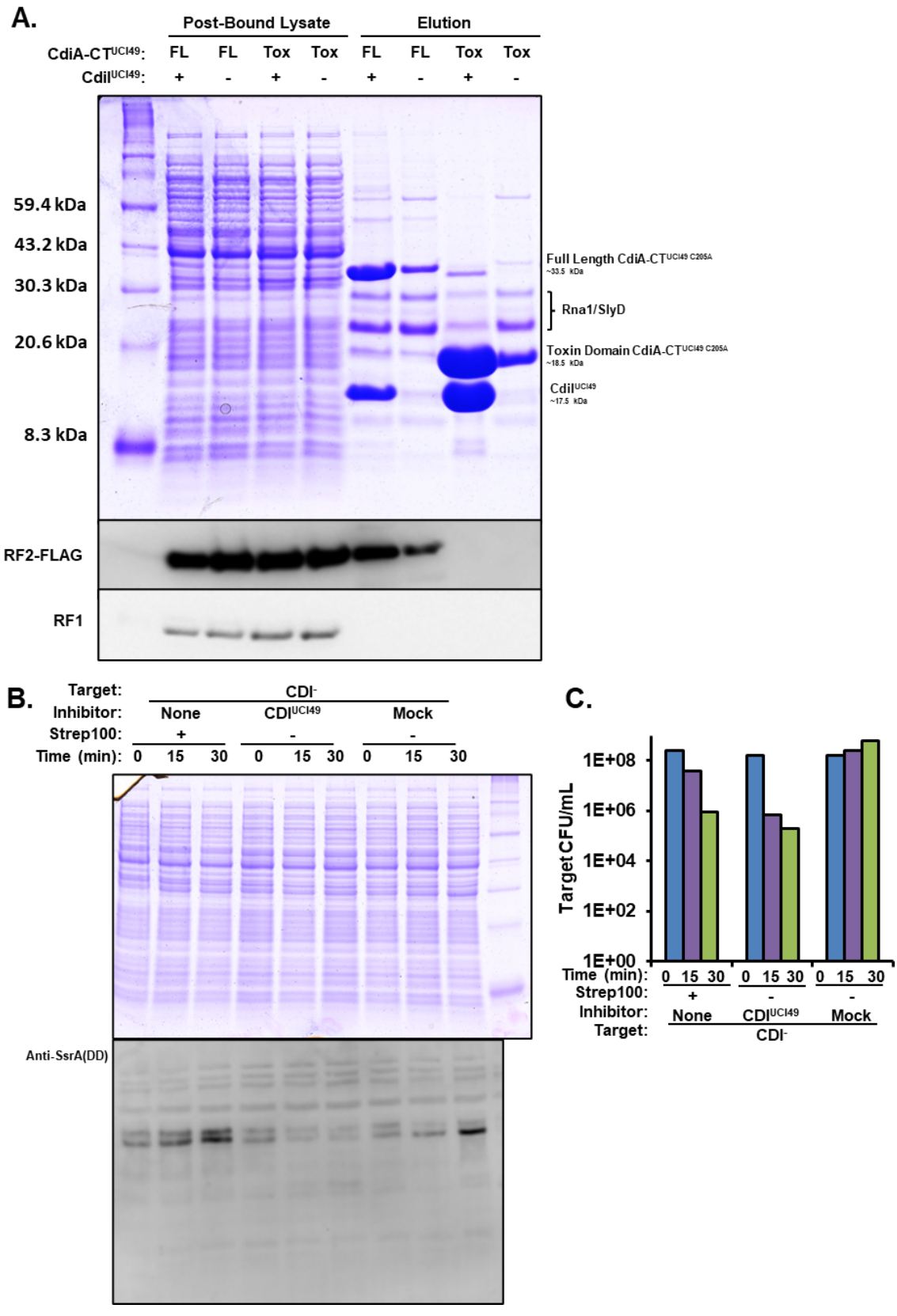
A.
Post-Bound Lysate
Elution
CdiA-CT^UCI49:
FL FL Tox Tox FL FL Tox Tox
CdiI^UCI49:
+ - + - + - + -
59.4 kDa
43.2 kDa
30.3 kDa
20.6 kDa
8.3 kDa
Full Length CdiA-CT^UCI49 C205A
~93.5 kDa
Rna1/SlyD
Toxin Domain CdiA-CT^UCI49 C205A
~18.5 kDa
CdiI^UCI49
~17.5 kDa
RF2-FLAG
RF1
B.
Target: CDI-
Inhibitor: None CDI^UCI49 Mock
Strep100: + - -
Time (min): 0 15 30 0 15 30 0 15 30
Anti-SsrA(DD)
C.
Target CFU/mL
1E+08
1E+06
1E+04
1E+02
1E+00
Time (min): 0 15 30 0 15 30 0 15 30
Strep100: + - -
Inhibitor: None CDI^UCI49 Mock
Target: CDI-

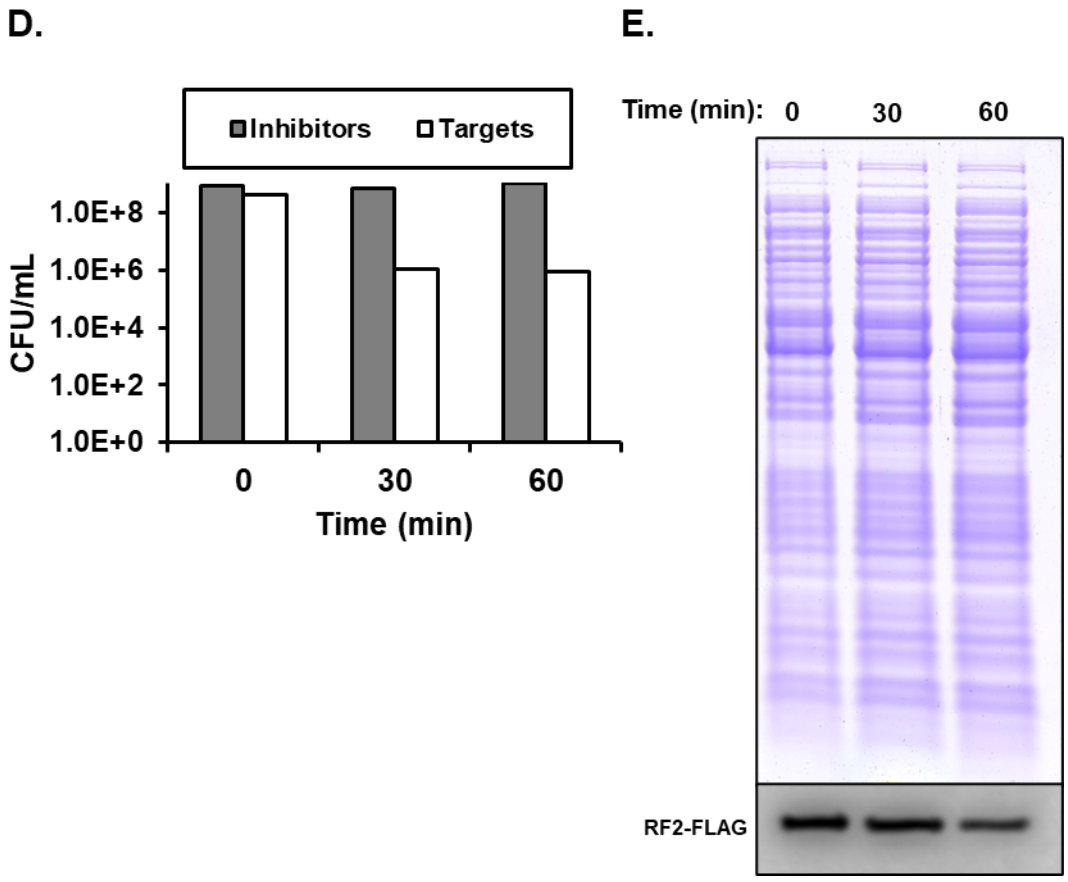

Figure 3. Investigation of Interactions Between CdiA-CT^{UCI49} and Class 1 Protein Release Factors.
A. Native purification of various CdiA-CT$^{UCI49\ C205A}$ constructs in cells bearing a FLAG tag on *prfB*, containing either the full length CdiA-CT ("FL") or only the effector domain ("Tox"), with or without co-expression of cognate immunity. Samples of lysate were collected after binding to Ni-NTA and normalized using Bradford reagent. After SDS-PAGE, gels were either stained with Coomassie G-250 or used for western blotting against indicated primary antibodies. Rna and SlyD are commonly co-purified protteins with Ni^{2+}-binding affinity.
B. Co-culture of CDI-sensitive CH8868 cells with chimeric CdiA^{EC93} -CT^{UCI49} inhibitors, mock inhibitors, or mono-culture of targets with 100 μg/mL streptomycin. Lysates from co-cultures were generated at the indicated times and normalized with Bradford reagent for SDS-PAGE. Gels were stained with either Coomassie G-250 or subjected to western blotting against SsrA(DD) primary antibody.
C. CFU/mL of target cells determined by serial dilution and spot plating from each of the lanes in Figure 3B.
D. Co-culture time course of chimeric CdiA^{EC93} -CT^{UCI49} inhibitors with *prfB-FLAG* CH4119 target cells.
E. Coomassie stain and anti-FLAG western blot of the co-cultures in Figure 3D at the indicated time points.

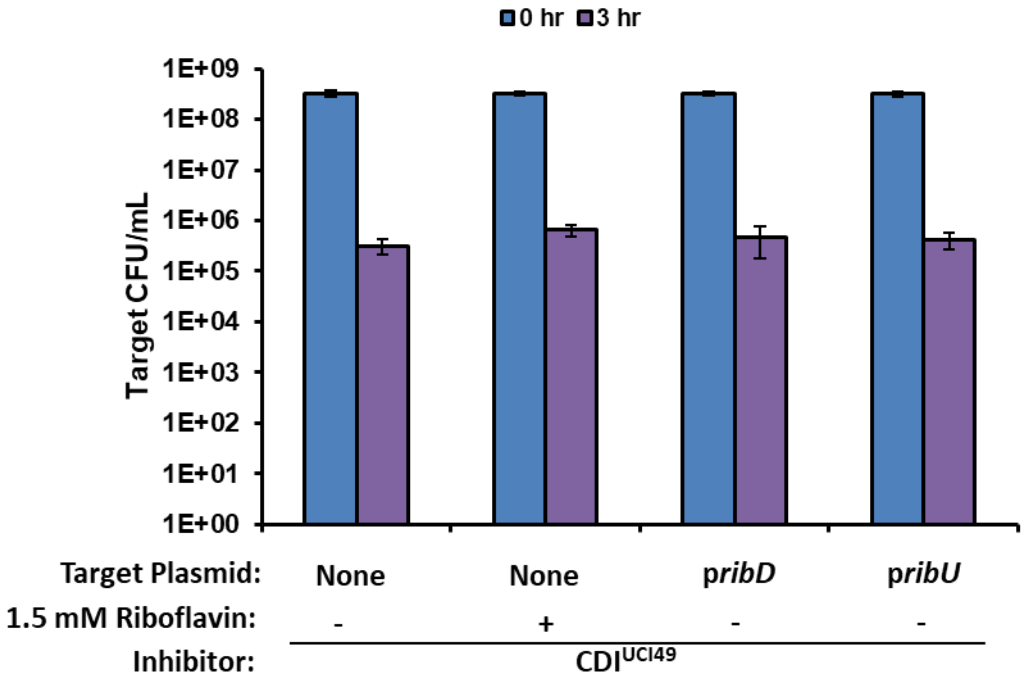

Figure 4. Investigation of Involvement of RibD and Riboflavin Biosynthesis in CDI^{UCI49} Toxicity
Target colony forming units/mL for competition co-cultures of CH2005 CDI^{UCI49} chimeric inhibitors with wild-type CH7286 cells bearing the indicated plasmids. The gene *ribD* comes from *E. coli* K-12 strains, while *ribU* comes from *Bacillus subtilis* 168. In one co-culture condition, 1.5 mM riboflavin was added to the media.

Materials and Methods

Table 3. Bacterial Strains

Strain	Genotype	Source
CH2016	X90 *(DE3) Δrna ΔslyD::kan* Rif^R Kan^R	170
CH3778	MG1655 *ΔwzbΔarfB bamA(Δ2014-2043)*	8
CH7157	X90 *ΔclpXΔclpA::kan* Rif^R Kan^R	169
CH4119	X90 *(DE3) prfB(flag)* Rif^R	172
CH2183	X90 *ssrA(DD)-kan* Rif^R Kan^R	173
X90	F' *lacIq lac' pro'/ara D(lac-pro) nal1 argE(Am) rifr thi-1.* Rif^R	-
CH7286	MG1655 *Δwzb::kan* Kan^R	17

Abbreviations: AmpR , ampicillin-resistant; CmR , chloramphenicol-resistant; KanR , kanamycin-resistance; RifR , rifampicin-resistant; TetR , tetracycline-resistant; TpR , trimethoprim-resistant

Table 4. Plasmids

Plasmid	Genotype	Source
pCH1764	pMCSG63::*H6-TEV-cdiA-CT-cdiI (C. rodentium* DBS100*),* IPTG inducible expression with T7 promoter for purification, Amp^R	This Study
pCH2005	Constitutive expression of chimeric $cdiA^{EC93}$-CT^{UCI49} and $cdiI^{UCI49}$, Amp^R	This Study
pCH2848	pCH450::*cdiA-CT-cdiI-DAS* (*E. cloacae* UCI49), Arabinose Inducible Degradation Construct, Tet^R	This Study
pCH8829	pCH450::*cdiA-CT-cdiI-DAS* (*E. cloacae* UCI49) (C205A), Arabinose Inducible Degradation Construct, Tet^R	This Study
pCH8831	pMCSG63::*H6-TEV-ToxinDomain-cdiI (C205A) (E. cloacae* UCI49*),* IPTG inducible expression with T7 promoter for purification, includes UCI49 toxin domain, Amp^R	This Study
pCH8538	pMCSG63::*H6-TEV-CdiA-CT-cdiI (E. cloacae* UCI49*),* IPTG inducible expression with T7 promoter for purification, Amp^R	This Study
pCH8839	pMCSG63::*H6-TEV-ToxinDomain-(C205A) (E. cloacae* UCI49*),* IPTG inducible expression with T7 promoter for purification, Amp^R	This Study
pCH8851	pMCSG63::*H6-TEV-ToxinDomain-cdiI (E. cloacae* UCI49*),* IPTG inducible expression with T7 promoter for purification, includes UCI49 toxin domain, Amp^R	This Study
pCH138	pTrc::*rbsK1-6*, IPTG-inducible expression of *rbsK1-6* (V72G), Amp^R	173
pCH8907	pTrc::*ribD*, IPTG-inducible expression of *ribD,* Amp^R	This Study
pCH8908	pCH405D::*ribU* (B. subtilis 168) constitutive expression of *ribU*, Tet^R	This Study

Abbreviations: AmpR , ampicillin-resistant; CmR , chloramphenicol-resistant; KanR , kanamycin-resistance; RifR , rifampicin-resistant; TetR , tetracycline-resistant; TpR , trimethoprim-resistant

Table 5. Oligonucleotides

Oligo Number	Name	Sequence	Description	Source
CH5760	UCI49-C205A-for	5'- TTG TAC GGA TGC CTC AGA TAT CG -3'	Forward oligo to introduce the C205A mutation into cdiA-CT(UCI49)	This Study
CH5795	UCI49-TEV-S156-Kpn-for	5'- TTT GGT ACC GAG AAC CTG TAC TTC CAA GGT TCT CCT TCA ATG GAT GAT CTT TTC -3'	Forward oligo to clone the toxin domain of UCI49 into an NT-H6 pMCSG63 construct	This Study
CH5796	UCI49-Tox-Xho-rev	5'- TTT CTC GAG TTA TTT TAA CCC CTG TAA TTT ATC AGA G -3'	Reverse primer to clone the toxin domain of UCI49 into an NT-H6 pMCSG63 construct	This Study
CH5838	UCI49-cdiI-Xho-rev	5'- TTT CTC GAG TTA TGC ATC ATA TCC AGC ATT TTT G -3'	Reverse primer to clone UCI49 cdiA-CT-cdiI into an NT-H6 pMCSG63 construct	This Study
CH5910	UCI49-cdiI-Eco-for	5'- TTT GAA TTC ATG TTT CCG ATA GGT AAG AAA G -3'	Forward primer to clone the immunity gene of UCI49 into a pCH400 series plasmid	This Study
CH4734	MGH20/UCI49C-Kpn/Nco-for	5'- TTT GGT ACC ATG GTT GAG AAT AAC TCG CTG AG -3'	Forward primer for cloning S611 UCI49-CT into the CdiA(EC93) inhibitor chimera and generation of the CdiA-CT-CdiI-DAS UCI49 construct with pCH450	This Study
CH4738	UCI49-cdiI-Spe-rev	5'- TTT ACT AGT TGC ATC ATA TCC AGC ATT T -3'	Reverse primer for generation of the CdiA-CT-CdiI-DAS UCI49 construct with pCH450	This Study
CH5741	UCI49-CT-Kpn-for	5'- TTT GGT ACC GAG AAC CTG TAC TTC CAA TCG CTG AGT GTC GGT ATA CAG G -3'	Forward oligo to clone the UCI49 cdiA-CT into an NT-H6 pMCSG63 construct	This Study
CH5915	ribD-Kpn-for	5'- TTT GGT ACC ATG CAG GAC GAG TAT TAC -3'	forward to amplify ribD from K-12, with native GTG start changed to ATG	This Study
CH5917	ribD-Xho-rev	5'- TTT CTC GAG TCA TGC ACC CAC TAA ATG CAG -3'	reverse to amplify ribD from K-12. Contains stop codon.	This Study
CH5918	fmnP-Kpn-for	5'- TTT GGT ACC ATG AAA GTA AAA AAA TTA GTT GTG GTC -3'	forward to amplify fmnP(ribU) from B. subtilis 168. Native GTG start changed to ATG	This Study
CH5919	fmnP-Xho-rev	5'- TTT CTC GAG TTA ATG GAT ATG TGC ACT TGC -3'	reverse to amplify fmnP(ribU) from B. subtilis 168 for cloning into pCH405D.	This Study

Prediction of Structural Homology and Modeling of the CdiA-CT^{UCI49} Proposed Active Site

Submission of the CdiA-CT^{UCI49} protein sequence to AlphaFold2 yielded a predicted .pdb file, which was then submitted to the EMBL Dali Protein Structure Comparison Server (http://ekhidna2.biocenter.helsinki.fi/dali/) . The top 10 matches of this search from the PDB-

90 output were selected for inclusion. Additionally, the AlphaFold2-predicted model of CdiA-CT^{UCI49} was imported into PyMol and illustrated as a secondary structure cartoon. Selected residues were illustrated as "sticks", colored by element.

Internal Expression and Growth Curves of cdiA-CT^{UCI49} Derivatives

Expression of *cdiA-CT^{UCI49}* or *cdiA-$CT^{UCI49\ C205A}$* was performed by first generating a construct consisting of the respective cognate *cdiA-CT^{UCI49}-cdiI^{UCI49}* pair in a pCH450-DAS backbone plasmid (Tet^R). This plasmid introduces a pBAD arabinose inducible promoter, and an ssrA(DAS) tag at the 3' end of the immunity gene. Translation of this sequence generates a suboptimal degradation tag at the C-terminus of CdiI. These constructs, stored in strains CH2848 and CH8829 were transformed into wild type CH7286 cells. After ice-cold incubation of cells and plasmid and heat shock at 42˚C, cells were recovered in LB and 0.8% glucose for 1 hour at 37˚C. After recovery, cells were pelleted, resuspended in a small volume of LB, then plated on LB-agar plates supplemented with 20 µg/mL tetracycline and either 0.4% glucose or 0.2% arabinose. Plates were incubated overnight at 37˚C.

The next day, transformants plated on 0.4% glucose were harvested with a sterile swab and used to inoculate 60 mL of LB containing 15 µg/mL tetracycline to an optical density at 600 nm around ~0.05. The OD_{600} of the culture was measured every 30 minutes with a spectrophotometer while shaking at 37˚C. Once reaching an OD_{600} near 0.25 (or after 2 hours), cultures were split into two 20 mL fractions and were supplemented with either 0.2% arabinose (for induction) or 0.4% glucose (for suppression). OD_{600} was continually monitored over the course of 4-5 hours post-induction. For microscopy of cells during internal expression, samples were taken at 2 hours post-induction.

Native Purification of CdiA-CTs

Expression vectors were generated by cloning *cdiA-CT-cdiI* immunity pairs bearing the C205A mutation into *pMCSG63*, containing a N-terminal polyhistidine tag fusion under a T7 promoter. In some cases, only the effector domain of *cdiA-CT*^{UCI49} was included and the *cdiI* gene was omitted, as indicated. These plasmids were transformed into CH2016, an expression strain of X90 carrying the DE3 lysogen with T7 polymerase and knockouts of *rna* and *slyD*. Native purification constructs used here include CH1764, CH8538, CH8831, CH8842, CH8844, and CH8851. As an alternative to CH2016, constructs purified for purposes of western blotting against RF2 were purified in an X90 (DE3) *prfB*-FLAG background (CH8836-8840). Overnight cultures of the strains was grown in LB + 150 µg/mL ampicillin and used to inoculate 200 mL LB supplemented with 150 µg/mL ampicillin at OD_{600} = 0.1. After the optical density reached ~0.6, expression of CdiA-CT was induced by addition of 1.5 mM isopropyl ß-D-1-thiogalactopyranoside (IPTG). After 2 hours of induction, cells were harvested by centrifugation at 6,000 rpm for 10 minutes and resuspended in 10 mL of 20 mM Tris-HCl pH 7.5, 500 mM NaCl, 30 mM imidazole (wash buffer). After centrifugation at 10,000 rpm for 10 minutes, clarified lysates were added to 30 µL Ni-NTA and incubated at 4˚C for 1 hour with rotating. Bound Ni-NTA protein-complexes were then collected by centrifugation and removal of supernatant, followed by two 10 mL washes in wash buffer. Then, Ni-NTA was added to an elution column and further washed with wash buffer. Finally, proteins were eluted in successive 200 µL volumes of wash buffer supplemented with 250 mM Imidazole. Elutions were assayed with Bradford reagent and combined, followed by loading of 12 µL of elution in SDS-PAGE and electrophoresis at 110 V for 1 hour. Gels were either stained with Coomassie R-250, or subjected to western blotting (see below).

Western Blotting

SDS-PAGE gels destined for western blots were first incubated in transfer buffer (Tris-Glycine + 20% methanol) and sandwiched between filter paper, stacked upon a PVDF membrane in the transfer apparatus. Transferring occurred at 17 V for 1 hour, followed by blocking of the PVDF membrane in 30 mL PBS + 6 g of milk powder for 30 minutes. The desired antibody (anti-FLAG or anti-RF1 in Figure 3A and anti-SsrA(DD) in Figure 3B) at a 1:20,000 dilution was then incubated with the membrane at 4˚C overnight. The next day, three washes were performed using 30 mL PBS, followed by 1 hour of incubation with HRP-conjugated secondary antibody (anti-mouse for anti-FLAg and anti-rabbit for anti-RF1 and anti-SsrA(DD)). Three more washes were then performed with 30 mL PBS, and the blotted membrane was imaged by addition of chemiluminescent substrate luminol and H_2O_2. Blots were exposed for 1 minute during imaging and adjusted using ImageJ.

Competition Co-Cultures

Overnight cultures of targets were grown in 50 µg/mL kanamycin and inhibitors were grown in either grown in 150 µg/mL ampicillin (for pET-derivative inhibitors) or 60 µg/mL chloramphenicol (for pDAL879-derivate inhibitors). Overnight cultures were diluted to OD_{600} = 0.1 in fresh LB without antibiotics and grown with shaking for 1.5 hours at 37˚C. The optical density of each fresh culture was then measured using a spectrophotometer and target cells and inhibitors were mixed by resuspending each to OD_{600} = 0.1 in 10 mL of LB. Co-cultures were incubated in baffled 125 mL flasks at 37˚C for 3 hours (unless otherwise stated) with shaking. Prior to incubation, a time = 0 point was taken by diluting cells 10-fold into M9, followed by further 10-fold serial dilution for spot plating. Aliquots were again taken at the final time point

and serial diluted, followed by spotting 10 µL of dilution on LB-agar containing either kanamycin (50 µg/mL) or ampicillin (150 µg/mL) to measure target and inhibitor CFU/mL. Competitive indices were calculated as the ratio of inhibitor:target CFU/mL at the final time point divided by the ratio of inhibitor:target CFU/mL at the initial time point.

SsrA(DD) Accumulation Assay

Co-culture competitions were set up as described above, except inhibitors and targets were instead resuspended at OD_{600} = 0.3. Inhibitors were either CH2005 cells or CH7092 (mock inhibitor) cells. In the case of addition of 100 µg/mL streptomycin, no inhibitor cells were added. At the indicated time points, 2 mL of cells were pelleted and lysed in urea lysis buffer, followed by a freeze-thaw cycle at -80˚C and centrifugation to harvest clarified lysate. Lysates were normalized with Bradford reagent by measurement of OD_{595} and dilution calculation (loaded volume = $1.5/A_{595}$). Samples were loaded in SDS-PAGE and subjected either to Coomassie staining or western blot as described above. Additionally, at each time point aliquots were taken and serially diluted to calculate CFU/mL of target CH8868 cells.

V. Conclusion

Contact dependent inhibition (CDI) type Vb secretion systems play important roles in interbacterial competition and likely help shape multicellular bacterial communities in diverse ecological niches[15,165]. Given their linkage to pathogenesis factors in the genome[16], the study of CDI systems may also yield insight into the physiology of human pathogens. Beyond effects in physiology, CdiA, in complex with CdiB, functions as a controlled molecular machine, using intrinsic and extrinsic mechanisms to adopt a variety of defined conformations which mediate delivery of the effector cargo. In the past 15 years, some aspects of CDI have become well understood, including the domain boundaries of CdiA and the general functions of each domain. However, certain mechanistic details have yet to be worked out and pose barriers to the complete engineering and repurposing of CDI systems. For example, while the receptor binding domain is known to interact with outer membrane epitopes[12,14,81] and is modular with other CDI receptor binding domains[8], the mechanism by which it causes resumption of secretion is not fully understood. Additionally, the ability of CdiA to utilize receptor binding domains from other proteins has not been explored. It's likely that further understanding of the mechanisms of native CDI systems is necessary before performing this kind of engineering. Once understood, expression of chimeric CDI proteins with receptor binding domains grafted from completely heterologous systems could function as valuable tools.

Another important and mysterious step in CDI that was touched upon in Chapter 2 is receptor recognition and the translocation mechanism of the cytoplasm entry domains of CdiA-CTs across the inner membrane of target cells. Given the broad genetic diversity of the currently characterized entry domains and the observation that CdiA-CT entry domains are limited in "host range"[96], it's possible that CDI provides selective pressures towards the

evolution of periplasmic regions in the inner membrane. While components exposed to the extracellular surface are constantly under selective pressures to avoid recognition by host immune systems and phages, proteins in the periplasm do not appear subject to the same pressures. CDI, in combination with other bacteriocin systems, could thus in part be responsible for divergence of these regions.

Some work has shown that inner membrane translocation appears to universally depend upon the proton motive force[82], suggesting a universal or similar mechanism of translocation between genetically and structurally distinct domains. It's possible that interaction with the periplasmic epitopes of one of the identified inner membrane proteins simply localizes CdiA-CT to the surface of the membrane, whereby the protein interacts with either the lipid bilayer and possibly with the transmembrane helices of the recognized proteins to pass through the membrane. This mechanism would imply a relatively hydrophobic surface of the entry domain, which may be facilitated through a molten-globule-like conformation as has been observed for a cytoplasm entry domain targeting MetI[116]. However, the mechanism could also imply that the C-terminal effector domain would need to share these properties to avoid the immense energetic cost of crossing an aliphatic barrier in a channel-independent manner. The requirement of co-factors for some CDI effectors to increase thermodynamic stability[88,118] may represent a driving force for net flow of CdiA-CT across the membrane. Additionally, an affinity of the entry domain for membranes could result in anchoring of CdiA-CT to the inner leaflet of the cytoplasmic membrane, limiting the ability of the effector domain to freely diffuse and find its substrates. Uncovering of the precise mechanistic details regarding this step in CDI could have powerful implications for the delivery of other effectors such as colicins, as well as the rational design of new proteins which deliver cargoes across membranes.

Perhaps the most challenging domain of all to characterize is the toxic effector domain at the extreme C-terminus of CdiA. The high degree of sequence polymorphism, combined with the highly specific and distinct activities of each of the currently characterized effectors makes characterizing these domains especially difficult. However, they are some of the most fascinating proteins, having evolved to specifically perturb distinct cellular functions and inhibit growth. Beyond the currently characterized nucleases[9,19,93] and pore formers[84], *in silico* work predicts homology of some families of uncharacterized *cdiA-CT*s to deaminases[166], methyltransferases, and proteases. In fact, the actual diversity of effector activities likely stretches substantially beyond that available in current sequence space.

This thesis covers functions of CdiA-CTs spanning across both the cytoplasm entry domains and effector domains of unique CDI systems. In chapter 2, novel inner membrane proteins were identified to be associated with previously uncharacterized CdiA-CT entry domains. Transposon mutagenesis and selection of mutagenized pools with chimeric CDI systems bearing various cytopolasm entry domains revealed that AroP, MtlA, AmpG, and YajC are associated with the import of distinct CdiA-CTs. Based upon previous findings, the native cellular functions of these proteins are unlikely to contribute to the mechanisms of translocation[18], and they may instead act as permissive receptors for target cell recognition and localization of CdiA-CT to the inner membrane. Additionally, the previously identified inner membrane proteins GltJK and FtsH[18] were identified to be associated with novel CdiA-CT entry domain sequences and structures. It appears likely that these entry domains recognize distinct epitopes on the periplasmic surfaces of these inner membrane proteins compared to the previously identified effectors.

In Chapters 3 and 4, I performed experiments attempting to characterize CdiA-CTs from *Enterobacter cloacae* S611 and UCI49 respectively. CdiA-CT^{S611} is predicted to have a *S*-adenosylmethionine (SAM) binding domain and could perform methyltransfer to cellular substrates in order to exhibit toxicity. Notably, this domain was not found to function in a similar manner to phage encoded SAM-binding domains, which act as SAMases. While the mechanism underlying this toxic effector remains elusive, an involvement with SAM and therefore methyltransferase activity, seems likely. The effector domain of CdiA-CT^{UCI49} is predicted resemble protein glutaminases and cysteine proteases. Consistent with this prediction, the domain contains a Cys-Asp-His catalytic triad, and mutation of the presumed active cysteine completely abrogates inhibitory activity. Co-purification of the inactive mutant of this CdiA-CT revealed multiple promising substrates, including protein release factor 2 (RF2) and the riboflavin biosynthetic enzyme RibD. However, it is not yet clear that either of these proteins are associated with CdiA-CT^{UCI49}, and attempts to rescue growth or probe for specific phenotypes associated with disruption of these proteins have failed. It remains possible that one of these proteins may act as a co-factor for toxicity. Further characterization of both CdiA-CT^{S611} and CdiA-CT^{UCI49} is necessary before any insight is to be gained into their mechanisms of growth inhibition, but both remain promising effectors for study.

References

1. Coker JA. Recent advances in understanding extremophiles [version 1; peer review: 2 approved]. *F1000Res*. 2019;8. doi:10.12688/F1000RESEARCH.20765.1/DOI
2. Moran NA. Symbiosis. *Current Biology*. 2006;16(20):R866-R871. doi:10.1016/J.CUB.2006.09.019
3. Green ER, Mecsas J. Bacterial Secretion Systems: An Overview. *Microbiol Spectr*. 2016;4(1). doi:10.1128/MICROBIOLSPEC.VMBF-0012-2015
4. Bernstein HD. Type V Secretion in Gram-Negative Bacteria. *EcoSal Plus*. 2019;8(2). doi:10.1128/ECOSALPLUS.ESP-0031-2018/ASSET/93D07053-8763-49A3-B549-EB3398297868/ASSETS/GRAPHIC/PSIB-0008-2018_FIG_002.JPG
5. Hachani A, Wood TE, Filloux A. Type VI secretion and anti-host effectors. *Curr Opin Microbiol*. 2016;29:81-93. doi:10.1016/J.MIB.2015.11.006
6. Costa TRD, Felisberto-Rodrigues C, Meir A, et al. Secretion systems in Gram-negative bacteria: structural and mechanistic insights. *Nat Rev Microbiol*. 2015;13(6):343-359. doi:10.1038/NRMICRO3456
7. Willett JLE, Ruhe ZC, Goulding CW, Low DA, Hayes CS. Contact-Dependent Growth Inhibition (CDI) and CdiB/CdiA Two-Partner Secretion Proteins. *Journal of Molecular Biology*. 2015;427(23):3754-3765. doi:10.1016/J.JMB.2015.09.010
8. Ruhe ZC, Nguyen JY, Xiong J, et al. CdiA effectors use modular receptor-binding domains to recognize target bacteria. *mBio*. 2017;8(2). doi:10.1128/MBIO.00290-17
9. Webb JS, Nikolakakis KC, Willett JLE, Aoki SK, Hayes CS, Low DA. Delivery of CdiA nuclease toxins into target cells during contact-dependent growth inhibition. *PLoS One*. 2013;8(2). doi:10.1371/JOURNAL.PONE.0057609
10. Aoki SK, Pamma R, Hernday AD, Bickham JE, Braaten BA, Low DA. Microbiology: Contact-dependent inhibition of growth in Escherichia coli. *Science (1979)*. 2005;309(5738):1245-1248. doi:10.1126/SCIENCE.1115109/SUPPL_FILE/AOKI-SOM.PDF
11. Aoki SK, Diner EJ, de Roodenbeke CTK, et al. A widespread family of polymorphic contact-dependent toxin delivery systems in bacteria. *Nature 2010 468:7322*. 2010;468(7322):439-442. doi:10.1038/nature09490
12. Beck CM, Willett JLE, Cunningham DA, Kim JJ, Low DA, Hayes CS. CdiA Effectors from Uropathogenic Escherichia coli Use Heterotrimeric Osmoporins as Receptors to Recognize Target Bacteria. *PLoS Pathog*. 2016;12(10). doi:10.1371/JOURNAL.PPAT.1005925
13. Ruhe ZC, Nguyen JY, Chen AJ, Leung NY, Hayes CS, Low DA. CDI Systems Are Stably Maintained by a Cell-Contact Mediated Surveillance Mechanism. *PLoS Genet*. 2016;12(6). doi:10.1371/JOURNAL.PGEN.1006145
14. Aoki SK, Malinverni JC, Jacoby K, et al. Contact-dependent growth inhibition requires the essential outer membrane protein BamA (YaeT) as the receptor and the inner membrane transport protein AcrB. *Molecular Microbiology*. 2008;70(2):323-340. doi:10.1111/J.1365-2958.2008.06404.X
15. Anderson MS, Garcia EC, Cotter PA. The Burkholderia bcpAIOB Genes Define Unique Classes of Two-Partner Secretion and Contact Dependent Growth Inhibition Systems. *PLOS Genetics*. 2012;8(8):e1002877. doi:10.1371/JOURNAL.PGEN.1002877

16. Rojas CM, Ham JH, Deng WL, Doyle JJ, Collmer A. HecA, a member of a class of adhesins produced by diverse pathogenic bacteria, contributes to the attachment, aggregation, epidermal cell killing, and virulence phenotypes of Erwinia chrysanthemi EC16 on Nicotiana clevelandii seedlings. *Proc Natl Acad Sci U S A*. 2002;99(20):13142-13147. doi:10.1073/PNAS.202358699
17. Ruhe ZC, Subramanian P, Song K, et al. Programmed Secretion Arrest and Receptor-Triggered Toxin Export during Antibacterial Contact-Dependent Growth Inhibition. *Cell*. 2018;175(4):921-933.e14. doi:10.1016/J.CELL.2018.10.033
18. Willett JLE, Gucinski GC, Fatherree JP, Low DA, Hayes CS. Contact-dependent growth inhibition toxins exploit multiple independent cell-entry pathways. *Proc Natl Acad Sci U S A*. 2015;112(36):11341-11346. doi:10.1073/PNAS.1512124112/SUPPL_FILE/PNAS.201512124SI.PDF
19. Michalska K, Quan Nhan D, Willett JLE, et al. Functional plasticity of antibacterial EndoU toxins. *Mol Microbiol*. 2018;109(4):509-527. doi:10.1111/MMI.14007
20. Liu G, Topping TB, Randall LL. Physiological role during export for the retardation of folding by the leader peptide of maltose-binding protein. *Proc Natl Acad Sci U S A*. 1989;86(23):9213-9217. doi:10.1073/PNAS.86.23.9213
21. den Blaauwen T, Terpetschnig E, Lakowicz JR, Driessen AJM. Interaction of SecB with soluble SecA. *FEBS Lett*. 1997;416(1):35-38. doi:10.1016/S0014-5793(97)01142-3
22. Zhou J, Xu Z. Structural determinants of SecB recognition by SecA in bacterial protein translocation. *NATURE STRUCTURAL BIOLOGY*. 2003;10. doi:10.1038/nsb980
23. Oswald J, Njenga R, Natriashvili A, Sarmah P, Koch HG. The Dynamic SecYEG Translocon. *Frontiers in Molecular Biosciences*. 2021;8:248. doi:10.3389/FMOLB.2021.664241/BIBTEX
24. Tsirigotaki A, de Geyter J, Šoštarić N, Economou A, Karamanou S. Protein export through the bacterial Sec pathway. *Nature Reviews Microbiology 2016 15:1*. 2016;15(1):21-36. doi:10.1038/nrmicro.2016.161
25. Crane JM, Randall LL. The Sec System: Protein Export in Escherichia coli . *EcoSal Plus*. 2017;7(2). doi:10.1128/ECOSALPLUS.ESP-0002-2017/ASSET/DA07B125-C2EC-49F9-9BF6-947CD0CB3BF7/ASSETS/GRAPHIC/ESP-0002-2017_FIG_011.JPG
26. Economou A, Wickner W. SecA promotes preprotein translocation by undergoing ATP-driven cycles of membrane insertion and deinsertion. *Cell*. 1994;78(5):835-843. doi:10.1016/S0092-8674(94)90582-7
27. Tsukazaki T, Mori H, Echizen Y, et al. Structure and function of a membrane component SecDF that enhances protein export. *Nature*. 2011;474(7350):235-238. doi:10.1038/NATURE09980
28. Steinberg R, Knüpffer L, Knüpffer K, Origi A, Asti R, Koch HG. Co-translational protein targeting in bacteria. *FEMS Microbiology Letters*. 2018;365:95. doi:10.1093/femsle/fny095
29. Kiefer D, Kuhn A. YidC-mediated membrane insertion. *FEMS Microbiol Lett*. 2018;365(12). doi:10.1093/FEMSLE/FNY106
30. Beckwith J. The Sec-dependent pathway. *Research in Microbiology*. 2013;164(6):497-504. doi:10.1016/J.RESMIC.2013.03.007

31. Thomas S, Holland IB, Schmitt L. The Type 1 secretion pathway - The hemolysin system and beyond. *Biochimica et Biophysica Acta - Molecular Cell Research*. 2014;1843(8):1629-1641. doi:10.1016/J.BBAMCR.2013.09.017
32. Masi M, Wandersman C. Multiple signals direct the assembly and function of a type 1 secretion system. *Journal of Bacteriology*. 2010;192(15):3861-3869. doi:10.1128/JB.00178-10
33. Thanabalu T, Koronakis E, Hughes C, Koronakis V. Substrate-induced assembly of a contiguous channel for protein export from E.coli: reversible bridging of an inner-membrane translocase to an outer membrane exit pore. *The EMBO Journal*. 1998;17(22):6487-6496.
34. Thomassin JL, Santos Moreno J, Guilvout I, Tran Van Nhieu G, Francetic O. The trans-envelope architecture and function of the type 2 secretion system: new insights raising new questions. *Molecular Microbiology*. 2017;105(2):211-226. doi:10.1111/MMI.13704
35. Douzi B, Ball G, Cambillau C, Tegoni M, Voulhoux R. Deciphering the Xcp Pseudomonas aeruginosa Type II Secretion Machinery through Multiple Interactions with Substrates. *The Journal of Biological Chemistry*. 2011;286(47):40792. doi:10.1074/JBC.M111.294843
36. Reichow SL, Korotkov K v., Gonen M, et al. The binding of cholera toxin to the periplasmic vestibule of the type II secretion channel. *Channels*. 2011;5(3):215. doi:10.4161/CHAN.5.3.15268
37. Korotkov K v., Sandkvist M. Architecture, Function, and Substrates of the Type II Secretion System. *EcoSal Plus*. 2019;8(2). doi:10.1128/ECOSALPLUS.ESP-0034-2018/ASSET/3DA4A312-6B77-4CDC-A334-E66D11299A0C/ASSETS/GRAPHIC/PSIB-0022-2018_FIG_003.GIF
38. Naskar S, Hohl M, Tassinari M, Low HH. The structure and mechanism of the bacterial type II secretion system. *Molecular Microbiology*. 2021;115(3):412-424. doi:10.1111/MMI.14664
39. Horna G, Ruiz J. Type 3 secretion system of Pseudomonas aeruginosa. *Microbiological Research*. 2021;246:126719. doi:10.1016/J.MICRES.2021.126719
40. Diepold A, Armitage JP. Type III secretion systems: the bacterial flagellum and the injectisome. *Philos Trans R Soc Lond B Biol Sci*. 2015;370(1679). doi:10.1098/RSTB.2015.0020
41. Barison N, Gupta R, Kolbe M. A sophisticated multi-step secretion mechanism: how the type 3 secretion system is regulated. *Cellular Microbiology*. 2013;15(11):1809-1817. doi:10.1111/CMI.12178
42. Galán JE, Wolf-Watz H. Protein delivery into eukaryotic cells by type III secretion machines. *Nature 2006 444:7119*. 2006;444(7119):567-573. doi:10.1038/nature05272
43. Fulde M, van Vorst K, Zhang K, et al. SPI2 T3SS effectors facilitate enterocyte apical to basolateral transmigration of Salmonella-containing vacuoles in vivo. *Gut Microbes*. 2021;13(1). doi:10.1080/19490976.2021.1973836
44. Lederberg J, Tatum EL. Gene recombination in Escherichia coli. *Nature*. 1946;158(4016):558. doi:10.1038/158558A0
45. Souza DP, Oka GU, Alvarez-Martinez CE, et al. Bacterial killing via a type IV secretion system. *Nature Communications 2015 6:1*. 2015;6(1):1-9. doi:10.1038/ncomms7453

46. Low HH, Gubellini F, Rivera-Calzada A, et al. Structure of a type IV secretion system. *Nature 2014 508:7497*. 2014;508(7497):550-553. doi:10.1038/nature13081
47. Costa TRD, Harb L, Khara P, Zeng L, Hu B, Christie PJ. Type IV secretion systems: Advances in structure, function, and activation. *Mol Microbiol*. 2021;115(3):436-452. doi:10.1111/MMI.14670
48. Cover TL, Lacy DB, Ohi MD. The Helicobacter pylori Cag Type IV Secretion System. *Trends Microbiol*. 2020;28(8):682-695. doi:10.1016/J.TIM.2020.02.004
49. Aksyuk AA, Leiman PG, Kurochkina LP, et al. The tail sheath structure of bacteriophage T4: a molecular machine for infecting bacteria. *The EMBO Journal*. 2009;28(7):821. doi:10.1038/EMBOJ.2009.36
50. Coulthurst S. The Type VI secretion system: A versatile bacterial weapon. *Microbiology (United Kingdom)*. 2019;165(5):503-515. doi:10.1099/MIC.0.000789/CITE/REFWORKS
51. Jana B, Salomon D. Type VI secretion system: a modular toolkit for bacterial dominance. *Future Microbiol*. 2019;14:1451-1463. doi:10.2217/FMB-2019-0194
52. Crisan C v., Hammer BK. The Vibrio cholerae type VI secretion system: toxins, regulators and consequences. *Environ Microbiol*. 2020;22(10):4112-4122. doi:10.1111/1462-2920.14976
53. Clemens DL, Lee BY, Horwitz MA. The Francisella Type VI Secretion System. *Front Cell Infect Microbiol*. 2018;8(APR). doi:10.3389/FCIMB.2018.00121
54. Jana B, Salomon D. Type VI secretion system: a modular toolkit for bacterial dominance. *Future Microbiol*. 2019;14:1451-1463. doi:10.2217/FMB-2019-0194/ASSET/IMAGES/LARGE/FIGURE2.JPEG
55. Fan E, Chauhan N, Udatha DBRKG, Leo JC, Linke D. Type V Secretion Systems in Bacteria. *Microbiology Spectrum*. 2016;4(1). doi:10.1128/MICROBIOLSPEC.VMBF-0009-2015
56. Meuskens I, Saragliadis A, Leo JC, Linke D. Type V secretion systems: An overview of passenger domain functions. *Frontiers in Microbiology*. 2019;10(MAY):1163. doi:10.3389/FMICB.2019.01163/BIBTEX
57. Leo JC, Grin I, Linke D. Type V secretion: mechanism(s) of autotransport through the bacterial outer membrane. *Philosophical Transactions of the Royal Society B: Biological Sciences*. 2012;367(1592):1088-1101. doi:10.1098/RSTB.2011.0208
58. Baud C, Hodak H, Willery E, et al. Role of DegP for two-partner secretion in Bordetella. *Molecular Microbiology*. 2009;74(2):315-329. doi:10.1111/J.1365-2958.2009.06860.X
59. Oliver DC, Huang G, Nodel E, Pleasance S, Fernandez RC. A conserved region within the Bordetella pertussis autotransporter BrkA is necessary for folding of its passenger domain. *Mol Microbiol*. 2003;47(5):1367-1383. doi:10.1046/J.1365-2958.2003.03377.X
60. st. Geme JW, Cutter D. The Haemophilus influenzae Hia adhesin is an autotransporter protein that remains uncleaved at the C terminus and fully cell associated. *J Bacteriol*. 2000;182(21):6005-6013. doi:10.1128/JB.182.21.6005-6013.2000
61. Emsley P, Charles IG, Fairweather NF, Isaacs NW. Structure of Bordetella pertussis virulence factor P.69 pertactin. *Nature*. 1996;381(6577):90-92. doi:10.1038/381090A0
62. Mistry D, Stockley RA. IgA1 protease. *The International Journal of Biochemistry & Cell Biology*. 2006;38(8):1244. doi:10.1016/J.BIOCEL.2005.10.005

63. Meuskens I, Saragliadis A, Leo JC, Linke D. Type V secretion systems: An overview of passenger domain functions. *Frontiers in Microbiology*. 2019;10(MAY):1163. doi:10.3389/FMICB.2019.01163/BIBTEX
64. Mühlenkamp M, Oberhettinger P, Leo JC, Linke D, Schütz MS. Yersinia adhesin A (YadA) - Beauty & beast. *International Journal of Medical Microbiology*. 2015;305(2):252-258. doi:10.1016/J.IJMM.2014.12.008
65. Simmerman RF, Dave AM, Bruce BD. Structure and function of POTRA domains of Omp85/TPS superfamily. *Int Rev Cell Mol Biol*. 2014;308:1-34. doi:10.1016/B978-0-12-800097-7.00001-4
66. Schleiff E, Maier UG, Becker T. Omp85 in eukaryotic systems: one protein family with distinct functions. *Biol Chem*. 2011;392(1-2):21-27. doi:10.1515/BC.2011.005
67. Gentle IE, Burri L, Lithgow T. Molecular architecture and function of the Omp85 family of proteins. *Molecular Microbiology*. 2005;58(5):1216-1225. doi:10.1111/j.1365-2958.2005.04906.x
68. Salacha R, Kovačić F, Brochier-Armanet C, et al. The Pseudomonas aeruginosa patatin-like protein PlpD is the archetype of a novel Type V secretion system. *Environmental Microbiology*. 2010;12(6):1498-1512. doi:10.1111/J.1462-2920.2010.02174.X
69. Leibiger K, Schweers JM, Schütz M. Biogenesis and function of the autotransporter adhesins YadA, intimin and invasin. *Int J Med Microbiol*. 2019;309(5):331-337. doi:10.1016/J.IJMM.2019.05.009
70. Leo JC, Oberhettinger P, Schütz M, Linke D. The inverse autotransporter family: Intimin, invasin and related proteins. *International Journal of Medical Microbiology*. 2015;305(2):276-282. doi:10.1016/J.IJMM.2014.12.011
71. Guerin J, Botos I, Zhang Z, Lundquist K, Gumbart JC, Buchanan SK. Structural insight into toxin secretion by contact-dependent growth inhibition transporters. *Elife*. 2020;9:1-22. doi:10.7554/ELIFE.58100
72. Ur Rahman S, Arenas J, Öztürk H, Dekker N, van Ulsen P. The polypeptide transport-associated (POTRA) domains of TpsB transporters determine the system specificity of two-partner secretion systems. *Journal of Biological Chemistry*. 2014;289(28):19799-19809. doi:10.1074/JBC.M113.544627
73. Guérin J, Baud C, Touati N, et al. Conformational dynamics of protein transporter FhaC: Large-scale motions of plug helix. *Molecular Microbiology*. 2014;92(6):1164-1176. doi:10.1111/MMI.12585/SUPINFO
74. Clantin B, Delattre AS, Rucktooa P, et al. Structure of the membrane protein FhaC: A member of the Omp85-TpsB transporter superfamily. *Science (1979)*. 2007;317(5840):957-961. doi:10.1126/SCIENCE.1143860
75. Maier T, Clantin B, Gruss F, et al. Conserved Omp85 lid-lock structure and substrate recognition in FhaC. *Nature Communications 2015 6:1*. 2015;6(1):1-9. doi:10.1038/ncomms8452
76. Delattre AS, Clantin B, Saint N, Locht C, Villeret V, Jacob-Dubuisson F. Functional importance of a conserved sequence motif in FhaC, a prototypic member of the TpsB/Omp85 superfamily. *The FEBS Journal*. 2010;277(22):4755-4765. doi:10.1111/J.1742-4658.2010.07881.X
77. Guédin S, Willery E, Tommassen J, et al. Novel topological features of FhaC, the outer membrane transporter involved in the secretion of the Bordetella pertussis

filamentous hemagglutinin. *Journal of Biological Chemistry*. 2000;275(39):30202-30210. doi:10.1074/JBC.M005515200
78. Clantin B, Hodak H, Willery E, Locht C, Jacob-Dubuisson F, Villeret V. The crystal structure of filamentous hemagglutinin secretion domain and its implications for the two-partner secretion pathway. *Proc Natl Acad Sci U S A*. 2004;101(16):6194-6199. doi:10.1073/PNAS.0400291101/SUPPL_FILE/00291FIG7.JPG
79. Kim S, Malinverni JC, Sliz P, Silhavy TJ, Harrison SC, Kahne D. Structure and function of an essential component of the outer membrane protein assembly machine. *Science (1979)*. 2007;317(5840):961-964. doi:10.1126/SCIENCE.1143993/SUPPL_FILE/KIMS.SOM.PDF
80. Delattre AS, Saint N, Clantin B, et al. Substrate recognition by the POTRA domains of TpsB transporter FhaC. *Mol Microbiol*. 2011;81(1):99-112. doi:10.1111/J.1365-2958.2011.07680.X
81. Halvorsen TM, Garza-Sánchez F, Ruhe ZC, et al. Lipidation of Class IV CdiA Effector Proteins Promotes Target Cell Recognition during Contact-Dependent Growth Inhibition. *mBio*. 2021;12(5). doi:10.1128/MBIO.02530-21/SUPPL_FILE/MBIO.02530-21-ST002.DOCX
82. Ruhe ZC, Nguyen JY, Beck CM, Low DA, Hayes CS. The proton-motive force is required for translocation of CDI toxins across the inner membrane of target bacteria. *Mol Microbiol*. 2014;94(2):466-481. doi:10.1111/MMI.12779
83. Jones AM, Virtanen P, Hammarlöf D, et al. Genetic Evidence for SecY Translocon-Mediated Import of Two Contact-Dependent Growth Inhibition (CDI) Toxins. *mBio*. 2021;12(1):1-14. doi:10.1128/MBIO.03367-20
84. Aoki SK, Webb JS, Braaten BA, Low DA. Contact-dependent growth inhibition causes reversible metabolic downregulation in Escherichia coli. *Journal of Bacteriology*. 2009;191(6):1777-1786. doi:10.1128/JB.01437-08/ASSET/94ABFA58-D59C-4950-AC3A-44EED9C05FEE/ASSETS/GRAPHIC/ZJB0060985500007.JPEG
85. Beck CM, Morse RP, Cunningham DA, et al. CdiA from Enterobacter cloacae delivers a toxic ribosomal RNase into target bacteria. *Structure*. 2014;22(5):707-718. doi:10.1016/J.STR.2014.02.012
86. Jones AM, Garza-Sánchez F, So J, Hayes CS, Low DA. Activation of contact-dependent antibacterial tRNase toxins by translation elongation factors. *Proc Natl Acad Sci U S A*. 2017;114(10):E1951-E1957. doi:10.1073/PNAS.1619273114/SUPPL_FILE/PNAS.201619273SI.PDF
87. Diner EJ, Beck CM, Webb JS, Low DA, Hayes CS. Identification of a target cell permissive factor required for contact-dependent growth inhibition (CDI). *Genes & Development*. 2012;26(5):515-525. doi:10.1101/GAD.182345.111
88. Johnson PM, Beck CM, Morse RP, et al. Unraveling the essential role of CysK in CDI toxin activation. *Proc Natl Acad Sci U S A*. 2016;113(35):9792-9797. doi:10.1073/PNAS.1607112113/SUPPL_FILE/PNAS.201607112SI.PDF
89. Tan K, Johnson PM, Stols L, et al. The structure of a contact-dependent growth-inhibition (CDI) immunity protein from Neisseria meningitidis MC58. *Acta Crystallogr F Struct Biol Commun*. 2015;71(Pt 6):702-709. doi:10.1107/S2053230X15006585
90. Morse RP, Nikolakakis KC, Willett JLE, et al. Structural basis of toxicity and immunity in contact-dependent growth inhibition (CDI) systems. *Proc Natl Acad Sci*

U S A. 2012;109(52):21480-21485. doi:10.1073/PNAS.1216238110/SUPPL_FILE/PNAS.201216238SI.PDF
91. Aoki SK, Poole SJ, Hayes CS, Low DA. Toxin on a stick. *http://dx.doi.org/104161/viru2416463*. 2011;2(4):356-359. doi:10.4161/VIRU.2.4.16463
92. Cascales E, Buchanan SK, Duché D, et al. Colicin biology. *Microbiol Mol Biol Rev*. 2007;71(1):158-229. doi:10.1128/MMBR.00036-06
93. Beck CM, Morse RP, Cunningham DA, et al. CdiA from Enterobacter cloacae Delivers a Toxic Ribosomal RNase into Target Bacteria. *Structure*. 2014;22(5):707-718. doi:10.1016/J.STR.2014.02.012
94. Batot G, Michalska K, Ekberg G, et al. The CDI toxin of Yersinia kristensenii is a novel bacterial member of the RNase A superfamily. *Nucleic Acids Res*. 2017;45(9):5013-5025. doi:10.1093/NAR/GKX230
95. Cuthbert BJ, Hayes CS, Goulding CW. Functional and Structural Diversity of Bacterial Contact-Dependent Growth Inhibition Effectors. *Front Mol Biosci*. 2022;9. doi:10.3389/FMOLB.2022.866854
96. Myers-Morales T, Sim MMS, DuCote TJ, Garcia EC. Burkholderia multivorans requires species-specific GltJK for entry of a contact-dependent growth inhibition system protein. *Mol Microbiol*. 2021;116(3):957-973. doi:10.1111/MMI.14783
97. Sennhauser G, Amstutz P, Briand C, Storchenegger O, Grütter MG. Drug export pathway of multidrug exporter AcrB revealed by DARPin inhibitors. *PLoS Biol*. 2007;5(1):0106-0113. doi:10.1371/JOURNAL.PBIO.0050007
98. Simon R, Priefer U, Puhl A. *A BROAD HOST RANGE MOBILIZATION SYfflM FOR IN VIVO GENRIC ENGINEERING: TRANSPOSON MUTAGENESIS IN GRAM NEGATIVE BAOERIA*.; 1983. http://www.nature.com/naturebiotechnology
99. Linton KJ, Higgins CF. The Escherichia coli ATP-binding cassette (ABC) proteins. *Molecular Microbiology*. 1998;28(1):5-13. doi:10.1046/J.1365-2958.1998.00764.X
100. Jumper J, Evans R, Pritzel A, et al. Highly accurate protein structure prediction with AlphaFold. *Nature 2021 596:7873*. 2021;596(7873):583-589. doi:10.1038/s41586-021-03819-2
101. Varadi M, Anyango S, Deshpande M, et al. AlphaFold Protein Structure Database: massively expanding the structural coverage of protein-sequence space with high-accuracy models. *Nucleic Acids Research*. 2022;50(D1):D439-D444. doi:10.1093/NAR/GKAB1061
102. Baba T, Ara T, Hasegawa M, et al. Construction of Escherichia coli K-12 in-frame, single-gene knockout mutants: the Keio collection. *Mol Syst Biol*. 2006;2. doi:10.1038/MSB4100050
103. Brown KD. Formation of Aromatic Amino Acid Pools in Escherichia coli K-12. *Journal of Bacteriology*. 1970;104(1):177-188. doi:10.1128/JB.104.1.177-188.1970
104. Chye ML, Pittard J. Transcription control of the aroP gene in Escherichia coli K-12: Analysis of operator mutants. *Journal of Bacteriology*. 1987;169(1):386-393. doi:10.1128/JB.169.1.386-393.1987
105. Cosgriff AJ, Pittard AJ. A topological model for the general aromatic amino acid permease, AroP, of Escherichia coli. *Journal of Bacteriology*. 1997;179(10):3317-3323. doi:10.1128/JB.179.10.3317-3323.1997

106. Cheng Q, Park JT. Substrate specificity of the AmpG permease required for recycling of cell wall anhydro-muropeptides. *Journal of Bacteriology*. 2002;184(23):6434-6436. doi:10.1128/JB.184.23.6434-6436.2002/ASSET/2BBB9BB3-4634-4BBE-83AE-0DE39A7BD28A/ASSETS/GRAPHIC/JB2320672001.JPEG
107. Jacobs C, Huang LJ, Bartowsky E, Normark S, Park JT. Bacterial cell wall recycling provides cytosolic muropeptides as effectors for beta-lactamase induction. *EMBO J*. 1994;13(19):4684-4694. doi:10.1002/J.1460-2075.1994.TB06792.X
108. Chahboune A, Decaffmeyer M, Brasseur R, Joris B. Membrane topology of the Escherichia coli AmpG permease required for recycling of cell wall anhydromuropeptides and AmpC β-lactamase induction. *Antimicrobial Agents and Chemotherapy*. 2005;49(3):1145-1149. doi:10.1128/AAC.49.3.1145-1149.2005/ASSET/418637BC-E302-4B06-BD05-1F669110CA1C/ASSETS/GRAPHIC/ZAC0030547530003.JPEG
109. Karzai AW, Roche ED, Sauer RT. The SsrA-SmpB system for protein tagging, directed degradation and ribosome rescue. *Nat Struct Biol*. 2000;7(6):449-455. doi:10.1038/75843
110. Sugiyama JE, Mahmoodian S, Jacobson GR. Membrane topology analysis of Escherichia coli mannitol permease by using a nested-deletion method to create mtlA-phoA fusions (bacterial phosphotransferase system/phoA fusions/membrane protein topology). *Proc Nati Acad Sci USA*. 1991;88:9603-9607.
111. Jacobson GR, Tanney LE, Kelly DM, Palman KB, Corn SB. Substrate and phospholipid specificity of the purified mannitol permease of Escherichia coli. *Journal of Cellular Biochemistry*. 1983;23(1-4):231-240. doi:10.1002/jcb.240230120
112. Lolkema JS, Dijkstra DS, ten Hoeve-Duurkens RH, Robillard GT. The membrane-bound domain of the phosphotransferase enzyme IImtl of Escherichia coli constitutes a mannitol translocating unit. *Biochemistry*. 1990;29(47):10659-10663. doi:10.1021/BI00499A012
113. Figge RM, Ramseier TM, Saier MH. The mannitol repressor (MtlR) of Escherichia coli. *J Bacteriol*. 1994;176(3):840-847. doi:10.1128/JB.176.3.840-847.1994
114. Komar J, Alvira S, Schulze RJ, et al. Membrane protein insertion and assembly by the bacterial holo-translocon SecYEG-SecDF-YajC-YidC. *Biochem J*. 2016;473(19):3341-32354. doi:10.1042/BCJ20160545
115. Törnroth-Horsefield S, Gourdon P, Horsefield R, et al. Crystal Structure of AcrB in Complex with a Single Transmembrane Subunit Reveals Another Twist. *Structure*. 2007;15(12):1663-1673. doi:10.1016/J.STR.2007.09.023
116. Bartelli NL, Sun S, Gucinski GC, et al. The Cytoplasm-Entry Domain of Antibacterial CdiA Is a Dynamic α-Helical Bundle with Disulfide-Dependent Structural Features. *J Mol Biol*. 2019;431(17):3203-3216. doi:10.1016/J.JMB.2019.05.049
117. Waterhouse AM, Procter JB, Martin DMA, Clamp M, Barton GJ. Jalview Version 2—a multiple sequence alignment editor and analysis workbench. *Bioinformatics*. 2009;25(9):1189-1191. doi:10.1093/BIOINFORMATICS/BTP033
118. Jones AM, Garza-Sánchez F, So J, Hayes CS, Low DA. Activation of contact-dependent antibacterial tRNase toxins by translation elongation factors. *Proc Natl Acad Sci U S A*. 2017;114(10):E1951-E1957. doi:10.1073/PNAS.1619273114
119. Jurėnas D, Journet L. Activity, delivery, and diversity of Type VI secretion effectors. *Molecular Microbiology*. 2021;115(3):383-394. doi:10.1111/MMI.14648

120. Benz J, Meinhart A. Antibacterial effector/immunity systems: it's just the tip of the iceberg. *Current Opinion in Microbiology*. 2014;17(1):1-10. doi:10.1016/J.MIB.2013.11.002
121. Oerum S, Meynier V, Catala M, Tisne C. A comprehensive review of m6A/m6Am RNA methyltransferase structures. *Nucleic Acids Res*. 2021;49(13):7239-7255. doi:10.1093/NAR/GKAB378
122. Kishimoto S, Tsunematsu Y, Matsushita T, et al. Functional and Structural Analyses of trans C-Methyltransferase in Fungal Polyketide Biosynthesis. *Biochemistry*. 2019;58(38):3933-3937. doi:10.1021/ACS.BIOCHEM.9B00702/ASSET/IMAGES/LARGE/BI9B00702_0005.JPEG
123. Struck AW, Thompson ML, Wong LS, Micklefield J. S-Adenosyl-Methionine-Dependent Methyltransferases: Highly Versatile Enzymes in Biocatalysis, Biosynthesis and Other Biotechnological Applications. *ChemBioChem*. 2012;13(18):2642-2655. doi:10.1002/CBIC.201200556
124. Kozbial PZ, Mushegian AR. Natural history of S-adenosylmethionine-binding proteins. *BMC Structural Biology 2005 5:1*. 2005;5(1):1-26. doi:10.1186/1472-6807-5-19
125. Whitney JC, Quentin D, Sawai S, et al. An interbacterial NAD(P)(+) glycohydrolase toxin requires elongation factor Tu for delivery to target cells. *Cell*. 2015;163(3):607-619. doi:10.1016/J.CELL.2015.09.027
126. Tang JY, Bullen NP, Ahmad S, Whitney JC. Diverse NADase effector families mediate interbacterial antagonism via the type VI secretion system. *J Biol Chem*. 2018;293(5):1504-1514. doi:10.1074/JBC.RA117.000178
127. Guo X, Söderholm A, Sandesh Kanchugal P, et al. Structure and mechanism of a phageencoded sam lyase revises catalytic function of enzyme family. *Elife*. 2021;10:1-29. doi:10.7554/ELIFE.61818
128. Furth JJ, Pizer LI. Deoxyribonucleic acid-dependent ribonucleic acid synthesis in Escherichia coli infected with bacteriophage T2. *Journal of Molecular Biology*. 1966;15(1):124-135. doi:10.1016/S0022-2836(66)80214-0
129. Eustáquio AS, Härle J, Noel JP, Moore BS. S-Adenosyl-L-Methionine Hydrolase (Adenosine-Forming), a Conserved Bacterial and Archeal Protein Related to SAM-Dependent Halogenases. *ChemBioChem*. 2008;9(14):2215-2219. doi:10.1002/CBIC.200800341
130. Newman EB, Budman LI, Chan EC, et al. Lack of S-Adenosylmethionine Results in a Cell Division Defect in Escherichia coli. *Journal of Bacteriology*. 1998;180(14):3614. doi:10.1128/JB.180.14.3614-3619.1998
131. Posnick LM, Samson LD. Influence of S-Adenosylmethionine Pool Size on Spontaneous Mutation, Dam Methylation, and Cell Growth of Escherichia coli. *Journal of Bacteriology*. 1999;181(21):6756. doi:10.1128/JB.181.21.6756-6762.1999
132. Newman EB, Budman LI, Chan EC, et al. Lack of S-adenosylmethionine results in a cell division defect in Escherichia coli. *Journal of Bacteriology*. 1998;180(14):3614-3619. doi:10.1128/JB.180.14.3614-3619.1998/ASSET/660BBB5D-49E7-4830-A20B-17C74891F8B6/ASSETS/GRAPHIC/JB1480417002.JPEG
133. Palmer BR, Marinus MG. The dam and dcm strains of Escherichia coli--a review. *Gene*. 1994;143(1):1-12. doi:10.1016/0378-1119(94)90597-5

134. Ueno T, Ito H, Kimizuka F, Kotani H, Nakajima K. Gene structure and expression of the MboI restriction--modification system. *Nucleic Acids Res*. 1993;21(10):2309-2313. doi:10.1093/NAR/21.10.2309
135. Johnston C, Polard P, Claverys JP. The DpnI/DpnII pneumococcal system, defense against foreign attack without compromising genetic exchange. *Mob Genet Elements*. 2013;3(4):e25582. doi:10.4161/MGE.25582
136. George J, Chirikjian JG. Sequence-specific endonuclease BamHI: relaxation of sequence recognition. *Proc Natl Acad Sci U S A*. 1982;79(8):2432-2436. doi:10.1073/PNAS.79.8.2432
137. SPOEREL N, HERRLICH P. Colivirus-T3-coded S-adenosylmethionine hydrolase. *Eur J Biochem*. 1979;95(2):227-233. doi:10.1111/J.1432-1033.1979.TB12957.X
138. Simon-Baram H, Kleiner D, Shmulevich F, et al. Samase of bacteriophage t3 inactivates escherichia coli's methionine s-adenosyltransferase by forming heteropolymers. *mBio*. 2021;12(4). doi:10.1128/MBIO.01242-21/SUPPL_FILE/MBIO.01242-21-SF007.PDF
139. Jerlström Hultqvist J, Warsi O, Söderholm A, et al. A bacteriophage enzyme induces bacterial metabolic perturbation that confers a novel promiscuous function. *Nat Ecol Evol*. 2018;2(8):1321-1330. doi:10.1038/S41559-018-0568-5
140. Hughes JA, Brown LR, Ferro AJ. Expression of the cloned coliphage T3 S-adenosylmethionine hydrolase gene inhibits DNA methylation and polyamine biosynthesis in Escherichia coli. *J Bacteriol*. 1987;169(8):3625-3632. doi:10.1128/JB.169.8.3625-3632.1987
141. Gu X, Orozco JM, Saxton RA, et al. SAMTOR is an S-adenosylmethionine sensor for the mTORC1 pathway. *Science (1979)*. 2017;358(6364):813-818. doi:10.1126/SCIENCE.AAO3265/SUPPL_FILE/AAO3265_GU_SM.PDF
142. Horiuchi KY, Eason MM, Ferry JJ, et al. Assay development for histone methyltransferases. *Assay Drug Dev Technol*. 2013;11(4):227-236. doi:10.1089/ADT.2012.480
143. Skinner SO, Sepúlveda LA, Xu H, Golding I. Measuring mRNA copy number in individual Escherichia coli cells using single-molecule fluorescent in situ hybridization. *Nature Protocols 2013 8:6*. 2013;8(6):1100-1113. doi:10.1038/nprot.2013.066
144. Amobonye A, Singh S, Pillai S. Recent advances in microbial glutaminase production and applications-a concise review. *Crit Rev Biotechnol*. 2019;39(7):944-963. doi:10.1080/07388551.2019.1640659
145. Anami Y, Tsuchikama K. Transglutaminase-Mediated Conjugations. *Methods Mol Biol*. 2020;2078:71-82. doi:10.1007/978-1-4939-9929-3_5
146. Masisi BK, el Ansari R, Alfarsi L, Rakha EA, Green AR, Craze ML. The role of glutaminase in cancer. *Histopathology*. 2020;76(4):498-508. doi:10.1111/HIS.14014
147. Park MS, Bitto E, Kim KR, et al. Crystal structure of human protein N-terminal glutamine amidohydrolase, an initial component of the N-end rule pathway. *PLoS One*. 2014;9(10). doi:10.1371/JOURNAL.PONE.0111142
148. Yamaguchi S, Jeenes DJ, Archer DB. Protein-glutaminase from Chryseobacterium proteolyticum, an enzyme that deamidates glutaminyl residues in proteins. *European Journal of Biochemistry*. 2001;268(5):1410-1421. doi:10.1046/J.1432-1327.2001.02019.X

149. Wilkesman J. Cysteine Protease Zymography: Brief Review. *Methods Mol Biol*. 2017;1626:25-31. doi:10.1007/978-1-4939-7111-4_3
150. Miller SI, Salama NR. The gram-negative bacterial periplasm: Size matters. *PLOS Biology*. 2018;16(1):e2004935. doi:10.1371/JOURNAL.PBIO.2004935
151. Zhou J, Korostelev A, Lancaster L, Noller HF. Crystal structures of 70S ribosomes bound to release factors RF1, RF2 and RF3. *Current Opinion in Structural Biology*. 2012;22(6):733-742. doi:10.1016/J.SBI.2012.08.004
152. Demo G, Svidritskiy E, Madireddy R, et al. Mechanism of ribosome rescue by ArfA and RF2. *Elife*. 2017;6. doi:10.7554/ELIFE.23687
153. Bolanos-Garcia M, Davies OR. Structural analysis and classification of native proteins from E. coli commonly co-purified by immobilised metal affinity chromatography. Published online 2006. doi:10.1016/j.bbagen.2006.03.027
154. Waters M, Tadi P. Streptomycin. *Kucers the Use of Antibiotics: A Clinical Review of Antibacterial, Antifungal, Antiparasitic, and Antiviral Drugs, Seventh Edition*. Published online May 8, 2022:2471-2487. doi:10.1201/9781315152110
155. Keiler KC, Waller PRH, Sauer RT. Role of a Peptide Tagging System in Degradation of Proteins Synthesized from Damaged Messenger RNA. *Science (1979)*. 1996;271(5251):990-993. doi:10.1126/SCIENCE.271.5251.990
156. Hayes CS, Bose B, Sauer RT. Stop codons preceded by rare arginine codons are efficient determinants of SsrA tagging in Escherichia coli. *Proc Natl Acad Sci U S A*. 2002;99(6):3440-3445. doi:10.1073/PNAS.052707199
157. Richter G, Fischer M, Krieger C, et al. Biosynthesis of riboflavin: characterization of the bifunctional deaminase-reductase of Escherichia coli and Bacillus subtilis. *J Bacteriol*. 1997;179(6):2022-2028. doi:10.1128/JB.179.6.2022-2028.1997
158. Vogl C, Grill S, Schilling O, Stülke J, Mack M, Stolz J. Characterization of riboflavin (vitamin B2) transport proteins from Bacillus subtilis and Corynebacterium glutamicum. *J Bacteriol*. 2007;189(20):7367-7375. doi:10.1128/JB.00590-07
159. García Angulo VA, Bonomi HR, Posadas DM, et al. Identification and characterization of ribN, a novel family of riboflavin transporters from rhizobium leguminosarum and other proteobacteria. *Journal of Bacteriology*. 2013;195(20):4611-4619. doi:10.1128/JB.00644-13/ASSET/7E42ED47-3C6E-4189-B59D-C9E456D2506B/ASSETS/GRAPHIC/ZJB9990928310007.JPEG
160. Hemberger S, Pedrolli DB, Stolz J, Vogl C, Lehmann M, Mack M. RibM from Streptomyces davawensis is a riboflavin/roseoflavin transporter and may be useful for the optimization of riboflavin production strains. *BMC Biotechnol*. 2011;11. doi:10.1186/1472-6750-11-119
161. Rie Heurgue Â -Hamard VÂ, Phanie Champ SÂ, Ke Engstro AÊ, Ns Ehrenberg MÊ, Buckingham RH. The hemK gene in Escherichia coli encodes the N5-glutamine methyltransferase that modifies peptide release factors. *The EMBO Journal*. 2002;21(4):769-778. doi:10.1093/EMBOJ/21.4.769
162. Hashizume R, Maki Y, Mizutani K, et al. Crystal Structures of Protein Glutaminase and Its Pro Forms Converted into Enzyme-Substrate Complex. *Journal of Biological Chemistry*. 2011;286(44):38691-38702. doi:10.1074/JBC.M111.255133
163. Roux KJ, Kim DI, Burke B, May DG. BioID: A Screen for Protein-Protein Interactions. *Curr Protoc Protein Sci*. 2018;91(1):19.23.1-19.23.15. doi:10.1002/CPPS.51

164. Hung V, Udeshi ND, Lam SS, et al. Spatially resolved proteomic mapping in living cells with the engineered peroxidase APEX2. *Nat Protoc*. 2016;11(3):456-475. doi:10.1038/NPROT.2016.018
165. Yin W, Wang Y, Liu L, He J. Biofilms: The Microbial "Protective Clothing" in Extreme Environments. *Int J Mol Sci*. 2019;20(14). doi:10.3390/IJMS20143423
166. Allen JP, Hauser AR. Diversity of Contact-Dependent Growth Inhibition Systems of Pseudomonas aeruginosa. *J Bacteriol*. 2019;201(14). doi:10.1128/JB.00776-18
167. Ferrières L, Hémery G, Nham T, et al. Silent mischief: bacteriophage Mu insertions contaminate products of Escherichia coli random mutagenesis performed using suicidal transposon delivery plasmids mobilized by broad-host-range RP4 conjugative machinery. *J Bacteriol*. 2010;192(24):6418-6427. doi:10.1128/JB.00621-10
168. Akiyama Y, Shirai Y, Ito K. Involvement of FtsH in protein assembly into and through the membrane. II. Dominant mutations affecting FtsH functions. *Journal of Biological Chemistry*. 1994;269(7):5225-5229. doi:10.1016/S0021-9258(17)37678-0
169. Nikolakakis K, Amber S, Wilbur JS, et al. The toxin/immunity network of Burkholderia pseudomallei contact-dependent growth inhibition (CDI) systems. *Mol Microbiol*. 2012;84(3):516-529. doi:10.1111/J.1365-2958.2012.08039.X
170. Garza-Sánchez F, Janssen BD, Hayes CS. Prolyl-tRNA(Pro) in the A-site of SecM-arrested ribosomes inhibits the recruitment of transfer-messenger RNA. *J Biol Chem*. 2006;281(45):34258-34268. doi:10.1074/JBC.M608052200
171. Chiang SL, Rubin EJ. Construction of a mariner-based transposon for epitope-tagging and genomic targeting. *Gene*. 2002;296(1-2):179-185. doi:10.1016/S0378-1119(02)00856-9
172. Schaub RE, Hayes CS. Deletion of the RluD pseudouridine synthase promotes SsrA peptide tagging of ribosomal protein S7. *Molecular Microbiology*. 2011;79(2):331-341. doi:10.1111/J.1365-2958.2010.07467.X
173. Garza-Sánchez F, Gin JG, Hayes CS. Amino acid starvation and colicin D treatment induce A-site mRNA cleavage in Escherichia coli. *J Mol Biol*. 2008;378(3):505-519. doi:10.1016/J.JMB.2008.02.065
174. Hayes CS, Bose B, Sauer RT. Stop codons preceded by rare arginine codons are efficient determinants of SsrA tagging in Escherichia coli. *Proc Natl Acad Sci U S A*. 2002;99(6):3440-3445. doi:10.1073/PNAS.052707199